

**Application of Polyelectrolyte Capsule for Drug Delivery
and Intracellular pH-Sensing**

Doctoral Thesis

To be awarded the degree of Doctor of Natural Sciences

Dr. rer. nat.

by the Department of Chemistry
of the Faculty of Mathematics, Computer Science and Natural Sciences of the
University of Hamburg

Sathi Roy

Hamburg, 2019

The presented work conducted under the supervision of Dr. Neus Feliu and Prof. Wolfgang. J. Parak at Phillips University of Marburg, Germany (from April 2016 to December 2017) and at the Center for Hybrid Nanostructure (CHyN) of the University of Hamburg (from January 2018 to June 2019.)

1. First Evaluator: Prof. Dr. Wolfgang J. Parak.
2. Second Evaluator: Prof. Dr. Alf Mews.
3. Date 12.06.2019

Table of content

Abstract.....	6
Zusammenfassung.....	8
Conference contributions and publications	10
List of Abbreviations.....	12
1. Introduction.....	14
1.1 Polyelectrolyte capsule	15
1.1.1 Synthesis of template core	15
1.1.2 Layer-by-Layer assembly of polyelectrolytes	16
1.1.3 Tuning the size and shape of capsule by controlled growth of CaCO ₃ core.....	18
1.2 Different applications of polyelectrolyte capsule.....	20
1.2.1 Delivery of cargo (Therapeutic agent or fluorescent dye).....	20
1.2.2 Ion-sensor.....	23
1.3 Alginate: A potential biodegradable polymer for pharmaceutical applications	25
1.3.1 Overview of alginate	25
1.3.2 Advantages and applications of alginate-based vehicle	26
1.4 Polyethyleneimine (PEI) for efficient Intracellular Delivery of therapeutic macromolecules	27
1.4.1 Physicochemical properties of PEI	27
1.4.2 Advantages of PEI in Therapeutics	28
1.4.3 Endosomal escape: 'Proton-sponge hypothesis'	28
2. Objective	30
3. Materials.....	32
3.1 Materials used for synthesis and application of alginate capsule.....	32
3.2 Materials used for pH sensor capsule synthesis and intracellular pH measurement	32
3.3 Materials used for cell culture.....	33
4. Experimental section	33
4.1 Synthesis and Characterization of biodegradable alginate capsules.	33
4.1.1 Synthesis of initial calcium carbonate cores	33
4.1.2 Synthesis of biodegradable alginate capsules	34
4.1.3 Structural characterization.....	35
4.1.4 Determination of capsule concentrations.....	35
4.1.5 Size distribution of capsules	36
4.2 Drug loading and encapsulation efficiency of capsules.....	37
4.3 In vitro release study of different capsules	40

4.4 Degradation study of capsules	43
4.5 Uptake studies of alginate capsules by CLSM	43
4.6 Synthesis and Characterization of different pH sensitive capsules	45
4.7. Biocompatibility study	47
4.7.1 Cell culture	47
4.7.2 Biocompatibility study of biodegradable capsules.....	48
4.6.3 Biocompatibility study of different pH sensor capsules & test samples	49
4.8 pH calibration curve of different pH sensor capsules	51
4.8.1 pH calibration curve of only capsules.....	51
4.8.2 pH calibration curve of capsules inside cell.....	52
4.9 Experimental scheme for monitoring intracellular pH.....	53
4.9.1 Monitoring lysosomal pH in presence of different PEI samples.....	53
4.9.2 Monitoring pH of intra and extracellular compartments by different capsules.....	55
4.10 Synthesis and characterization of PEI-polyplex.....	56
4.11 Co-localization study of capsule, labeled-PEI or PEI-plasmid polyplex & lysosome	57
4.12 Study the effect of PEI on fluorescence of pH sensitive dye SNARF	58
4.13 Uptake studies by flow cytometry	59
4.13.1 Uptake studies of biodegradable capsules	59
4.13.2 Uptake studies of different pH sensor capsules	61
4.13.3 Uptake study of labeled PEI	62
5. Results and discussion	64
5.1 Biodegradable alginate capsules as biocompatible potential delivery agents	64
5.1.1 Synthesis and characterization of biodegradable alginate capsules.....	64
5.1.2 Drug loading and encapsulation efficiency of capsules	67
5.1.3 In vitro release study from different capsules.....	69
5.1.4 Biodegradation study of capsules.....	71
5.1.5 Biocompatibility studies of capsules	73
5.1.6 Uptake studies of the capsules.....	74
5.2 pH sensor capsule - a reporter of PEI-mediated Lysosomal pH change and capsule trafficking	76
5.2.1 Synthesis and characterization of pH sensor capsule	76
5.2.2 pH dependence of different pH sensor capsules	77
5.2.3 Cytotoxicity of different pH sensor capsules	80
5.2.4 Understanding the Intracellular trafficking of pH-sensor capsules by FACS	81
5.2.5 Monitoring intracellular pH by different pH-sensor capsule	87
5.2.6 Co-localization study of pH-sensor capsule, PEI and lysosome	93

6. Conclusion and outlook	96
7. List of Hazardous Substances used according to GHS.....	98
References.....	100
A. Acknowledgments	106

Abstract

In recent years, tremendous efforts have been devoted in pharmaceutical research area to the development of future Nano medicines that can be used as an effective drug delivery system (DDS). Polyelectrolyte capsule (PEC) formed through layer-by-layer (LbL) technology has emerged as a potential technique for different cargo encapsulation and successful release of cargo at desired site. In case of drug delivery application, despite of having several advantages, bigger size ($>2\mu\text{m}$) of capsule limits from any real application. Therefore, one of the aim of my research work was to synthesize small PEC based DDS through completely biocompatible process. Here we have reported formation of a small PEC ($<1\mu\text{m}$) made of biodegradable polymers, alginate (ALGI) and Poly-L-arginine (PARG) with a pH sensitive outer layer of EUDRAGIT L 100 (EuL) polymer. As a model drug, a natural hydrophobic extract curcumin was used. Curcumin possesses a wide range of biological activities including antioxidant, anti-inflammatory, anticancer and antimicrobial effects. In case of poor water soluble drug like curcumin, one of the major issues is reduced bioavailability after internalization into body. Encapsulation inside capsule protected the therapeutic activity and also increases bioavailability of these kinds of drugs. The viability study and uptake study of these drug loaded Nano capsule supports potentiality of this system for drug delivery.

Another aspect that highlighted in my research work is potentiality of PEC based sensor for intracellular pH analysis using high throughput analysis techniques Flow cytometry (FACS). Investigation of change in different ion concentration inside cell can reveal many unknown facts regarding various intracellular processes that can be induced by some external or internal factors. Different nanomedicine exposed to cell is also an external factor that can trigger different intracellular ion changes and understanding these facts will help us to design better pharmaceutical compounds. Most of these Nano carriers enters into cell through different endocytic process and have a tendency to get entrapped into lysosome which is the enzyme factory of cell. For effective intracellular delivery from Nano carriers containing different biopharmaceuticals requires release of it into cytosol by endosomal escape. Longer entrapment into lysosome will destroy

reactivity of therapeutics. Various researches are going on to develop efficient Nano carriers made of different pH sensitive polymers which can trigger endosomal escape by pH-induced structural change of lysosome. Polyethyleneimine (PEI) is one of such pH-sensitive polymer which has been widely explored for non-viral gene delivery and also for designing Nano carriers, efficient for therapeutic release to cytosol. The mechanism behind high efficiency of PEI for endosomal escape has been explained by the well accepted 'Proton-sponge' hypotheses. This hypothesis emphasizes high buffering capacity of PEI inside lysosome along with subsequent increase in lysosomal pH which is considered as one of the main factor behind endosomal escape. However, the experimental evidence to prove lysosomal pH change occurring in presence of PEI, is not satisfactory. Herein we have used SNARF loaded polyelectrolyte capsule as an intracellular pH sensor to investigate this phenomenon by monitoring lysosomal pH change in presence of different PEI exposed to cell. SNARF is a pH sensitive dye and it has dual emission property which enables ratio metric pH sensing without using any further reference fluorophore. The pH-sensor capsules were formed using polystyrene sulfonate (PSS) and polyallylamine hydrochloride (PAH) polymer by L-b-L method. In addition to exposing free PEI to cell, the outer layers of pH-sensor capsule were also modified with PEI in order to measure pH of lysosome (pH_{lyso}). A detailed quantitative analysis of pH_{lyso} has revealed influence of PEI on lysosomal pH rise. The comprehensive uptake study of PEI modified sensor capsule as compared to non-modified sensor capsule (control system) has also supported this result.

Zusammenfassung

In den letzten Jahren wurden im Bereich der pharmazeutischen Forschung enorme Anstrengungen unternommen, um zukünftige Nanomedizin zu entwickeln, die als wirksames Wirkstoffabgabesystem (DDS) eingesetzt werden kann. Polyelektrolyt-Kapseln (PEC), die durch Schicht für Schicht (LbL) -Technologie gebildet werden, haben sich als potentieller Träger für die unterschiedliche Einkapselung von Fracht und das erfolgreiche Freisetzen von Fracht an der gewünschten Stelle herausgebildet. Im Falle einer Medikamentenabgabe ist ihre größere Größe ($> 2 \text{ } \mu\text{m}$; μm) von jeder realen Anwendung abhängig, obwohl sie mehrere Vorteile hat. Daher bestand das Ziel meiner Doktorarbeit darin, kleine PEC-basierte DDS durch ein vollständig biokompatibles Verfahren zu synthetisieren. Hier haben wir die Bildung von kleinem PEC ($\sim 1 \mu\text{m}$) aus biologisch abbaubaren Polymeren, Alginat (ALGI) und Poly-L-Arginin (PARG) mit einer pH-empfindlichen äußeren Schicht aus EUDRAGIT L 100 (EuL) - Polymer beschrieben. Als Modellarzneimittel wurde ein natürlicher hydrophober Extrakt Curcumin verwendet. Curcumin verfügt über ein breites Spektrum an biologischen Aktivitäten, einschließlich antioxidativer, entzündungshemmender, antimikrobieller und antimikrobieller Wirkungen. Bei schlecht wasserlöslichen Arzneimitteln ist eines der Hauptprobleme die verminderte Bioverfügbarkeit nach der Internalisierung im Körper. Die Verkapselung des wasserunlöslichen Modellarzneimittels Curcumin in der Kapsel schützte deren therapeutische Aktivität und steigerte auch die Bioverfügbarkeit. Die Durchführbarkeitsstudie und die Aufnahmestudie dieser mit Wirkstoff beladenen Nanokapseln unterstützen das Potenzial dieses Systems für die Wirkstoffabgabe.

Ein weiterer Aspekt, der in meiner Forschungsarbeit hervorgehoben wurde, ist das Potenzial eines PEC-basierten Sensors für die intrazelluläre pH-Analyse durch Hochdurchsatz-Analysetechniken unter Verwendung von Durchflusszytometrie (FACS). Die Untersuchung der Veränderung der unterschiedlichen Ionenkonzentration innerhalb einer Zelle kann viele unbekannte Tatsachen bezüglich verschiedener intrazellulärer Prozesse aufdecken, die durch externe oder interne Faktoren ausgelöst werden können. Unterschiedliche Nanomedizin, die der Zelle ausgesetzt ist, ist auch ein externer Faktor, der verschiedene intrazelluläre Ionenveränderungen auslösen kann,

und das Verständnis dieser Fakten wird uns dabei helfen, bessere pharmazeutische Verbindungen zu entwickeln. Die meisten dieser Nanotransporter dringen durch unterschiedliche endozytische Prozesse in die Zelle ein und neigen dazu, im Lysosom eingeschlossen zu sein, das die Enzymfabrik der Zelle ist. Für eine effektive intrazelluläre Abgabe von Nanocarriern, die verschiedenen Biopharmaka enthalten, ist die Freisetzung in Cytosol durch endosomale Flucht erforderlich. Ein längerer Einschluss in das Lysosom zerstört die Reaktivität von Therapeutika. Verschiedene Forschungen arbeiten an der Entwicklung effizienter Nanotransporter aus verschiedenen pH-empfindlichen Polymeren, die durch pH-induzierte strukturelle Veränderungen des Lysosoms das endosomale Entweichen auslösen können. Polyethylenimin (PEI) ist ein solches pH-empfindliches Polymer, das für die nicht-virale Genabgabe und auch für das Design von Nanoträgern, die für die therapeutische Freisetzung von Cytosol wirksam sind, vielfach erforscht wurde. Der Mechanismus hinter der hohen Effizienz von PEI für die endosomale Flucht wurde durch die allgemein akzeptierte "Proton-Schwamm-Hypothese" erklärt. Diese Hypothese hebt die hohe Pufferkapazität von PEI im Lysosom und die anschließende Erhöhung des lysosomalen pH-Werts hervor, die als einer der Hauptfaktoren für das endosomale Entweichen angesehen wird. Die experimentellen Beweise für den Nachweis der Veränderung des lysosomalen pH-Werts in Gegenwart von PEI sind jedoch nicht zufriedenstellend. Hier haben wir eine mit SNARF beladene Polyelektrolytkapsel als intrazellulären pH-Sensor verwendet, um dieses Phänomen zu untersuchen, indem die Veränderung des lysosomalen pH-Werts in Gegenwart von verschiedenen PEI-Zellen überwacht wird. SNARF ist ein pH-empfindlicher Farbstoff und besitzt eine duale Emissionseigenschaft, die eine pH-Messung des Verhältnismaßes ohne Verwendung eines weiteren Referenzfluorophors ermöglicht. Die pH-Sensorkapseln wurden unter Verwendung von Polystyrolsulfonat- (PSS) und Polyallylaminhydrochlorid- (PAH) -Polymer durch das L-b-L-Verfahren gebildet. Zusätzlich zur Freisetzung von freiem PEI für Zellen wurden die äußeren Schichten der pH-Sensorkapsel auch mit PEI modifiziert, um den pH-Wert des Lysosoms (pH_{lyso}) zu messen. Eine detaillierte quantitative Analyse von pH_{lyso} hat den Einfluss von PEI auf den pH-Anstieg von Lysosomen gezeigt. Die umfassende

Aufnahmestudie der PEI-modifizierten Sensorkapsel im Vergleich zu einer nicht modifizierten Sensorkapsel (Kontrollsystem) hat dieses Ergebnis ebenfalls unterstützt.

Conference contributions and publications

In context with this work, the following contributions have been presented at conferences and published journal articles.

Conference contributions – poster/ oral presentation

❖ E-MRS 2019 Spring Meeting, Nice, France.
(Poster titled as “*Evaluating Poly(ethylenimine)-Mediated Lysosomal pH Alteration with Capsule-Based Fluorescent Sensor*”). Received The Best Student Poster Award.

❖ E-MRS 2018 Fall Meeting, Warsaw University of Technology – POLAND.
(Poster titled as “*Synthesis of a Novel Biocompatible Layer-by-Layer Nano capsule for Drug Delivery*”).

❖ Oral presentation at Raman4Clinic, Training School organized by COST 2018, European cooperation in science and technology at University of Coimbra, Portugal.
(Oral titled as “*pH sensitive capsule as reporter of lysosomal pH change*”).

List of publications

Published/ Accepted:

❖ **S. Roy**, N. Elbaz, W. J. Parak and N. Feliu (2019), “Biodegradable alginate polyelectrolyte capsules as plausible biocompatible delivery carriers.” ACS Applied Bio Materials. (Just accepted, DOI: 10.1021/acsabm.9b00203)

Contribution: Contributed in planning of the project, execution of the all experimental parts and developing protocol for new capsule synthesis, data analysis and result interpretation, presentation of manuscript figures and writing manuscript.

❖ Zhao, S., F. Caruso, L. Dähne, G. Decher, B. G. De Geest, J. Fan, N. Feliu, Y. Gogotsi, P. T. Hammond, M. C. Hersam, A. Khademhosseini, N. Kotov, S. Leporatti, Y. Li, F. Lisdat, L. M. Liz-Marzán, S. Moya, P. Mulvaney, A. L. Rogach, **S. Roy**, D. G. Shchukin, A. G. Skirtach, M. M. Stevens, G. B. Sukhorukov, P. S. Weiss, Z. Yue, D. Zhu and W. J. Parak (2019). "The Future of Layer-by-Layer Assembly: A Tribute to ACS Nano Associate Editor Helmuth Möhwald." ACS Nano. (Just accepted, DOI: 10.1021/acsnano.9b03326)

Contribution: Contributed in writing manuscript, specially the section 'Layer-by-Layer-based encapsulation for delivery vehicles', compiling the figures of the articles and proof reading.

❖ Zhu, D., **S. Roy**, Z. Liu, H. Weller, W. J. Parak and N. Feliu (2019). "Remotely controlled opening of delivery vehicles and release of cargo by external triggers." Advanced Drug Delivery Reviews **138**: 117-132.

Contribution: Contributed in writing manuscript, specially the sections 'Light triggered release', manuscript figures compilation and proof reading.

❖ Chakraborty, N. Feliu, **S. Roy**, K. Dawson and W. J. Parak (2018). "Protein-Mediated Shape-Control of Silver Nanoparticles." Bioconjugate Chemistry **29**: 1261–1265.

Contribution: Study the nanoparticle intracellular interaction through cytotoxicity study and Uptake study of differently shaped silver particles, data analysis and interpretation of result, writing manuscript and proof reading.

❖ N. Feliu, J. Hühn, M. V. Zyuzin, S. Ashraf, D. Valdeperez, A. Masood, A. H. Said, A. Escudero, B. Pelaz, E. Gonzalez, M. A. C. Duarte, **S. Roy**, I. Chakraborty, M. L. Lim, S. Sjöqvist, P. Jungebluth and W. J. Parak (2016). "Quantitative uptake of colloidal particles by cell cultures." Science of the Total Environment **568**: 819-828.

Contribution: Contributed in presentation of manuscript figures and writing manuscript, making the detailed table about different 'Mechanisms for cellular uptake of particles' and proof reading.

Manuscript under Preparation:

❖ **S. Roy**, Zhu. D., N. Feliu., W. J. Parak. "In situ measurements of lysosomal proton-buffering by pH-sensitive fluorescent polymer microcapsules"

Note: This is one of my major research project during the doctoral research time period and will be published very soon. Some unpublished data/ figures has been used here to write this PhD thesis and those will be used in main manuscript during publication later. The whole work has been executed by me and project planning has been done under supervision of my supervisor Prof. W.J. Parak and co-supervisor Dr. N. Feliu.

List of Abbreviations

PEC	Polyelectrolyte capsule
LbL	layer-by-layer
ALGI	Alginic acid sodium salt
PSS	Sodium poly-(styrene sulfonate)
PAH	Poly(allylamine hydrochloride)
PARG	Poly-L-arginine hydrochloride
DEX	Dextran sulfate sodium salt
EuL	Eudragit L 100
EDTA	Ethylenediaminetetraacetic acid disodium salt
PVP	Polyvinyl pyrrolidone
PLL	Poly-L-lysine
SNARF	Seminaphtharhodafluor
PBS	Phosphate-buffered saline
SDS	Sodium dodecyl sulfate
PEG	Polyethylene glycol

BPEI	Branched Poly(ethyleneimine)
LPEI	Linear Poly(ethyleneimine)
Rh-B	Rhodamine-B isothiocyanate
HA	Hyaluronic acid
SERS	Surface enhanced Raman scattering
Cq	Chloroquine
HBSS	Hank's Balanced Salt Solution
HEPES	4-(2-hydroxyethyl)-1-piperazineethanesulfonic acid
DMEM	Dulbecco's Modified Eagle's medium Minimum
FBS	Fetal bovine serum
HeLa	Human cervical adenocarcinoma cells
TEM	Transmission electron microscopy
CLSM	Confocal laser scanning microscopy
DLS	Dynamic light scattering
d_h	Hydrodynamic diameters
C_{cur}	Concentration of curcumin
η_{EE}	Encapsulation efficiency
η_{LC}	Loading capacity
Ctrl	Control
λ [nm]	Wavelength
I [a.u.]	Intensity
η_{CR}	Cumulative release
ζ [mV]	Zeta potential
SD	Standard deviation
WGA	Wheat Germ Agglutinin
TMRA	Tetramethylrhodamine

RT	Room temperature
HeLa	Human cervical adenocarcinoma cells
V [%]	Cell viability
FACS	Fluorescence-activated cell sorting/ Flow cytometry (FCM)
FSC	Forward-scattering
SSC	Side scattering
RCU	Relative capsule uptake

1. Introduction

1.1 Polyelectrolyte capsule

Since the revolutionary work by Caruso and Moñhwalld *et al.* at 1998, research on developing hollow capsule structure with distinct properties compare to solid nano/micro particles has received tremendous interest and shows significant promise in wide range of applications.[1] Polyelectrolyte capsules are hollow structures synthesized by adding different polyelectrolyte layers around a template core and subsequent removal of the core via etching. The void space inside the capsule acts as a storage system that can encapsulate a variety of substances and can be used for different applications, including protections of therapeutics, controlled cargo release, catalysis and sensing.

1.1.1 Synthesis of template core

Formation of a stable hollow capsule structure is highly dependent on the size, morphology and texture of template core. Various inorganic and organic templates can be used for the fabrication of capsules like, melamine formaldehyde (MF),[2] polystyrene (PS),[3] carbonates (MnCO_3 , CaCO_3 , CdCO_3)[4-6] , silica particles, and even cells. [7] Among them, calcium carbonate (CaCO_3) is the most promising candidate as a template because of its great biocompatibility and high porosity. Nevertheless, the inside core is easily removal after the capsule formation using nontoxic chelating agent ethylene diamine tetra acetic acid (EDTA), in contrary to the hares chemicals used for the removal of MF [acid, $\text{pH} = 1.3$], silica [alkaline or hydrofluoric acid(HF) etching] and PS [Tetrahydrofuran (THF)] cores. The simplest synthesis method of mixing CaCl_2 and Na_2CO_3 salt solutions lead to precipitation of three anhydrous polymorphs (calcite, aragonite, and vaterite) of CaCO_3 particles. The vaterite form of CaCO_3 particle holds great potential in different biomedical applications due to its high water solubility, porous nature and biological inertness. However, calcite is the most stable CaCO_3 polymorphs. As stated by Ostwald's rule of stages, the least stable polymorphs crystallize first to form more stable polymorph, the least stable vaterite CaCO_3 are prone to further recrystallization. Uniform, nearly spherical, vaterite CaCO_3 micro particles has be synthesized by rapid mixing of supersaturated aqueous solution (alkaline pH) of CaCl_2 and Na_2CO_3 under thorough agitation on magnetic stirrer followed by leaving the reaction mixture without stirring for few minutes at room

temperature (25- 45 °C).[8] The high abundance of vaterite polymorphs is extensively dependent upon several factors such as reactant (CaCl_2 and Na_2CO_3) concentration, pH, temperature, speed and intensity of agitation. For instance, high pH (pH 7-11) leads to super saturation of reactant carbonate ion, leading to formation of more vaterite particles. Control over crystal nucleation is possible by adjusting different parameters.

1.1.2 Layer-by-Layer assembly of polyelectrolytes

LbL technology for micro- and Nano encapsulation was introduced about 20 years ago.[9-13]. This technique brings the possibility of assembling therapeutics in between polyelectrolyte layers protecting the cargo, and, at the same time, introducing multiple functional groups available in the polyelectrolyte, which can be engineered to generate a stealth coating or for targeting delivery. Different types of biodegradable and nonbiodegradable polyelectrolyte capsules have been prepared by depositing oppositely charged layers onto the spherical template. The most common nonbiodegradable polymers used for capsule synthesis are negatively charge poly(styrene sulfonate) and positively charged poly(allylamine hydrochloride) (PSS/PAH). A variety of biodegradable polymers has been explored for making layers, such as, positively/ negatively charged poly-L-arginine hydrochloride/ dextran sulfate sodium salt (PARG/ DEXS), chitosan/ alginate (CHI/ ALGI) etc. These polyelectrolyte layers are self-assembled onto solid surface mostly by electrostatic interaction force. The fabrication of layers is highly dependent upon different physicochemical properties of the polymer solutions like, ionic strength, pH, temperature etc. This kind of biodegradable capsules are very much efficient for delivering active pharmaceutical ingredients into cell. However, high semipermeable property of the L-b-L layers makes encapsulation of small molecules challenging. Even for the very dense polyelectrolyte system polyallylamine/ polystyrene sulfonate (PAH/PSS), high release rates were found for water soluble molecules with molecular weights below 5 kDa.[14] In contrary large molecules of molecular weights above 10 kDa can be permanently immobilized in capsules. Sukhorukov et al. have reported a biodegradable composite polyelectrolytes/silica capsules that showed great potential for successful encapsulation of small molecules.[15] This composite silica capsules were synthesized by adding a

last layer of silica around as synthesized biodegradable (PARG/DEX) capsule of predetermined numbers of layers. Addition of silica coating is a typical sol-gel synthesis where silica forms concrete layers around PEC upon addition of Tetraethyl ortho silicate (TEOS) which then hydrolyzed and condensed to form a strong shell. Nowadays, LbL technology still has its potential in particular in the areas where other technologies are not available. A number of studies demonstrated on various cell types ranging from macrophages, dendritic cells to neurons, and stem cells, that internalization of capsules in cells showed no significant effect on cell viability. [16, 17] Whereas mechanical properties of capsules facilitate their uptake as the capsules can be easily deformed during internalization.[18-20] In another word, the cells are tolerant to capsule intake, which is not always a case for many other delivery systems. In this way polyelectrolyte capsule offers a good platform to deliver encapsulated cargo inside cells, which will be discussed in terms of application of LbL capsule in the following paragraphs.

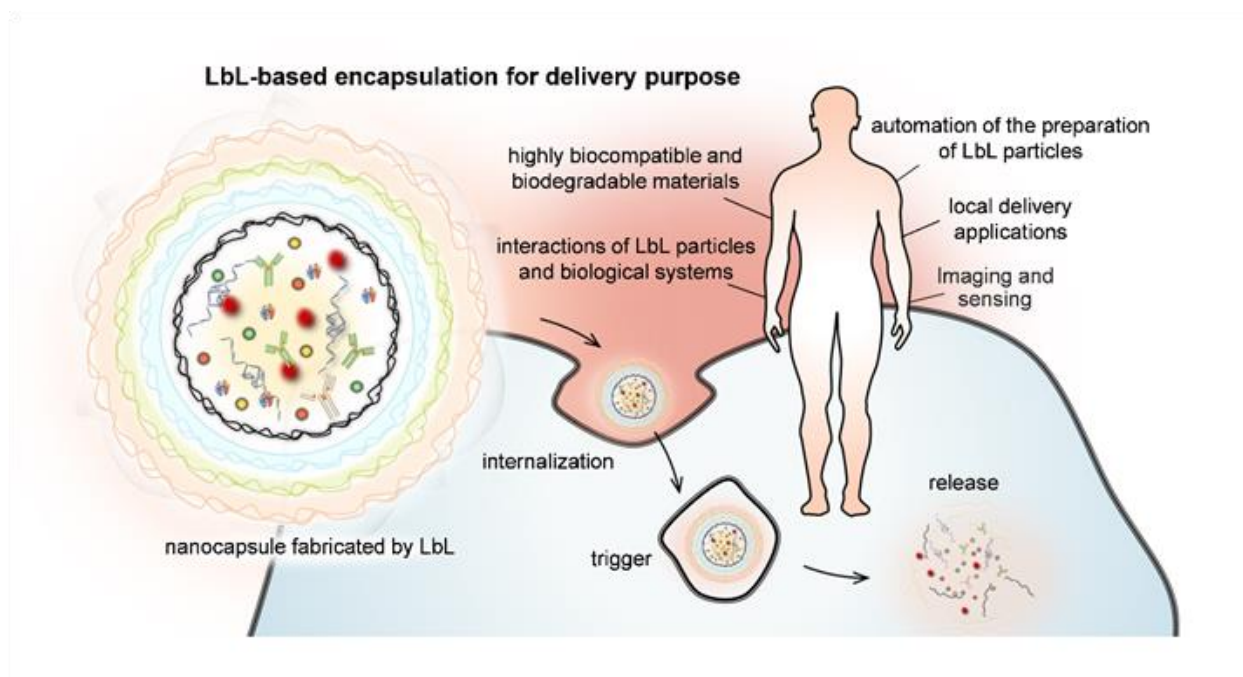


Figure 1. LbL polyelectrolyte capsule used as platform for delivery purpose.[21]

1.1.3 Tuning the size and shape of capsule by controlled growth of CaCO_3 core

The template core mostly governs the size and shape of polyelectrolyte capsules. Therefore, synthesis of monodisperse template core with distinct size distribution is an essential factor. In aqueous solution, CaCO_3 forms three anhydrous polymorphs, calcite, aragonite, and vaterite. Among them vaterite particles are most effective for loading cargo due to high porous nature and for adding different polymer layers. However, calcite is the most stable polymorphs. CaCO_3 particles are formed by mixing CaCl_2 and Na_2CO_3 solution. Vigorous mixing of reactants, initially results into solid dispersion of CaCO_3 , followed by transformation and dissolution-recrystallization resulting in a mixture of different CaCO_3 polymorphs.[22] High abundance of vaterite particles can be achieved by controlling different reaction conditions. The different parameters responsible for tuning the size, shape and morphologies are, stoichiometric ratio of mixing reactants, pH of reaction medium, temperature, speed of mixing and nucleation time. The CaCO_3 particles of 2 to 15 μm size are highly reproducible from saturated mixture of reactants, at alkaline pH and RT. Different additives are also responsible for modification of size and shape of CaCO_3 particles. For e.g.. CaCO_3 particles of 150 nm to 500 nm can be produced in presence of poly (vinyl sulfonic acid) whereas in n-butyl alcohol and hexadecyl trimethylammonium bromide, particles of 100 to 400 nm are forms. Although high polydispersity is a matter of concern here. Trushina et al. studied the influence of Polyols (ethylene glycol (EG), glycerol, and erythritol) on the particle size.[8] The higher viscosity of reaction medium in presence of polyols increases the super saturation and facilitates nucleation making the nucleation predominant over the particle growth process. In a detailed investigation by *Parak et al.* demonstrated the ratio of water/EG, pH of the mixture, stirring time and aspect ratio of CaCl_2 and Na_2CO_3 mixture, can initiate anisotropic growth of particles.[23] Different polymers also affect this nucleation and growth process. Polymers such as poly (sodium 4-styrenesulfonate) (PSS) and poly (allylamine hydrochloride) (PAH), helps to block the growth stage of particles and produces smaller particles of 600 nm to 1 μm size.[22] In principle, small particles are able to produce smaller hollow capsules after adding different layers of polymers by L-b-L assembly. However, different physiochemical

parameters also need optimization to make successful assembly of layers around particles avoiding aggregation.

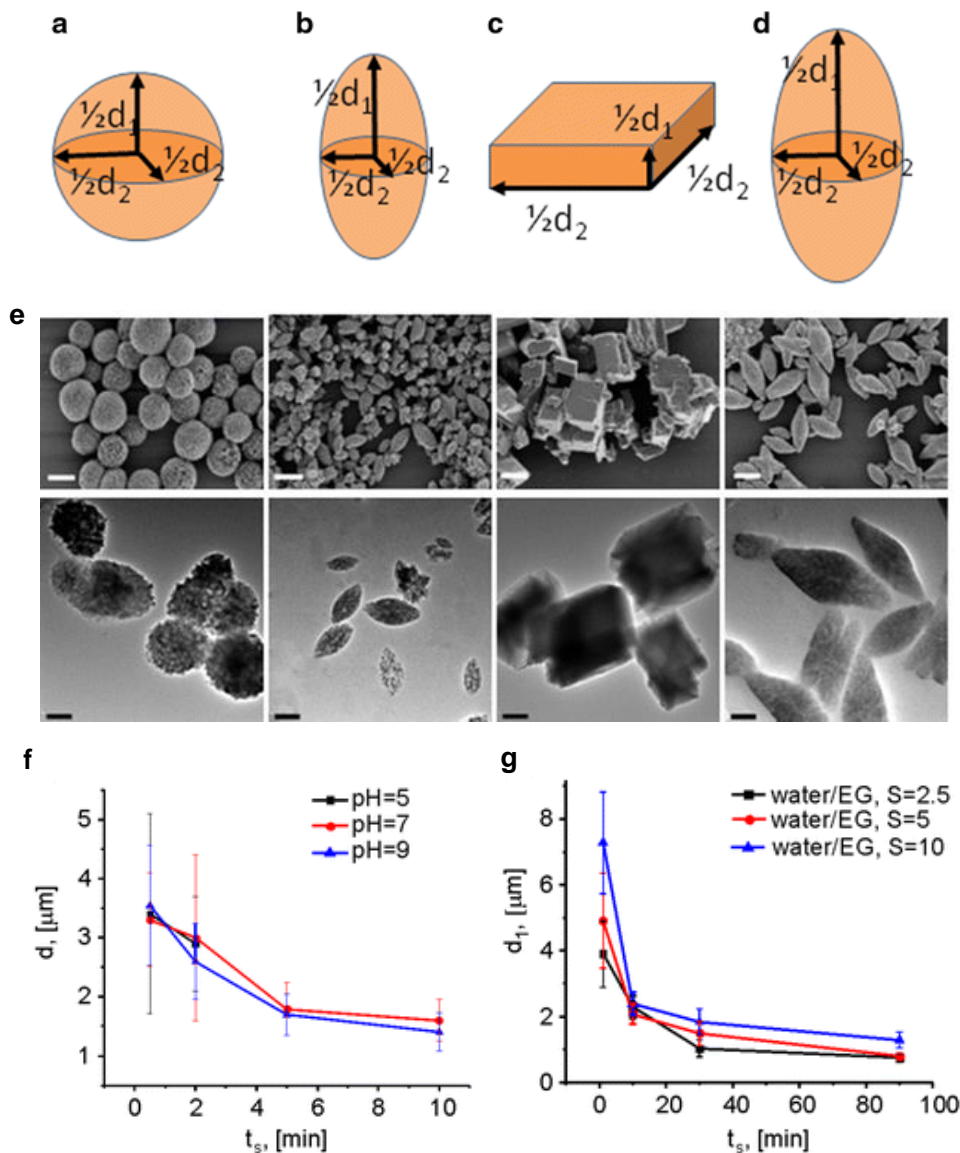


Figure 2. Anisotropic growth of CaCO_3 particles under variation of different parameters (a, b, c, d). All particles have symmetry in the x–y plane. d_1 describes the extension of the particles along the axis of symmetry, and d_2 the extension perpendicular to this axis. (e) SEM (1st row) and TEM (2nd row) images of the different particles formed from (a) through (d). The scale bars in all images correspond to 2 μm and 1 μm for SEM and TEM images respectively. (f, g) Tuning the sizes of particles. (f) The size variation (d =

$d_1 = d_2$) of spherical CaCO_3 particles by varying the stirring time (t_s) of the CaCl_2 and Na_2CO_3 mixture at different pH values with a sodium carbonate to calcium chloride ratio (S) = 1. (g) Tuning the length (d_1) of ellipsoidal CaCO_3 particles by varying the t_s at different salt concentration ratios (S) in water/ethylene glycol = 1/5 solutions of pH = 9.5. Adapted with permission from *Parak et al.* [23]

1.2 Different applications of polyelectrolyte capsule

1.2.1. Delivery of cargo (Therapeutic agent or fluorescent dye)

Polyelectrolyte capsules possess excellent potential to be used as a drug delivery system. Different therapeutics or fluorophore can be easily loaded into these capsules and by various techniques, it is possible to release the cargo at a particular site inside cell.

Capsule disintegration and endo/ lysosomal escape of molecular cargo

The multilayered system must degrade in order to deliver, encapsulated therapeutics into cell. PEC are internalized by cells *via* endocytosis process [24] and eventually reach lysosomes, [16, 18, 25] which is the most acidic compartment of the cell having several enzymes. Therefore, the most effective and simple strategy to release the payload from capsule by enzymatic degradation inside cell. Biodegradable capsules made of dextran sulfate/poly-L-arginine (DEXS/PARG), are capable to release molecular cargo through enzymatic degradation. As an example, self-quenched DQ-ovalbumin (DQ-OVA, ~ 45 kDa, Thermofisher), [26] known to be a fluorogenic substrate for proteases, was encapsulated into both non-degradable poly(styrene sulfonate)/poly(allylamine hydrochloride) (PSS/PAH) and bio-degradable dextran sulfate/poly-L-arginine (DEXS/PARG) microcapsules. DQ-OVA comprises ovalbumin heavily labelled with BODIPY dyes. The green fluorescence of DQ-OVA is self-quenched due to close proximity of BODIPY molecules, which may restore upon enzymatic degradation of DQ-OVA into peptide fragments. After internalization into cell, for PSS/PAH capsules no green fluorescence appeared due to enzymatic degradation of DQ-OVA. Whereas DEXS/PARG capsules and encapsulated DQ-OVA were almost completely degraded after 3–5 days. This phenomenon was confirmed by reappearance of green fluorescence due to release of BODIPY molecules. (Fig. 3a, b). However, most of DQ-

OVA fragments were still trapped inside lysosomes, which eventually will lead to exocytosis. Specially for delivering genetically modified plasmid molecules, lysosomal entrapment is a major issue. In another work, degradable silica capsules were prepared and found highly efficient to deliver intact mRNA (mGFP) able to serve as a template for the synthesis of proteins in the cytosol. This properties makes capsule system interesting for the delivery of sensitive molecules that otherwise will be degraded before reaching the target cells.[27]

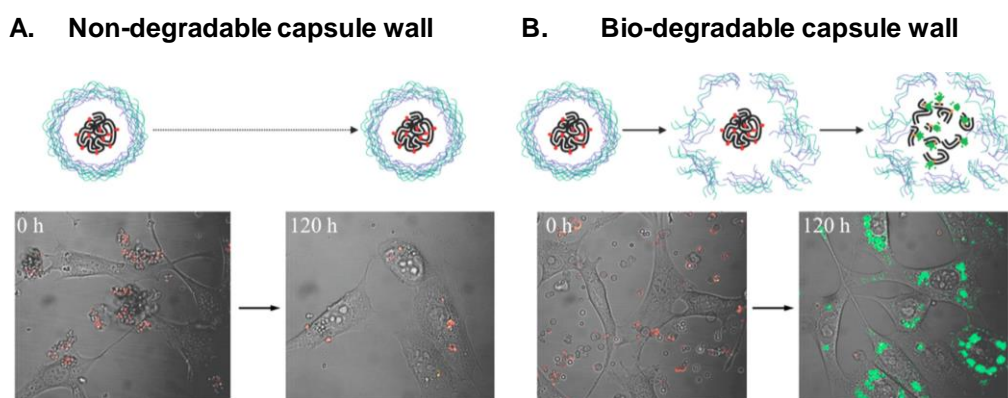


Figure 3. Release of protein cargo from capsule, through enzymatic cleavage. Embryonic NIH/3 T3 fibroblasts were incubated with (a) nondegradable PSS/PAH or (b) degradable DEXS/PARG capsules encapsulating DQ-OVA. Images were taken 0 h and 120 h after capsules exposure.[28]

Light-mediated capsule opening

Light-mediated photo thermal release of molecular cargo from a capsule can be achieved by embedding plasmonic NPs into the polyelectrolyte shell of the vehicle, inside which the molecular cargo is embedded. Employed plasmonic NPs include silver NPs [29, 30], gold sulfide NPs [31], spherical gold NPs [32],[33], agglomerated gold NPs [27],[34],[35], gold nanorods [36],[37] and gold nanostars [38], as also non-plasmonic NPs such as magnetite NPs [39]. As first example live cell imaging based on intracellular immunostaining with impermeable fluorescence reporters has been described. Fluorescent labeling of intracellular organelles for live cell imaging is challenging. Specially for immunostaining, it requires fixation and permibilization of cell

as many fluorescent reporters, e.g. fluorescence-labelled antibodies targeting specific intracellular organelles cannot penetrate the cell membrane. In addition, single cell staining within a cell culture is almost impossible.

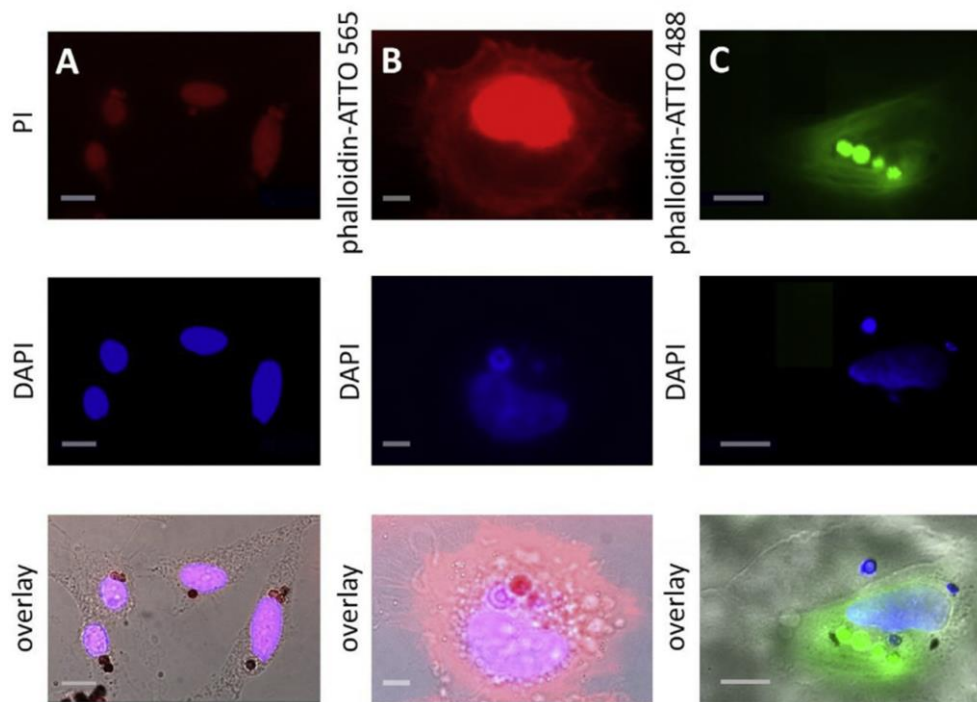


Figure 4. Multiplexed intracellular opening of capsules with different encapsulated fluorescent reporters. a) Combination of propidium iodide (PI) and (4',6-diamidino-2-phenylindole) (DAPI). The scale bars indicate 20 μm . b) Combination of phalloidin-ATTO-565 and DAPI. The scale bars correspond to 10 μm . c) Combination of phalloidin-ATTO-488 and DAPI. The scale indicate 20 μm . [28]

In a recent study by Parak et al. reported specific staining of single cell in a controlled manner by light triggered capsule opening process. For that membrane-impermeable ATTO-488 labelled phalloidin, propidium iodide (PI), and 4,6-diamidino-2-phenylindole (DAPI) were encapsulated in PSS/PAH polyelectrolyte capsules decorated with gold stars. As shown in Fig.4, multiplexed NIR opening of capsules loaded with different fluorophores enabled dual staining of the nuclei and F-actin within single live cells in a controlled and specific manner.

1.2.2 Ion-sensor

In different biomedical application, sensing analyte concentrations inside cell under the influence of various external conditions is very important. Inside cell, a huge variation in different ion concentration can be observed between the intracellular and extracellular environment.[40] Variation of these ion concentrations in our body can lead to pathological disturbances. Typical analysis technique involves ion-sensitive sensor based on optical detection.[41] Fluorescence ion-sensitive dyes show change in their spectral property upon chemical interaction with respective ions. One of the major drawback of using free dye as ion sensor is it's high cytotoxicity effect to the cell.[42] Encapsulation of these dyes into capsule system restricts direct interaction to the cell which reduces toxic effects at the same time protects it from intracellular degradation.[42] Polyelectrolyte capsules are made of different polymer layers. Fluorescent dyes when connected to dextran moiety it cannot get out of the system whereas the ions can easily pass through the permeable layers of capsule. Apart from this, multiple ion-sensitive fluorophores are also possible to load into same capsule. For instance, PEC was loaded with pH sensitive dye FITC and reference dye AF594 i.e. pH insensitive, and both dyes were conjugated with dextran in order to avoid any leakage. The pH quantification was possible by making a ratio of change in FITC fluorescence w.r.t pH to fluorescence of pH insensitive dye AF594.[43] Other than that, The sodium sensitive dye, sodium-binding benzofuran isophthalate (SBFI), and the potassium sensitive dye, potassium-binding benzofuran isophthalate (PBFI), were also loaded into capsule and used as ion indicators for the fluorimetric determination of intracellular concentrations of Na^+ and K^+ , respectively. In a study by Parak et al. showed quantum dot (QD) barcoded capsule acts like a smart multiple ion sensor.[44] Here different capsules were loaded with different ion sensitive dyes (FITC, SBFI and PBFI which responds to H^+ , Na^+ , and K^+ ions respectively) along with a reference dye. Each different capsule was tagged with QD barcode in the wall using combination of three different QD colors. (fig 5) QDs are organic fluorophores with broad excitation spectrum and a narrow, sharply defined emission peak, which enables excitation of multicolor QDs simultaneously with single light source. In case of multiple ion sensing, cross-talk among different dyes is a major issue, like sodium and potassium sensitive fluorophores

SBFI and PBFI shows huge cross-talk with different ion concentrations. However, due to presence of additional barcode with QD, it was possible to quantify response of different dyes w.r.t respective ions. In such a configuration, the sensor and reference fluorophores conjugated to dextran molecules are loaded within the inner cavity, whereas the QDs tags are embedded in the outer shell. The empty cavities beyond inside core serve as spacers which physically and optically separate the fluorescence signals of the inner fluorophores from the fluorescence signal of the QDs. This region avoids overlay of fluorescence signals and therefore the cross-talk between them.

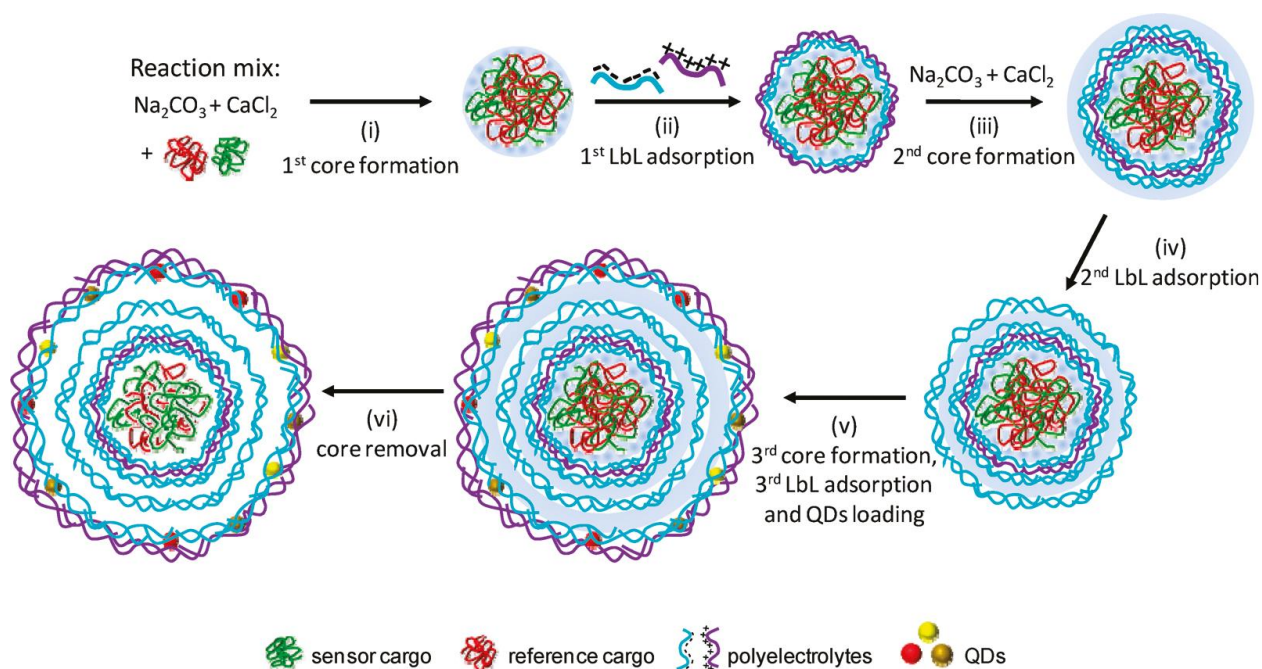


Figure 5. Synthetic Scheme of LbL assembly of a multilayer polyelectrolyte double-wall sensor capsule loaded with sensor and reference fluorophore. The resulting core-shell particles, formed after 2nd step, are subjected to a second co-precipitation leading to the formation of a second CaCO_3 compartment. At step (v) a third CaCO_3 compartment was formed that accompanied by LbL absorption of a multilayer polyelectrolyte and one layer of QDs. Finally, CaCO_3 compartments are removed by dissolution with EDTA in order to obtain multilayer capsules with double cavities and double shells. Adapted with permission from Parak *et al.*[44]

1.3 Alginate: A potential biodegradable polymer for pharmaceutical applications

1.3.1 Overview of alginate

Alginate is a naturally occurring anionic polysaccharide composed of (1-4)- β -D-mannuronic acid (M) and α -L-guluronic acid (G) in various sequence. It is a block copolymers containing blocks of consecutive G residues (GGGG), consecutive M residues (MMMM) or alternating M/G residues (GMGMGM). The physicochemical properties of alginate are highly dependent on their Mw and M/G ratio which is further dependent on their source. Typically most commercially available alginates are extracted by chemical process from brown seaweeds for e.g. *Laminaria hyperborean*, *Laminaria digitata* etc. [45] However, alginate with more defined chemical structure and physical properties can be also produced from bacterial biosynthesis including two bacterial genera, *Azotobacter vineladii* and *Pseudomonas spp.* Recent development in bacterial alginate production may enable more tailor-made synthesis of alginate. Unlike alginate extracted from seaweeds, having no acetylation, bacterial alginate show high degree of actylation and slightly higher M/G ratio. High acetyl group correspond to higher viscosity and flexibility of alginate, whereas gelling property is governed by the presence of G subunits in alginate. All these tunable characteristic of alginate allowed it's applications as biomaterials in many different biomedical applications.[46]

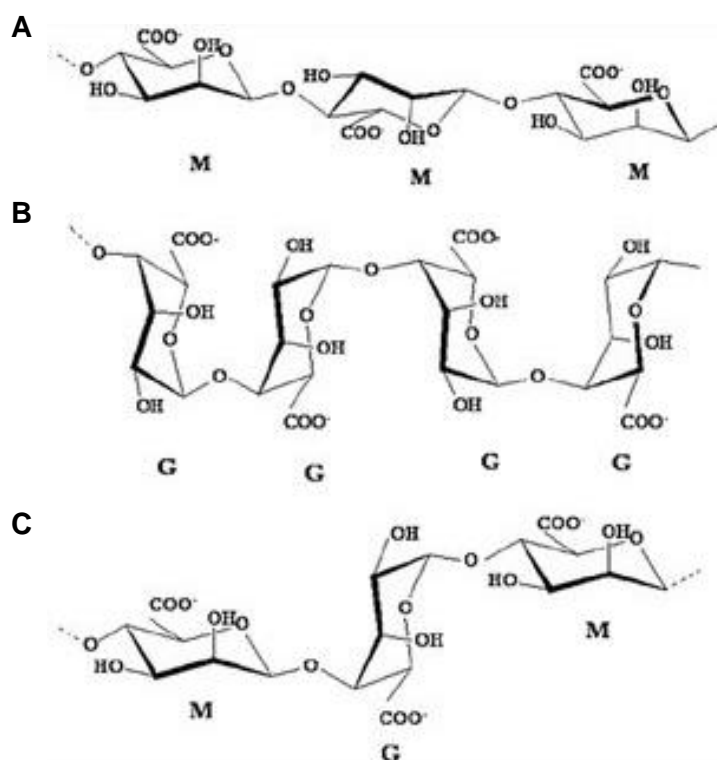


Figure 6. Components of alginates: (A) M–M, (B) G–G, and (C) M–G blocks. Block structure homopolymeric M- and G-, and MG- block heteropolymeric, constitute the molecule of alginate. Adapted with permission from *Chan et. al.*[46]

1.3.2 Advantages and applications of alginate-based vehicle

Alginate has received tremendous attention in microencapsulation and biomedical applications due to its high biocompatibility and unique physicochemical properties.[47] Aqueous solutions of alginate can easily form gels in presence of divalent cationic cross-linkers.[46, 48] The most commonly used agent for ionic cross-linking is calcium chloride (CaCl_2). The Ca^{+2} ions can form high coordination with G block of alginate, which is explained by 'egg-box model'. That G block of one polymer then form junction with other G block of another polymer, resulting in a gel structure. Therefore, different macromolecules or drugs can be loaded into such ionically cross-linked alginate networks. [47, 49, 50] For instance, a multifunctional hollow alginate capsule synthesis using CaCO_3 as a templet recently reported. On top of the alginate network, silver NP was grown that showed great potential for drug delivery as well as SERS detection.[49] Furthermore, alginate gels have interesting swelling properties dependent on the pH of the environment, which has been extensively explored to prepare drug delivery systems enabling controlled release.[51]

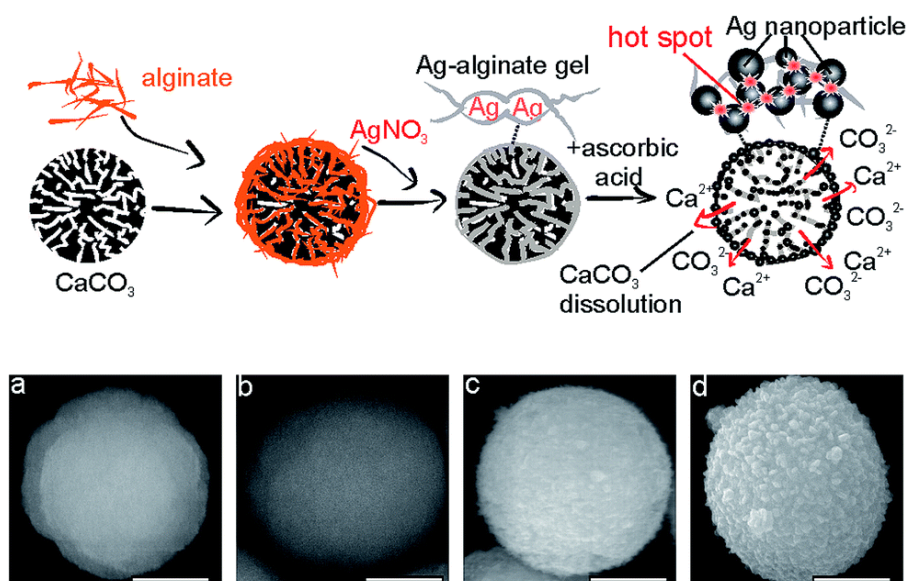


Figure 7. Synthesis scheme of hollow silver alginate hydrogel microspheres using CaCO_3 as a templet. The growth of the silver nanoparticles is accomplished using ascorbic acid that also eliminates calcium carbonate forming the hollow structure. SEM images corresponding to (a) calcium carbonate; (b) calcium carbonate covered with sodium alginate; (c) calcium carbonate covered with sodium alginate after the injection of silver nitrate; (d) silver alginate hydrogel microspheres. The scale bars correspond to 1 μm . Adapted with permission from *Parakhonskiy et. al.*[49]

1.4 Polyethyleneimine (PEI) for efficient Intracellular Delivery of therapeutic macromolecules

1.4.1 Physicochemical properties of PEI

PEI is a cationic polymer and it has two configurations, branched (BPEI) and linear (LPEI) structure. (fig 8) Acid-catalyzed polymerization of aziridine monomer produces BPEI and ring-opening polymerization of 2-ethyl-2-oxazoline followed by hydrolysis gives rise to LPEI.[52] Several BPEI and LPEI of different molecular weights are commercially available. All BPEIs are found as liquid under R.T whereas LPEI are available as solid at R.T. BPEI contains all primary, secondary and tertiary amine groups on contrary LPEI only have primary and secondary amine groups. All the primary, secondary and tertiary amine groups are present as 1:2:1 ratio into BPEI molecule. The pK_a value of these amine groups covers the physiological pH range and can act as a buffer. As the pH decreases from 7.4 to 5.0, the degree of protonation of these amine groups changes from 20% to 45%.[53]

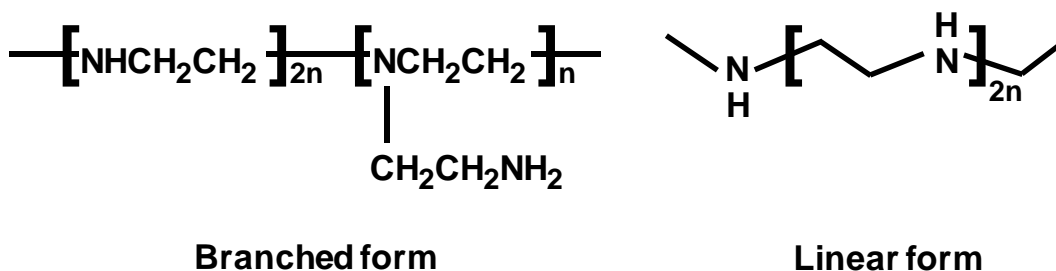


Figure 8. Chemical structure of branched and linear PEI.

1.4.2 Advantages of PEI in Therapeutics

PEI is one of the most effective and commonly used nonviral vectors for gene transfection.[54] Gene transfection is a process of transferring externally modified nucleic acids into specific cells of patients. It is a very effective and promising approach for treating genetically related diseases. Successful gene therapy is dependent upon safe, efficient and controlled delivery of nucleic acids/ plasmid molecules into cell. Viral vectors, such as adenovirus, retrovirus are highly efficient for that purpose but it also causes severe side effects. In contrary to viral vectors, non-viral vectors are safer and economically advantageous [55, 56]. Different cationic polymers like PEI is found to be more efficient transfecting agent, although their toxicity effect is also a matter of concern.[57] However, ketalized linear polyethylenimine (KL-PEI) was found efficient for intracellular target-specific and biocompatible siRNA delivery. The siRNA/KL-PEI polyplexes is acid-degradable. This modification of PEI resulted in much higher RNA interference efficiency than unmodified L-PEI via selective cytoplasmic localization of the polyplexes and efficient disassembly of siRNA from the polyplexes, which were promoted upon acid-hydrolysis of amino ketal linkages.[58]. In another study it was shown, modification of amine moiety in PEI by acetylation or succinylation reduces it's toxicity resulting in efficient SiRNA carrier.[52] Not only gene therapy, potentiality of PEI is also explored to modify and stabilize NP surface as well as for stimuli responsive drug delivery. For instance, Lee et al. reported a cysteamine modified gold nanoparticles (AuCM)/siRNA/polyethyleneimine, (PEI)/hyaluronic acid (HA) complex, developed through a layer-by-layer method for target-specific intracellular delivery of siRNA by HA receptor mediated endocytosis. [59] Moreover, this system was found highly efficient as a target-specific siRNA therapeutics for the treatment of various liver diseases.

1.4.3 Endosomal escape: 'Proton-sponge hypothesis'

The gene-delivery through non-viral vectors or in case of designing nano-drug delivery system one of the major challenge is to successfully release therapeutic to the cytosol.[60] As mentioned before these kind of delivery vehicle need to pass through different intracellular vesicles like endosome and lysosome. Lysosome is the acidic compartments of cell containing different enzymes. Long-term entrapment into these vesicles will destroy the activity of therapeutic. Therefore, different cationic polymers like

PEI are used for gene transfection as well as NP surface modification.[61] First tested cationic polymer for gene transfection was polylysine (PLL), although it could only transfect cell in presence of chloroquine which can initiate endosome disruption. In 1995 Boussif et al. tested efficiency of PEI as a transfecting agent. It was found that these kind of cationic polymers, specially containing multiple amine groups, have high buffering capacity and can cause efficient transfection without adding any membrane disruptive agents. This mechanism is theoretically explained by well-accepted 'Proton-sponge hypothesis.'[62] In 1997, Behr and colleagues summarized the concept of the proton sponge hypothesis as follows: "The accumulation of protons brought in by the endosomal ATPase is coupled to an influx of chloride anions. In the presence of PEI there will be a large increase in the ionic concentration within the endosome resulting in osmotic swelling of the endosome.[60] Moreover, PEI protonation will also expand its polymeric network by internal charge repulsion. Therefore, due to the two phenomena occurring simultaneously, it is expected that endosomal life expectancy is sorely reduced. Considering the protonation profile of PEI we can expect that about a third of the N-atoms in the molecule participate in the swelling action, making the molecule a virtual proton sponge." A schematic representation of the proton sponge hypothesis is depicted in Figure 9.[63] The 'Proton-sponge hypothesis' states due to presence of nonprotonated amine groups at physiological pH, these polymers can act as a buffer inside endocytic vesicles. The buffering capacity will allow entry of more numbers of protons through V-ATPase proton-pump along with an influx of chloride ions in it. This will inhibit lysosomal nuclease activity, which have an acidic optimal pH. Finally, this will cause disruption of the lysosome and release the therapeutic to cytosol. Altogether, this hypothesis well explains the possible mechanism behind high transfection efficiency of PEI.[64] However, this hypothesis is not supported with any experimental proof. Infact a lot of contradictory research finding regarding this topic, has been reported over the year. This part has been elaborated in the section 2 (objective).

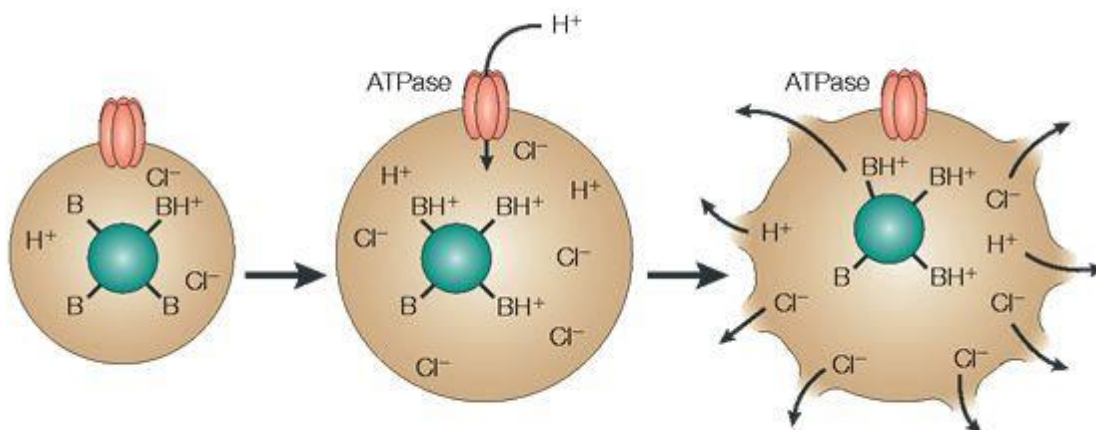


Figure 9. Protonation of the proton-sponge polymer like PEI (green) causes increased influx of protons (and counter-ions) into endocytic vesicles. Increasing osmotic pressure causes the vesicle to swell and rupture. Adopted with permission from *Stayton et. al.*[63]

2. Objective

The capsules made out of different biodegradable or nonbiodegradable polymers by the Layer-by-Layer (LbL) technique poses huge potential for effective encapsulation and in vitro delivery of therapeutics.[28, 65-67] Also encapsulation of different ion sensitive fluorophores allows sensing of ion alteration during different intracellular processes. The objective of my research was to develop new biocompatible delivery vehicles aimed for drug delivery and establish a high throughput intracellular pH-sensing protocol with pH sensor capsules.

Monodisperse spherical CaCO_3 particles of 4-12 μm size are easily synthesized by mixing different equivalent ratios of calcium chloride and sodium carbonate solutions.[68] The capsules prepared from these micron size particles have been tested towards in vivo delivery of drugs[69] and vaccines[70]. However, for drug delivery applications a smaller overall size is preferable and also use of biocompatible polyelectrolytes for the capsule assembly is advantageous. In one of my research work, a new biocompatible polymer capsule system was developed for active transport and controlled release of drug into cell by enzymatic degradation. One interesting pharmaceutical agent curcumin was used as model drug. It is a naturally occurring

polyphenolic compound having huge clinical advantages. Despite its possible therapeutic effects, the poor solubility of curcumin limits its clinical applicability. For this reason, different approaches have been utilized to enhance the solubility of curcumin, including solid dispersion techniques[71], nanoparticle encapsulation[72] and others, which enables the use of curcumin for treatment of several diseases. For instance, Priya et al. encapsulated curcumin into carboxymethyl cellulose and casein nanogels and studied its potent anticancer effect in a melanoma skin cancer cell model.[73] Herein a solid dispersion of curcumin was prepared by making complex with PVP in order to increase its aqueous solubility. The encapsulation of it into capsules also enhances bioavailability of the drug. A fully biocompatible synthetic route was explored for preparing polyelectrolyte capsules with diameters below 1 μm made of the biocompatible polyelectrolytes alginate (ALGI) and poly-L-arginine (PARG) based on LbL assembly. These capsules were further modified with a pH-sensitive outer layer of Eudragit L 100 (EuL). Capsule stability, capsule degradation, and drug release from capsules were studied as a function of pH.

Another important application of capsule is to sense intracellular ion change associated to different diseased conditions. Capsule as sensor possess many advantages compare to free ion sensitive dye, such as reduced toxic effect of dye, protecting dye from leakage and increasing noise to signal ratio enabling more sensitive quantification.[42, 74] Here we have established a new high throughput quantitative analysis protocol, for sensing intracellular pH alteration in response to different physicochemical changes, by Flow Cytometry. Ions play a very important role in different intracellular process. Understanding the fundamentals of these processes can help us to better design different therapeutic agents for e.g. Cationic polymers for non-viral transfection. One of my major research objective was focused on validating 'Proton Sponge Hypothesis' a well-accepted theory, supporting high transfection efficiency of polyethylene imines (PEI). As mentioned in sec 1.4.3, PEI facilitates endosomal escape process during transfection. The proton sponge hypothesis theoretically explains the mechanism of this process. Although the claim of this hypothesis regarding lysosomal pH change need experimental validation.[75] For instance, Wilson et al. prepared a Triple-fluorophore-labeled nucleic acid pH nanosensor to monitor post-transfection intracellular pH around

the delivered DNA using PEI and PLL (poly-L-lysine) separately.[61] This study showed highly cationic polymer such as PEI can avoid acidification of lysosome during post-transfection periods. Whereas Andresen et al. carried out quantitative measurements of lysosomal pH as a function of PEI content using Triple-fluorophore labeled polyacrylamide matrix based nanosensors and correlate the results to the “proton sponge” hypothesis. According to his study, PEI did not influence lysosomal pH.[76] Therefore, these contradictory results accelerate the urgent need for detailed investigation of this hypothesis.

3. Materials

3.1 Materials used for synthesis and application of alginate capsule

Calcium chloride dihydrate ($\text{CaCl}_2 \cdot 2\text{H}_2\text{O}$, Sigma), sodium carbonate (Na_2CO_3 , Merck, Germany), sodium poly-(styrene sulfonate) (PSS, molecular weight $M_w = 70$ kDa, Sigma), poly-L-arginine hydrochloride (PARG, $M_w = 15,000$ -70,000 kDa, Sigma), alginic acid sodium salt (ALGI, Sigma), eudragit L 100 (EuL, Evonik), ethylenediaminetetraacetic acid disodium salt (EDTA, Sigma), phosphate-buffered saline (PBS, Biochrom AG), curcumin (cur, Sigma), polyvinyl pyrrolidone (PVP, $M_w = 55$ kDa, Sigma), polyethylene glycol (PEG, $M_w = 50$ kDa), and sodium dodecyl sulfate (Sigma) were used as received.

3.2 Materials used for pH-sensor capsule synthesis and intracellular pH measurement

Poly(sodium 4-styrenesulfonate) (PSS, M_w 70 kDa, #243051), poly(allylamine hydrochloride) (PAH, M_w 56 kDa, #283223), calcium chloride dehydrate (CaCl_2 , #223506), sodium carbonate (Na_2CO_3 , #S7795), ethylenediaminetetraacetic acid disodium salt dihydrate (EDTA disodium salt, #E5134), 4-(2-hydroxyethyl)-1-piperazineethanesulfonic acid (HEPES; #H3375), Linear Poly(ethyleneimine) (LPEI, M_w 250kDa, #24314), Branched Poly(ethyleneimine) (BPEI, 25kDa, #408727), Linear Poly(ethyleneimine) (LPEI, M_w 20kDa, #764965), Poly-L-arginine hydrochloride (M_w 15-70kDa, #P7762), Rhodamine-B isothiocyanate (M_w 536.08 Da, #283924), monensin sodium hydrate (#46468), nigericin sodium salt (#N7143), were purchased from Sigma-

Aldrich (Germany). Branched Poly(ethyleneimine) (BPEI, Acros organics, Mw 60kDa, # 9002-98-6), Branched Poly(ethyleneimine) (BPEI, Acros organics, Mw 2kDa, # 408700), DY-647-NHS ester (Dyomics, Mw 761.85, # 647-01), Sodium chloride (Roth, NaCl, #HN00.2). SNARF-1-dextran (Mw 170 kDa, #D3304), Cascade blue dextran (Mw 10kDa, #D1976) from Life Technologies (Germany) and ultrapure double distilled water (ddH₂O) with a resistivity greater than 18.2 M cm was used for all experiments.

3.3 Materials used for cell culture

Human cervical adenocarcinoma cells (HeLa) were obtained from American Type Culture Collection (ATCC) (Manassas, USA). Cells were cultured in Dulbecco's Modified Eagle's medium Minimum (DMEM Fisher Scientific) supplemented with 10% fetal bovine serum (FBS, Biochrom, Germany), and 1% penicillin/streptomycin (P/S, Fisher Scientific, Germany). The cells were kept at 37 °C in a humidified atmosphere of 5% CO₂ in air. When cells reached 90% of confluence, cells were washed once with PBS and detached with 0.05 % trypsin ethylenediaminetetraacetic acid (EDTA) solution (Fisher Scientific, Germany). Cells were then seeded in flasks for cell passaging or seeded in plates for performing the *in vitro* experiments.

4. Experimental section

4.1¹ Synthesis and Characterization of biodegradable alginate capsules.

4.1.1 Synthesis of initial calcium carbonate cores

Calcium carbonate cores (PSS-CaCO₃) [65] were prepared by mixing 0.615 mL of 0.33 M aqueous solution of calcium chloride (CaCl₂) and 0.75 mL of 25 mg/mL polystyrene sulfonate (PSS) solution under magnetic stirring (1000 rpm, stirrer "Magnetprüher IKA-

¹ Parts of this work have been published in "Biodegradable alginate polyelectrolyte capsules as plausible biocompatible delivery carriers." **S. Roy**, N. Elbaz, W. J. Parak and N. Feliu (2019), ACS Applied Bio Materials. (Just accepted, DOI: 10.1021/acsabm.9b00203). Part of the capsule synthesis and characterization was performed by Nancy Elbaz.

RO 5 power") at room temperature (RT) for 5 min. Next, 0.615 mL of 0.33 M aqueous solution of sodium carbonate (Na_2CO_3) was added to the mixture under vigorous stirring (1000 rpm, "Magnetrührer IKA-RO 5 power") and stirred for 60 s at RT. Then the solution was transferred into an Eppendorf tube of 2 mL. PSS- CaCO_3 particles of 800 – 1000 nm size were formed. The solution was centrifuged at 1400 rcf for 2 min to separate the precipitate. The precipitated PSS- CaCO_3 particles were then washed three times with 1 mL Millie-Q water to remove unreacted salts and were then re-suspended in 1 mL of Millie-Q water. The PSS- CaCO_3 cores were used to synthesize the capsules by the layer by layer (LbL) approach [77] as described in the following.

4.1.2 Synthesis of biodegradable alginate capsules

Biodegradable polyelectrolyte capsules prepared by LbL assembly of oppositely charged polyelectrolytes around small PSS- CaCO_3 cores. Two different types of capsules were prepared, i.e. (PARG/ALGI)₂ and (PARG/ALGI)₂(PARG/EuL). A general sketch of the synthesis route is depicted in Figure1. Capsules were prepared using a modified synthesis from literature[43],[78]. Briefly, 0.5 mL of poly-L-arginine solution (8 mg/mL) dissolved in 0.05 M NaCl (pH 6) was mixed with the as-synthesized PSS- CaCO_3 cores in a 2 mL Eppendorf tube and sonicated for 5 min, followed by shaking for 20 min at RT. Then, the excess polyelectrolyte solution was removed by centrifugation at 1400 rcf for 2 min at RT. Capsules were washed three times with 1 mL Millie-Q water and by centrifugation, similar to the washing procedure as described before for the PSS- CaCO_3 particles. Afterwards, 0.5 mL of alginate solution (8 mg/mL) dissolved in 0.05 M NaCl (pH 6) was added [79] and a similar washing process was followed as described before. These synthesis steps of adding alternately charged polyelectrolyte layers were repeated until forming 2-bilayered (PARG/ALGI)₂ capsules. Next, hollow microcapsules were obtained by dissolving the CaCO_3 cores in 0.2 M aqueous EDTA buffer (pH 7.4) overnight at 4 °C. Finally, the sample was centrifuged at 175 rcf for 40 min and washed twice with 1 mL of Millie-Q water as described before. The capsules were then re-dispersed in 1 mL of Millie-Q water and kept at 4 °C until further use. (PARG/ALGI)₂ PARG capsules were prepared as described above, with an additional layer of PARG added. Then 0.5 mL of Eudragit-100 (8 mg/mL) dissolved in 0.05 M NaCl

(pH 7) was added to the (PARG/ALGI)₂PARG capsules in an Eppendorf tube, followed by 5 min sonication and 20 min shaking at RT. The excess of polyelectrolyte was separated by performing three washing steps as described before. Finally, the CaCO₃ core was removed by incubation with EDTA buffer (pH 7.4) overnight at 4 °C. The sample was finally centrifuged at 175 rcf for 40 min and washed twice with 1 mL of Millie-Q water. Then the capsules were re-dispersed in 1 mL of Millie-Q water and kept at 4 °C until further use.

4.1.3 Structural characterization

The fluorescence of the capsules was measured with a Horiba FluoroLog fluorimeter upon excitation at $\lambda_{\text{ex}} = 420 \text{ nm}$ and 488 nm (*cf.* Figure 2(A)-(B)). The geometry of the different capsules was analyzed with transmission electron microscopy (TEM, *cf.* Figure 2(C)-(F)) and CLSM (*cf.* Figure 2(G)-(H)). TEM images of the curcumin-loaded capsules were taken by using a field emission gun JEM 2100F UHR (JEOL, Japan) TEM equipped with a high angle annular dark field (HAADF) detector. The TEM was operated at an accelerating voltage of 200 kV along the full study. Fluorescence images of curcumin-loaded capsules were taken with a LSM 510 META confocal microscope from Zeiss, equipped with lasers allowing excitation at 405, 488, 543, and 633 nm. Capsules were excited with the 488 nm laser and a band pass (BP) filter of 500 - 580 nm was used to collect the emission at $540 \pm 20 \text{ nm}$. The hydrodynamic diameters d_h of the spherical capsules was measured by dynamic light scattering (DLS) and the zeta-potential (ζ) with laser Doppler anemometry, as carried out in a Malvern ZetasizerNano particle analyzer ZEN 3600 instrument (*cf.* Figure 2(I)-(N)). The results summarized in Table 1.

4.1.4 Determination of capsule concentrations

Capsule concentrations were determined as average number n_{capsules} of capsule/mL from three independent dilution series by counting. The dilutions were prepared from the stocks solution. For the counting, 10 μL of curcumin-loaded capsule solution was evaluated by using a Hemocytometer (counting chamber (Neubauer-improved 0.1 mm),

Marienfeld) under the confocal microscope, using 488 nm laser excitation and a BP filter 500-580 nm, and the capsules were counted. Results shown in Figure 10.

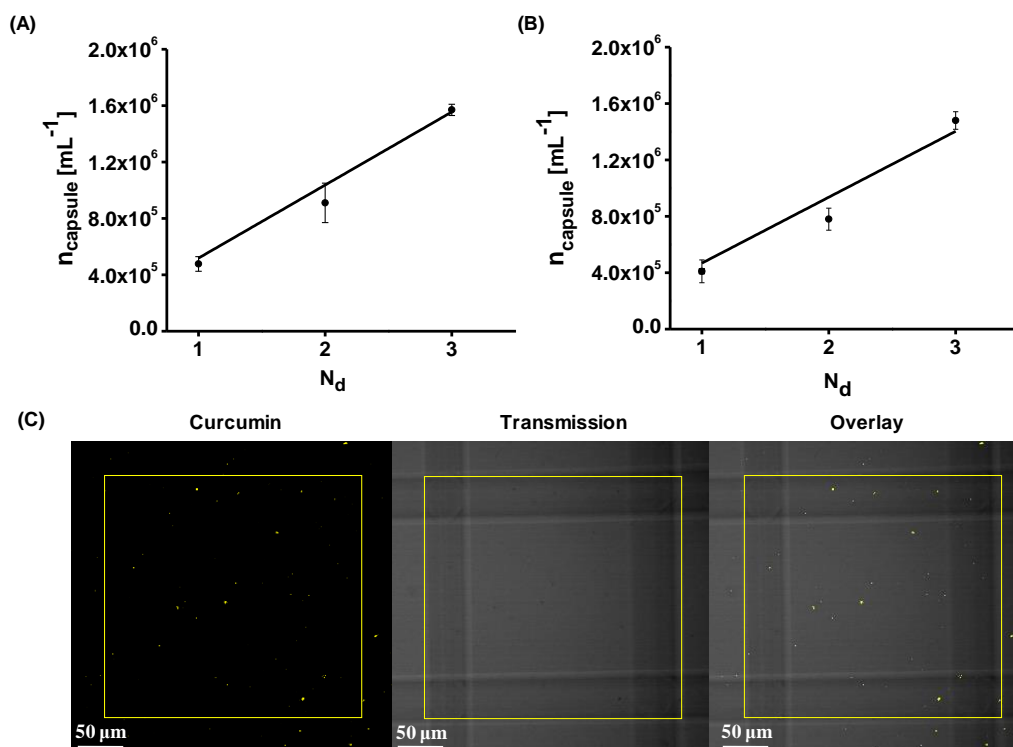


Figure 10. Determination of capsule concentrations. Results from the counting of capsules from three different dilutions of (A) (PARG/ALGI)₂(PARG/EuL) and (B) (PARG/ALGI)₂ capsules, as quantify by confocal microscopy (CLSM). N_d ($= 1,2,3$) in the x-axis corresponds to 100, 200, and 400 times dilution of the original stock solution from each capsule ($n= 4$). $n_{\text{capsules}} [\text{mL}^{-1}]$ provides the number of capsules per mL of solution. (C) Confocal image of curcumin-loaded (PARG/ALGI)₂ capsules inside the counting chamber, in which 10 μL of diluted capsule solution is analyzed.

4.1.5 Size distribution of capsules

The size distribution of two different capsules (PARG/ALGI)₂ and (PARG/ALGI)₂(PARG/EuL) were measured by analysing different TEM images of curcumin loaded capsules by image j software. Figure SI-10, shows size distribution of (PARG/ALGI)₂ and (PARG/ALGI)₂(PARG/EuL) capsules.

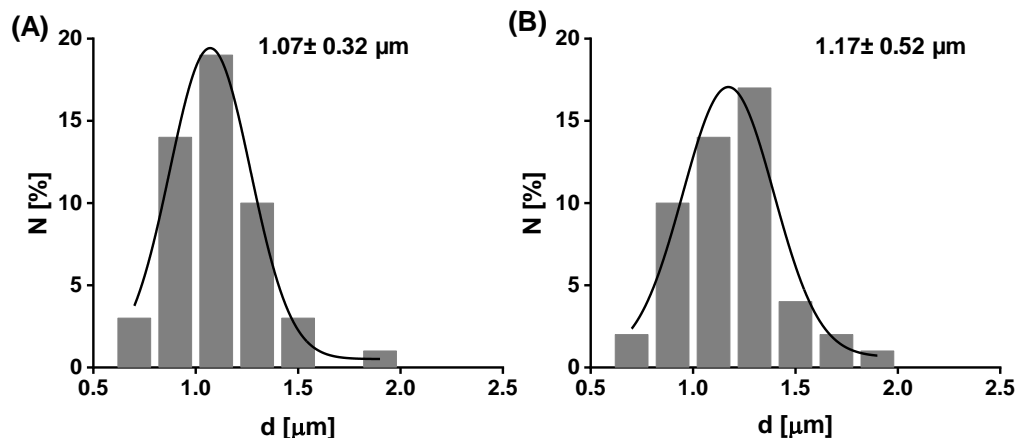


Figure 11. The diameter of two different capsules **(A)** (PARG/ALGI)₂ and **(B)** (PARG/ALGI)₂(PARG/EuL) obtained from TEM images. The data corresponds to (mean ± standard deviation (SD)) from almost 50 capsule images.

4.2 Drug loading and encapsulation efficiency of capsules

The goal of the here described investigation was to enhance the aqueous solubility of curcumin and thus to enhance its bioavailability. Solid dispersion formulations of curcumin were prepared using different surfactants such as polyethylene glycol (PEG), sodium dodecyl sulfate (SDS), and polyvinyl pyrrolidone (PVP). Solid dispersion was conducted using two different methods, the melting method and the solvent evaporation method.[71] Briefly, the melting method includes melting 50 mg of PEG followed by mixing with 50 mg of curcumin at 60 °C and then drying in air. The solvent evaporation method was carried out by dissolving 50 mg of SDS or PVP in 20 mL ethanol in a beaker. 50 mg of curcumin was added and the solution was stirred overnight. Afterwards, the co-precipitates were air-dried for 24 h. Solubility measurements were performed according to the method reported by Higuchi and Connors[80] add reference]. The solubility of curcumin was measured spectrophotometrically at 430 nm using an UV–Vis absorption spectrophotometer and at 540 nm with a fluorimeter. For the further experiments, the PVP curcumin solid dispersion was used as it showed better solubility in water.

Curcumin was loaded into the capsules by the co-precipitation method. Briefly, 0.5 mL ($C_{\text{cur}} = 1 \text{ mg/mL}$) of aqueous curcumin solution was mixed under stirring for 5 min (1000 rpm, stirrer "Magnetrührer IKA-RO 5 power") with 0.615 mL 0.33 M CaCl_2 and 0.75 mL 25 mg/mL PSS solution in a glass vial. After that, 0.615 mL 0.33 M sodium carbonate (Na_2CO_3) was added to the mixture under vigorous stirring (1000 rpm, Magnetrührer IKA-RO 5 power) for 60 s at RT. The particle precipitate was washed 2 times with Millie-Q water. Next, $(\text{PARG/ALGI})_2$ and $(\text{PARG/ALGI})_2(\text{PARG/EuL})$ capsules were prepared as described in section 4.1. The encapsulation efficiency (η_{EE}) and loading capacity (η_{LC}) of curcumin loaded capsules were evaluated by both, indirect and direct methods, as described below.

As indirect method, after co-precipitation the UV-Vis absorption spectra (A_{420}) of non-absorbed curcumin (i.e. curcumin which had not been integrated in the PSS- CaCO_3 cores) found in the supernatants was measured. From this absorption @420 nm the concentration of non-encapsulated curcumin $c_{\text{cur}}(\text{non-bound})$, which remained free in solution was determined. The concentration of curcumin (C_{cur}) was estimated hereby from calibration curve $A_{420}(C_{\text{cur}})$ of curcumin in Millie-Q water (*cf.* Figure 12B). Based on that, the curcumin loading was determined by subtracting the non-absorbed curcumin concentration $c_{\text{cur}}(\text{non-bound})$ from the initial curcumin concentration $c_{\text{cur}}(\text{added})$: $c_{\text{cur}}(\text{bound}) = c_{\text{cur}}(\text{added}) - c_{\text{cur}}(\text{non-bound})$. Note, C_{cur} [mole/L] is the molar concentration, whereas C_{cur} [g/L] is the mass concentration of curcumin. $C_{\text{cur}} = c_{\text{cur}} \cdot M_{\text{W}}(\text{cur})$ with the molar mass $M_{\text{W}}(\text{cur})$ of curcumin.

As direct method, 0.05 mL capsule solution incubated with 0.25 mL (2 mg/mL) pronase solution at 37 °C for 24 h. After 24 h incubation, an UV-Vis absorption spectrum of released curcumin from the capsules was measured and the curcumin concentration $c_{\text{cur}}(\text{bound})$ was determined from the calibration curve $A_{420}(C_{\text{cur}})$ of curcumin in 2 mg/mL pronase solution (*cf.* Figure 11C). η_{EE} and η_{LC} determined by the following equation. $n_{\text{capsules}} = N_{\text{capsules}}/V$ is the number of capsules N_{capsules} per volume V of solution.

$$\eta_{\text{EE}} [\%] = [(c_{\text{cur}}(\text{bound})/c_{\text{cur}}(\text{added})) \cdot 100\%$$

$$\eta_{LC} = C_{cur}(\text{bound})/n_{capsules}$$

Those results summarized in Table 4 in the section 5.1.2.

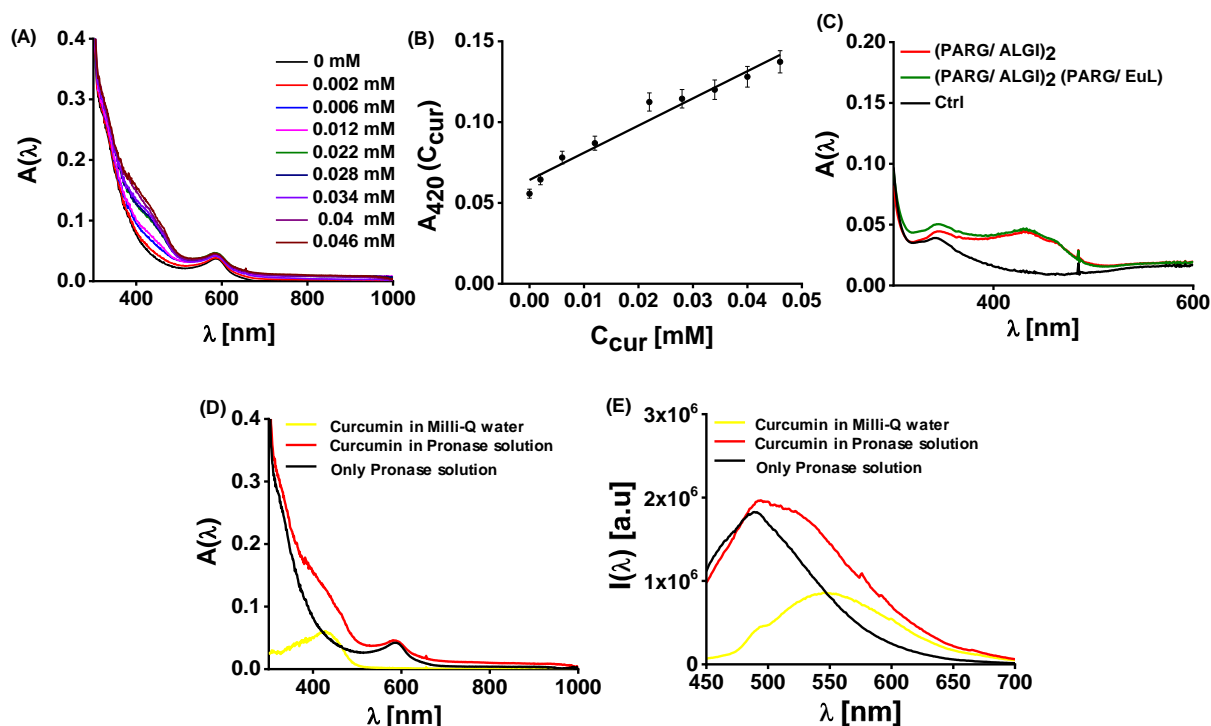


Figure 12. (A) UV-Vis absorption spectra $A(\lambda)$ of curcumin in presence of pronase. The absorption spectra were measured with increasing concentration of curcumin (C_{cur} from 0 - 0.046 mM) in 2 mg/mL pronase solution in PBS buffer pH 7. (B) Calibration curve of curcumin in the presence of pronase (the average of $n = 2$ experiments is shown). The absorption maximum A_{420} at $\lambda = 420$ nm is plotted versus the curcumin concentration. (C) UV-Vis absorption spectra $A(\lambda)$ of released curcumin from $(PARG/ALGI)_2$ and $(PARG/ALGI)_2(PARG/EuL)$ capsules after 24 h incubation with pronase at 37°C. Pronase only was used as control ("Ctrl"). (D) Effect of pronase on the UV-Vis absorption spectra and (E) the fluorescence spectra $I(\lambda)$ of curcumin after 24 h incubation at 37°C. Curcumin solution in Millie-Q water used as a control for the data shown in D and E.

4.3 In vitro release study of different capsules

A release study of curcumin from (PARG/ALGI)₂ and (PARG/ALGI)₂(PARG/EuL) capsules was performed by two different methods, either using dialysis tubes (Spectra/Pro, Folat-A-Lyzer G2, MWCO 100 kDa) or centrifuge filters (Amicon centrifuge filter, Ultracel- 100 kDa) for separating released curcumin from the capsules. (Figures 13 - 14) Dialysis tubes containing 1 mL solution of curcumin-loaded capsule solution ($C_{\text{cur}}(\text{added}) = 40 \mu\text{g/mL}$) were immersed in 6 mL buffer solutions of different pH (pH 3, 5, and 7). The dialysis performed at 37 °C under mild stirring conditions at 40 rcf. At different time intervals (1, 2, 4, 6, 24, and 48 h), 1 mL released media was withdrawn for analysis and it was replaced with the same volume of buffer to maintain conditions. The amount of released curcumin ($C_{\text{cur}}(\text{released})$) in the buffer solution was quantified by using a calibration curve of absorbance and fluorescence spectra of curcumin as prepared at 0 h, 24 h, and 48 h in different pH buffers.

The release study with centrifuge filters was performed by incubating capsules in 0.5 mL of buffers of different pH (pH 3, 5, and 7) at 37 °C for 24 h and 48 h. After 24 h incubation the supernatant of the capsule solution ($C_{\text{cur}} = 80 \mu\text{g/mL}$) was removed by centrifugation at 175 rcf for 40 min as flow through. The retained capsules re-dispersed in different pH buffers and incubated with fresh pH buffers for another 24 h at 37 °C. The supernatant again collected by centrifugation with a centrifuge filter (1400 rcf, 15 min) as flow through. The amount of released curcumin $C_{\text{cur}}(\text{released})$ found in the flow-through with the different pH buffers was quantified using the above described calibration curves. The amount of cumulative release η_{CR} of curcumin was calculated using the following equation:

$$\eta_{\text{CR}} [\%] = (C_{\text{cur}}(\text{released}) / C_{\text{cur}}(\text{added})) \cdot 100\%$$

Results are shown in Figure 29, and additional data are presented in Figure 15 and Table 1.

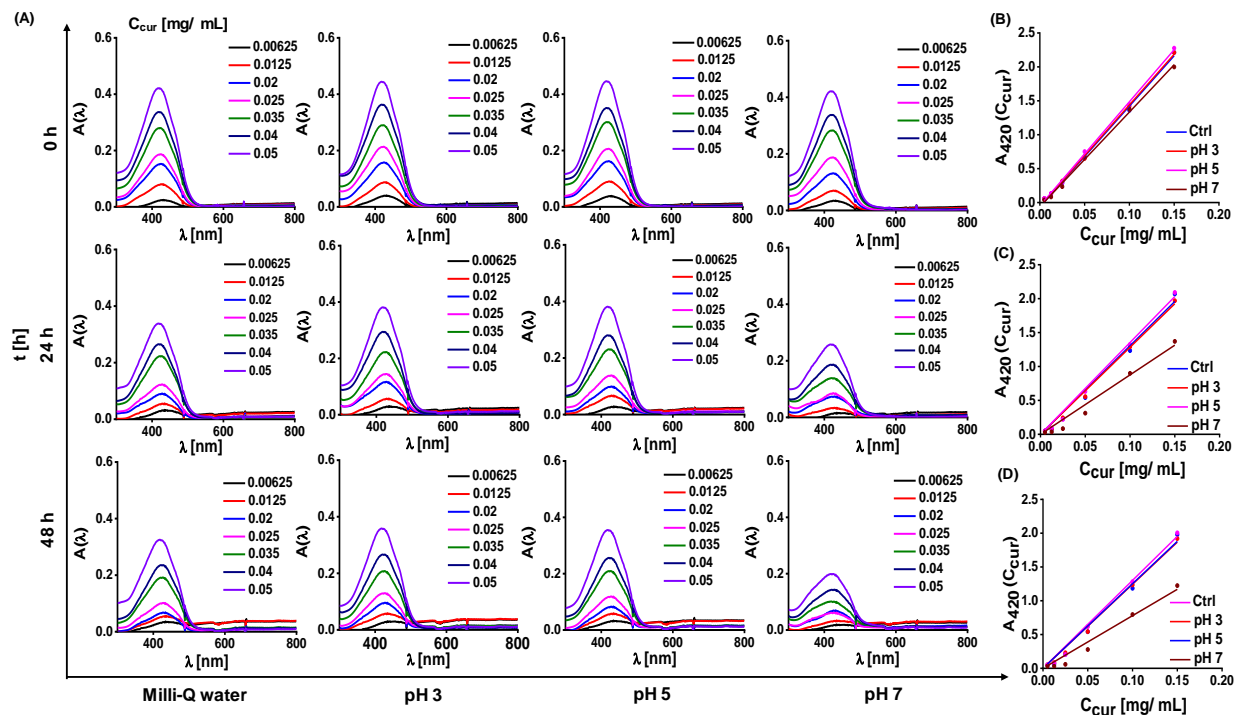


Figure 13. Curcumin characterization at different pH values. (A) Absorption spectra $A(\lambda)$ of a series of curcumin concentrations C_{cur} (from 0 - 0.05 mg/mL) in Millie-Q water, pH 3, 5, and 7 at $t = 0$ h, 24 h, and 48 h after immersion in buffer. (B-D) Calibration curves of curcumin in water (Ctrl), pH 3, 5 and 7 at 0 h, 24 h, and 48 h. The absorbance A_{max} at $\lambda = 420$ nm has been used for making the calibration curve $A_{420}(C_{cur})$.

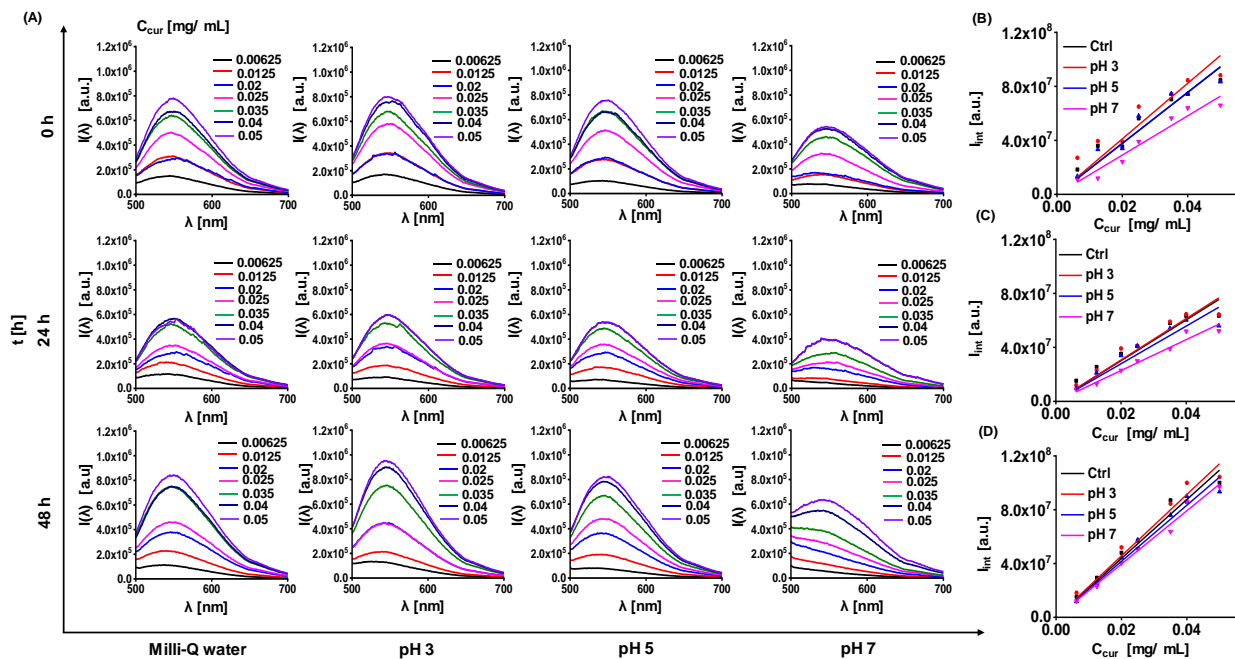


Figure 14. Curcumin characterization at different pH values. (A) Fluorescence spectra $I(\lambda)$ of a series of curcumin concentrations C_{cur} (from 0 - 0.05 mg/mL) in Millie-Q water, pH 3, 5, and 7 at $t = 0$ h, 24 h, and 48 h after immersion in buffer. (B-D) Calibration curves of curcumin in water (Ctrl), pH 3, 5, and 7 at 0 h, 24 h, and 48 h. The integrated area I_{int} under the $I(\lambda)$ curve has been used for making the calibration curve $I_{\text{int}}(C_{\text{cur}})$.

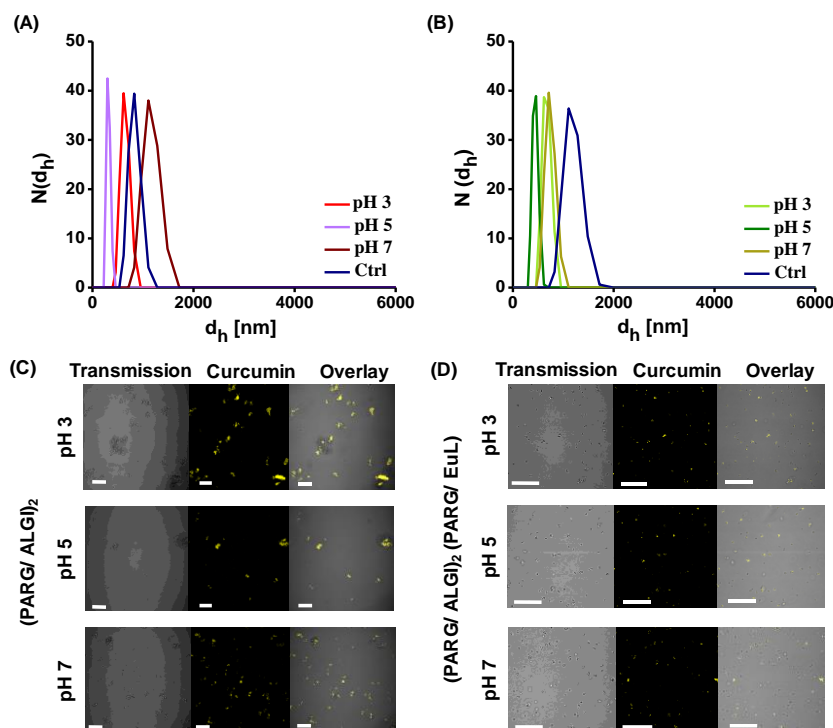


Figure 15. Colloidal and structural characterization of biodegradable capsules $((\text{PARG/ALGI})_2$ and $(\text{PARG/ALGI})_2(\text{PARG/EuL})$) after the release study carried out by dialysis. As control (Ctrl) the capsules before dialysis experiments ($t = 0$) were used. (A,B) Number distribution $N(d_h)$ of hydrodynamic diameters are determined by dynamic light scattering (DLS). Mean values are given in Table SI-1. (C,D) Confocal microscope images of (C) $(\text{PARG/ALGI})_2$ and (D) $(\text{PARG/ALGI})_2(\text{PARG/EuL})$ capsules at different pH (3, 5, 7) after dialysis ($t = 48$ h). Scale bar corresponds to 20 μm .

Capsule Type	Before Dialysis		After Dialysis					
	Millie-Q water		pH 3		pH 5		pH 7	
	dh [nm]	ζ [mV]	dh [nm]	ζ [mV]	dh [nm]	ζ [mV]	dh [nm]	ζ [mV]
(PARG/ALGI) ₂	840 ± 12.27	-26.4 ± 2.4	618 ± 12.4	-9.38 ± 1.34	350 ± 5.98	-1.22 ± 0.58	1150 ± 21.2	-0.059 ± 0.021
(PARG/ALGI) ₂ (PARG/EuL)	1100 ± 14.2	-39.2 ± 3.5	635 ± 8.2	-7.28 ± 0.87	450 ± 22.7	-1.26 ± 1.0	750 ± 15.3	-3.17 ± 1.93

Table 1. Hydrodynamic diameter d_h and zeta potential ζ of curcumin-loaded (PARG/LGI)₂ and (PARG/ALGI)₂(PARG/EuL) capsules at different pH (3, 5, 7) after dialysis (t = 48 h). Data are represented as (mean ± standard deviation (SD)) from n = 3 independent experiments.

4.4 Degradation study of capsules

An enzymatic degradation study of curcumin-loaded (PARG/ALGI)₂ and (PARG/ALGI)₂(PARG/EuL) capsules was carried out using pronase as example of a proteolytic enzyme. 15 µL of (PARG/ALGI)₂ capsules ($n_{\text{capsules}} = 2.4 \cdot 10^8$ capsules/mL) and (PARG/ALGI)₂(PARG/EuL) capsules ($n_{\text{capsules}} = 2 \cdot 10^8$ capsules/mL) were incubated with 75 µL of 2 mg/mL pronase (pH = 7) at 37 °C for 2, 4, 6, 24, 48, and 72 h. A series of similar sets at different time points was prepared for each capsule at pH = 7 in PBS. Variation in hydrodynamic diameter and zeta potential of capsules at each time point were measured with a Malvern ZetasizerNano particle analyzer ZEN 3600 instrument. CLSM images of capsules at each time point were also taken. Data are presented in Figure 30.

4.5 Uptake studies of alginate capsules by CLSM

Internalization of capsules was evaluated by confocal microscopy (CLSM). For that, 12,000 HeLa cells per well were seeded in ibidis 8-well plates (area per well: 1 cm², medium per well: 300 µL). Cells were incubated overnight. The next day, cells were exposed to curcumin-loaded (PARG/ALGI)₂ and (PARG/ALGI)₂(PARG/EuL) capsules at

concentration of $N_{\text{capsules/cell}} = 50$ capsules/cell in complete cell medium for 24 h. After the exposure time, cells were stained using two different approaches. First, the cell membrane was stained with Wheat Germ Agglutinin, Tetramethylrhodamine conjugate from ThermoFisher (WGA-TMRA). For that cell with internalized capsule were washed 3 times with 200 μL of Hank's Balanced Salt Solution (HBSS) and were then incubated with 70 μL of 25 $\mu\text{g/mL}$ WGA-TMRA solution in HBSS buffer at 37°C for 10 min. After the incubation cells were washed 3 times with 200 μL HBSS. Next, nucleus staining was performed with Hoechst 33342 solution by incubating with 70 μL of 5 mg/mL Hoechst solution in PBS at RT for 15 min. Finally, cells were washed one time with 200 μL PBS fresh complete medium was added. Second, lysosomes were stained. For that, cells were incubated with 75 nM LysoTracker red- DND 99 solution in complete media at 37°C for 120 min. Then, nucleus staining performed with Hoechst dye as described above.

Fluorescence micrographs of HeLa cells with the internalized capsules were recorded with a confocal microscope (Zeiss LSM 510 Meta Confocal Microscope). Images were taken with a Plan-Apochromat $63\times/1.40$ Oil DIC M27 objective, and the pin hole was set to 0.86–1.32 airy units. A laser diode emitting at 405 nm and a bandpass BP 420-480 emission filter were used to visualize the nucleus labelling with Hoechst. An argon laser with a line at 488 nm and a bandpass emission filter BP 505– 570 were used to visualize curcumin. A helium–neon laser for excitation at 543 nm and a BP 560–615 emission filter was used to visualize the WGA-TAMRA. A helium–neon laser for excitation at 543 nm together with a BP 560–615 emission filter were used for recording fluorescence of LysoTracker. All images were further processed with the image J software to reduce background noise and to enhance contrast for clear visualization of cellular images. All images processed with the same settings. Images are shown in Figures 33 and 16.

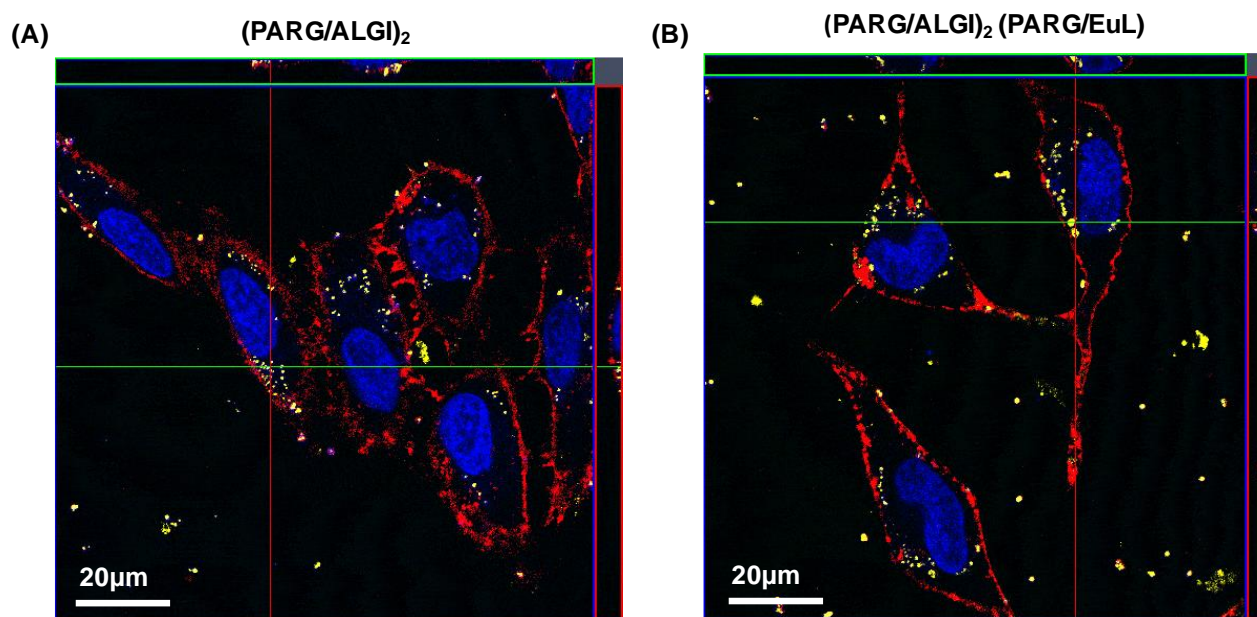


Figure 16. Confocal image of cells exposed to (A) (PARG/ALGI)₂ and (B) (PARG/ALGI)₂(PARG/EuL) capsules for 24 h. WGA-TAMRA, and Hoechst were used for cell membrane and nucleus staining, respectively. Images represent Z-scans parallel to the culture plate surface of cells exposed to capsules for 24 h at the concentration of 50 capsules/cell added. The scale bars correspond to 20 μm.

4.6² Synthesis and Characterization of different pH sensor capsules

Synthesis

Different capsules loaded with the pH indicator SNARF (here termed as pH sensitive, +/- capsules, PEI capsules, PEI-end capsules) were synthesized by Layer-by-Layer assembly of oppositely charged polyelectrolytes onto a SNARF loaded spherical calcium carbonate (CaCO₃) template. The carboxy-SNARF dye was covalently linked to 170 kDa amino-dextran molecules. CaCO₃ particles filled with SNARF-dextran produced via co-precipitation of SNARF-dextran with equivalent amount of calcium

² parts of this work are currently prepared for publication: **Sathi Roy**, Dingcheng Zhu, Wolfgang J. Parak, Neus Feliu, "In situ measurements of lysosomal proton-buffering by pH-sensitive fluorescent polymer microcapsules".

chloride (CaCl_2) and Sodium carbonate (Na_2CO_3). Briefly, 0.615 mL of 0.33 M CaCl_2 and 40 μL of 5 mg/ mL SNARF-dextran solution mixed. Next, 0.615 mL of 0.33 M Na_2CO_3 added under stirring (1000 rpm) condition and stirred for 30 s followed by another 2 mins standing time without stirring. SNARF loaded CaCO_3 particles washed 2 times with Millie-Q water to remove unbound SNARF. (+) Capsule, ($\text{CaCO}_3@(\text{PAH/PSS})_4\text{PAH}$) & (-) capsules ($\text{CaCO}_3@(\text{PAH/PSS})_4$) were prepared by adding alternate layers of negative polystyrene sulfonate, (PSS, 2 mg/ mL in 0.5 M NaCl, pH 6.5) and positive polyallylamine hydrochloride, (PAH, 2 mg/ mL in 0.5 M NaCl, pH 6.5) polymers onto the SNARF loaded micro particles until desired numbers of layers had been established. To make PEI capsule ($\text{CaCO}_3@(\text{PAH/PSS})(\text{PEI/DEX})_3\text{PARG}$), one bilayer of (PAH/PSS) were added and then 3 alternate (PEI/DEX) bilayers of BPEI 25 kDa (PEI, 4 mg/ mL in 0.05 M NaCl, pH 5.5) & dextran sulfate (DEX, 4 mg/ mL in 0.05 M NaCl, pH 5.5) were added. The final layer was prepared with poly-L-arginine (PARG, 2 mg/ mL in 0.5 N NaCl, pH 6.5) polymer to make stable monodisperse particles. PEI-end capsule ($\text{CaCO}_3@(\text{PAH/PSS})_3(\text{PEI/DEX})_3\text{PEI}$) were prepared in same way by adding 3 bilayers of nonbiodegradable (PAH/PSS) layers followed by one bilayer of (PEI/DEX) and the last layer was finished with another layer of PEI. Finally, the CaCO_3 template cores were chemically dissolved with ethylenediaminetetraacetic acid (EDTA, 1mL 0.1 N). The resulting different SNARF capsules were washed three times with ultrapure water to remove excess EDTA and stored at 4 °C. The size of the resulting capsules ranged between 3 to 5 μm .

Characterization

The fluorescence of 4 different pH sensitive capsules dispersed into Mili-Q water were measured with a Horiba FluoroLog fluorimeter upon excitation at $\lambda_{\text{ex}} = 561 \text{ nm}$.

The fluorescence images of SNARF-loaded capsules were taken with a LSM 510 META confocal microscope from Zeiss, equipped with lasers allowing excitation at 405, 488, 543, and 633 nm. Capsules were excited with the 543 nm laser and a band pass (BP) filter of 560 - 615 nm & 615 - 750 nm were used to collect the dual emissions of SNARF at 580 nm and 640 nm.

The zeta-potential (ζ) after addition of alternate polyelectrolyte layers around each capsule were measured with laser Doppler anemometry, as carried out in a Malvern ZetasizerNano particle analyzer ZEN 3600 instrument. Similarly, final charge of different capsules was also measured. Characterizations of all different pH sensor capsules are shown in figure 34 and zoomed in confocal images of capsules are presented in figure 17.

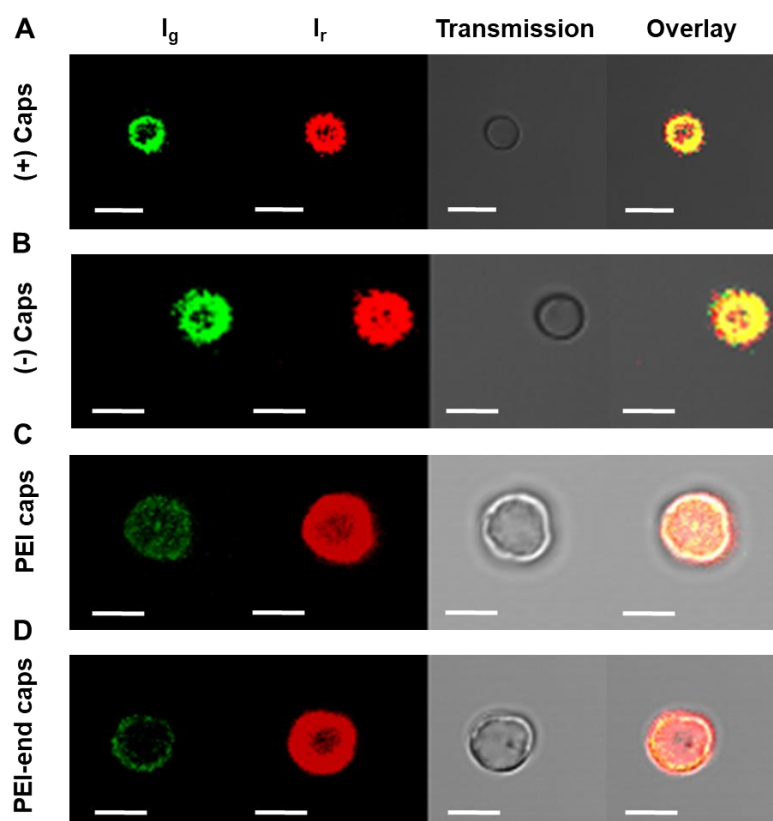


Figure 17: (A- D) Zoomed in Confocal images of 4 different SNARF loaded pH sensitive capsules, (PAH/PSS)4PAH capsule [(+) caps] (A), (PAH/PSS)4 capsule [(-) caps] (B), (PAH/PSS) (PEI/DEX)3 PARG capsule [PEI caps] (C) and (PAH/PSS)3(PEI/DEX) PEI capsule [PEI-end caps] (D), in water. Scale bar in each image corresponds to 5 μm .

4.7 Biocompatibility study

4.7.1 Cell culture

Human cervical adenocarcinoma cells (HeLa) were obtained from American Type Culture Collection (ATCC) (Manassas, USA). Cells were cultured in Dulbecco's Modified

Eagle's medium Minimum (DMEM Fisher Scientific) supplemented with 10% fetal bovine serum (FBS, Biochrom, Germany), and 1% penicillin/streptomycin (P/S, Fisher Scientific, Germany). The cells were kept at 37 °C in a humidified atmosphere of 5% CO₂ in air. When cells reached 90% of confluence, cells were washed once with PBS and detached with 0.05 % trypsin ethylenediaminetetraacetic acid (EDTA) solution (Fisher Scientific, Germany). Cells were then seeded in flasks for cell passaging or seeded in plates for performing the *in vitro* experiments.

4.7.2 Biocompatibility study of biodegradable capsules

Cell viability studies of HeLa cells exposed to two different types of curcumin-loaded biodegradable capsules were investigated by the resazurin assay as previously reported[81], [82]. For that, 7,500 HeLa cells were seeded into 96 well plates (area per well: 3.4 mm², medium per well: 100 µL) and were kept overnight at 37 °C, 5% CO₂. The next day, the HeLa cells were exposed to (PARG/ALGI)₂ and to (PARG/ALGI)₂(PARG/EuL) capsules at different concentrations N_{capsules/cell} (4 - 2000 capsules/cell) in serum-supplemented media for 24 h and 48 h. After incubation, HeLa cells were washed three times with PBS (100 µL). Then, 100 µL of 10% of resazurin solution (Sigma-Aldrich) in complete cell media was added to the cells and cells were incubated for 4 h at 37 °C, 5% CO₂. Then, the fluorescence intensity of the wells was measured with a microplate-reader equipped fluorimeter (Fluorolog-3, from Horiba JobinYvon, Germany). For that, the samples were excited at a wavelength of 560 nm and the emission was recorded in the range of 570 - 620 nm. The background-subtracted mean fluorescence intensity of each sample was normalized to the fluorescence of a reference sample to which no capsules had been added (control sample). The control sample was ascribed 100% cell viability (V), defined as their normalized fluorescence in respect to the control. The viability data are provided as mean value ± standard deviation (SD) from three independent experiments using HeLa cells at different passage numbers.

4.7.3 Biocompatibility study of different pH sensor capsules & test samples

Biocompatibility studies were carried out on the basis of the metabolic activity of living cells using a Resazurin based assay (Sigma-Aldrich, TOX-8). Resazurin (7-Hydroxy-3Hphenoxazin-3-one 10-oxide) acts as an oxidation-reduction indicator in cell viability assays. For that, 7,500 HeLa cells were seeded into 96 well plates (area per well: 3.4 mm², medium per well: 100 µL) and kept overnight at 37 °C, 5% CO₂. Next day, the HeLa cells were exposed to different test samples in serum-supplemented media for different time points at 4, 24, 48 h for different PEI & chloroquine (Cq) samples. Concentration range of all different test samples are presented in table 2.

PEI Samples	Range of Conc. used		15 caps/ cell + PEI conc. used	
	[µM]	[µg/ ml]	[nM]	[µg/ ml]
BPEI 2 kDa	[10800 - 5.27]	[21600 – 10.54]	[25× 10 ⁵ - 8000]	[500 - 16]
BPEI 25 kDa	[192 – 2.289×10 ⁻⁵]	[4800 – 5.72×10 ⁻⁴]	[200 - 12.5]	[5 - 0.312]
BPEI 60 kDa	[360 – 4.29× 10 ⁻⁵]	[21600 – 2.574× 10 ⁻³]	[176 – 11]	[10.56 – 0.66]
LPEI 250 kDa	[10.92 – 1.3× 10 ⁻⁶]	[2730 – 3.25× 10 ⁻⁴]	[86 - 5.37]	[21.5 – 1.34]
LPEI 20 kDa	[40- 7.8× 10 ⁻⁵]	[800 – 1.56× 10 ⁻⁶]	[300 – 9.4]	[6 – 0.188]
Chloroquine (Cq) 320 Da	[40 – 8.94× 10 ⁻⁶]	[12.8 – 2.8× 10 ⁻⁶]	--	--

Table 2: The ranges of concentration of the different test samples used for the viability assays are presented.

Another toxicity study was performed with (+) pH sensor capsule and different PEI samples together. Therefore 15 caps/ cell concentration was exposed to the cell together with dilution series of different PEI samples for 24 and 48 h in media containing serum. After incubation, HeLa cells were washed three times with PBS (100 µL). Then, 100 µL of 10% of resazurin solution (Sigma-Aldrich) in complete cell media was added

to the cells and incubated for 4 h at 37 °C, 5% CO₂. After that, the fluorescence intensity of the wells was measured with a microplate-reader equipped with fluorimeter (Fluorolog-3, from Horiba JobinYvon, Germany), excited at a wavelength of 560 nm and the emission was recorded in the range of 570 - 620 nm. The background-subtracted mean fluorescence intensity of each sample was normalized to the fluorescence of a reference sample. Reference sample was only cell where no samples had been added (control sample). The control sample was ascribed 100% cell viability V, defined as their normalized fluorescence in respect to the control. Cell viability of all test samples are depicted in figure 18.

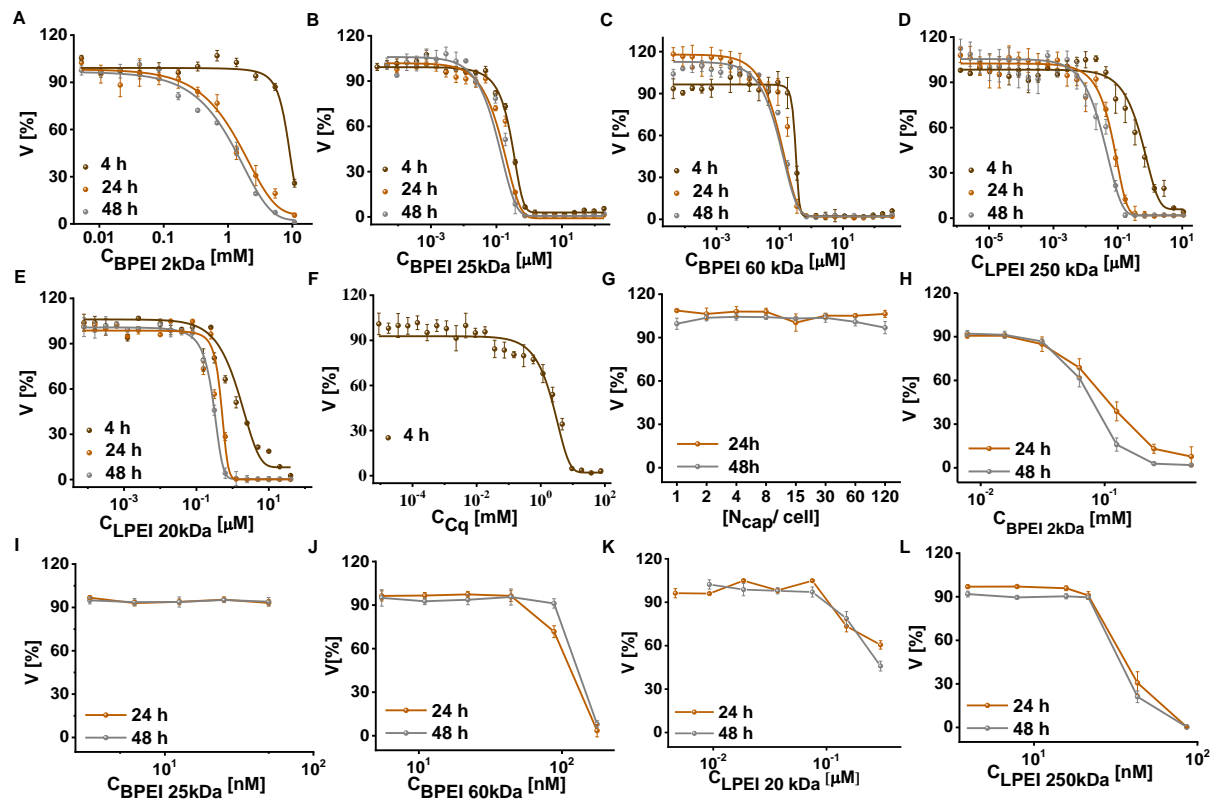


Figure 18. Biocompatibility studies of different PEI samples (A-E), chloroquine (F), pH sensitive (+) capsule (G) and different PEI samples with (+) capsule (H-L). 5 different PEI samples were used, BPEI 2 kDa, BPEI 25 kDa, BPEI 60 kDa, LPEI 20 kDa, LPEI 250 kDa. HeLa cells were exposed to various concentrations of PEI samples (A-E) for 4 h, 24 h and 48 h, chloroquine (Cq) samples (F) for 4h, (+) capsules for 24h and 48h (G), and different PEI samples with (+) capsule for 24 & 48 h (H-L) in serum-supplemented

media. (G-H) HeLa cells exposed to (+) capsule with a concentration of 15 capsule/ cell for 4 h in serum-supplemented media. After that media was replaced by various concentrations of PEI samples in fresh serum-supplemented media for 24 h and 48 h. Results are presented as percent of cell viability V [%] (mean value) from three independent experiments (A-L) and curves were fitted with a sigmoidal function (A-F).

The cell viability of capsules was also performed as described before by exposing a dilution series of different capsules (120 to 1 caps/ cell) for 24 & 48 h in serum supplemented media (See figure 3). The viability data are provided as mean value \pm standard deviation (SD) from three independent experiments using HeLa cells at different passage numbers.

4.8 pH calibration curve of different pH sensor capsules

4.8.1 pH calibration curve of only capsules

pH Calibration curve of 4 different pH sensitive capsules were prepared by using phosphate-citric acid buffer (pH range 3 - 8). Buffer solutions of different pH were prepared with 0.2 M dibasic sodium phosphate and 0.1 M citric acid. Sodium chloride, potassium chloride and magnesium sulfate salt concentration were maintained at 150, 4 and 1 mM respectively in each buffer solution.

Fluorescence of pH sensitive (+) capsules immersed into different buffers were measured by fluorimeter with different excitation wavelengths $\lambda_{\text{ex}} = 488, 514, 543 \text{ \& } 561$ nm. Intensity ratio (I_r/I_g) vs pH was plotted to make pH calibration curve of (+) capsules for different excitations. Maximum change in intensity ratio w.r.t pH was found for $\lambda_{\text{ex}} = 561$ nm and hence this wavelength has been used for characterizing different capsules by fluorimeter as well as Flow cytometry (See figure 19 A and B). pH calibration curve of (+) capsules were also prepared by taking fluorescence images of capsules in different buffers by CLSM (Zeiss LSM 510 Meta Confocal Microscope). A helium–neon laser for excitation at 543 nm together with a BP 560–615 nm (I_g) & 615-750 nm (I_r) emission filters were used for recording fluorescence emission of SNARF at two different wavelengths (580 & 640 nm). Finally, fluorescence intensities of different images were

calculated by image analysis with image J software and (I_r/I_g) vs pH was plotted to make calibration curve of (+) capsule by CLSM (See figure 19 C).

The pH dependent standard curve of 4 different capsules were prepared by fluorimeter upon excitation at $\lambda_{ex} = 561$ nm and flow cytometer (BD LSR Fortessa Biosciences, German) with $\lambda_{ex} = 561$ nm. Different capsules were immersed into different buffers for 10 min prior to the fluorescence measurement by different methods. Intensity ratio $(I_{640}/I_{580} = I_r/I_g)$ vs pH were plotted to make pH calibration curve of each capsules by fluorimeter. By flow cytometry fluorescence emission was collected at $I_r = 670 \pm 30$ nm and $I_g = 586 \pm 15$ nm and (I_r/I_g) ratio vs pH was plotted to make pH calibration curve of different capsules. (See figure 19 A-C)

4.8.2 pH calibration curve of capsules inside cell

The pH calibration curve of (+) capsule inside cell were prepared by exposing capsules to the cell for different times. For that, 15 (+) caps/cell were exposed to the HeLa cell for 8 h, 24h & 48 h in complete cell media and same process was followed as described below. These calibration curves were used for analyzing FACS data after exposing different test samples (See figure 19 D, E, F).

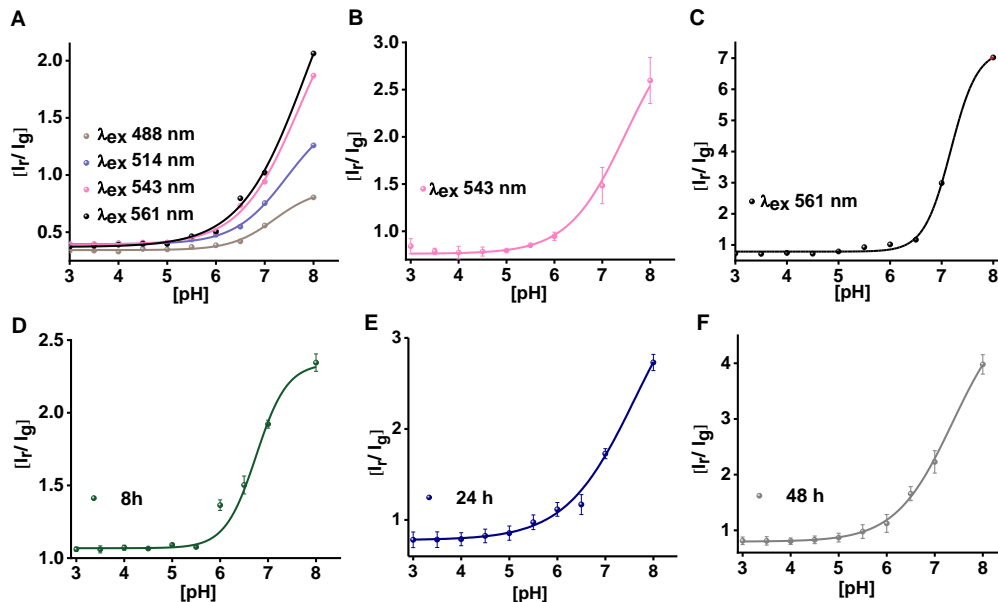


Figure 19: pH Calibration curves of (+) capsules only (A-C) and pH Calibration curves of (+) capsules inside cell (D-F). The ratio of green to red fluorescence intensity (I_r/I_g) vs

pH curves of (+) capsules only as measured by Fluorimeter (A), CLSM (B) and Flow cytometry (C). The data points in (B) correspond to the mean value of 10 different capsules and the corresponding standard deviations. Calibration curves of (+) capsules inside Hela cell were prepared after capsule exposure for different time intervals and fluorescence intensity measured by Flow cytometry. Hela cells are exposed to 15 caps/cell for 8 h (D), 24 h (E) and 48 h (F). The ratio (I_r/I_g) is plotted versus the pH of buffer solution in which capsule loaded cells were dispersed. The data correspond to the mean value of 3 independent experiments and the corresponding standard deviations. Curves were fitted with a sigmoidal function.

To make pH calibration of capsules inside cell, in each buffer solutions, ethanol solutions of monensin and nigericin were added at final concentrations of 20 μ M and 10 μ M respectively in order to equilibrate the pH of intracellular compartments to the extracellular pH buffer.[83] The pH Calibration curve of capsule inside cell was prepared by measuring change in fluorescence intensity of internalized capsules in cell by Flow cytometry (FACS). For that, Hela cells were exposed to 4 different capsules (+ caps, - caps, PEI caps, PEI-end caps) at 15 & 7 capsule/cell concentration in media supplemented with FBS for 24 hrs. After exposing capsules for desired time, cells were washed 3 times with PBS, collected and immersed into different buffer solutions containing nigericin and monensin for 15 mins prior to FACS measurements ($\lambda_{ex} = 561$ nm, emission collected at $I_r = 670 \pm 30$ nm & $I_g = 586 \pm 15$ nm). 10,000 cells were counted per sample. The results were analyzed by FlowJo software v10 and (I_r/I_g) vs pH calibration curve was plotted in the same way like before.

4.9 Experimental scheme for monitoring intracellular pH

4.9.1 Monitoring lysosomal pH in presence of different PEI samples

Lysosomal pH change was monitored by (+) pH sensor capsules due to exposure of different branched (BPEI) & linear (LPEI) polyethylene imines samples, by flow cytometry. Chloroquine has been used as a positive control for monitoring lysosomal pH change. It is a weak base and lysosomotropic substances, which is well known for increasing lysosomal pH. Hela cells were grown overnight in 24 well plates (1.9 cm² surface area per well; 1 mL of medium added per well) at 40,000 cell/ well

concentration. The next day, cells were exposed to the (+) capsules ($N_{\text{capsules/cell}} = 15$ capsules/cell) in complete cell medium for 24h & 4h separately. A dilution series of selected nontoxic concentrations of different PEI samples were exposed to the cells with internalized capsules (24h & 4h separately) for different time points. Two different experiments were performed for this study. For 1st experiment (+) capsules were exposed for 24h in complete cell medium. After that cell was washed with PBS, three times and different PEI samples (BPEI 2, 25, 60, & LPEI 250 kDa) were exposed for 2, 5, 8, 24 & 8+24 h in complete cell medium. Here 8+ 24 h means 8h exposure of PEI in serum supplemented medium and after that media was replaced with fresh complete medium. In 2nd experiment sensor capsules were exposed (15 caps/cell) for 4 h and then different dilutions of different PEI (BPEI 2, 25, 60, & LPEI 20, 250 kDa) were exposed in fresh complete cell medium for 2, 4, 6, 24 h. For both experiments 25 μ M of Chloroquine was considered as + ve control and exposed for 2, 5 & 8 h in 1st experiment and 2, 4, 6 h in 2nd experiment. HeLa cell with only sensor capsule without exposing any samples were used as control at each time points. At each time points, after incubation with test samples, cells were washed three times with PBS, collected through trypsinisation, followed by neutralization with PBS, centrifugation and further dispersed into fresh PBS for flow cytometric analysis. Fluorescence of (+) pH sensor capsule inside cell was measured by FACS using same settings as before used for uptake study. Analyzed data presented in figure 20 and 45 for 1st and 2nd experiments respectively.

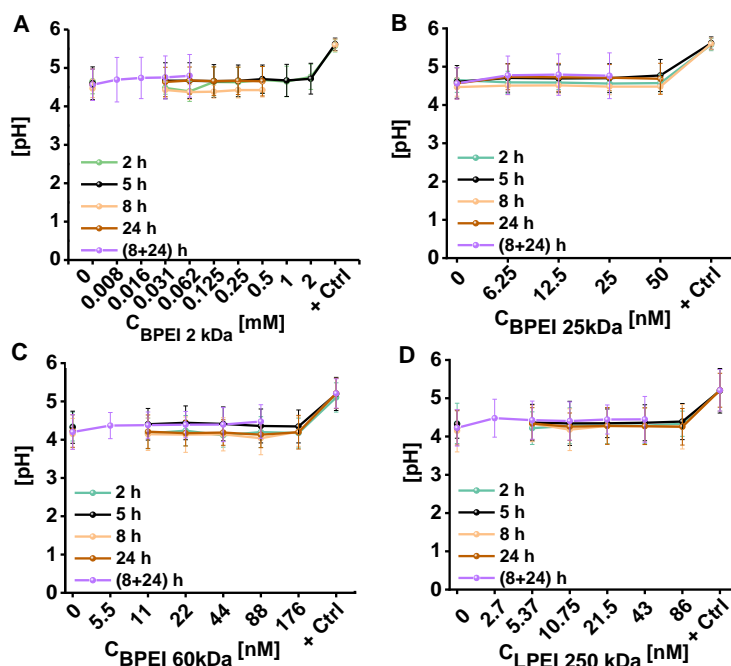


Figure 20: Measurements of lysosomal pH in response to different branched (A-C) and linear (D) polyethylenimine (BPEI & LPEI) over time. Hela cells are allowed to internalize + ve pH sensor capsule at 15 caps/ cell in serum supplemented media for 24 h followed by exposure to series of dilutions of different PEI samples for 2 h, 5h, 8h, 8+ 24 h and 24 h. The time point 8+ 24 h means 8 h PEI exposure, washing and kept further in fresh serum supplemented media for another 24 h. The Data point at zero corresponds to reference cell or control. As + Control (+ ctrl) 25 uM chloroquine solution has been exposed to cells for 2h, 5h and 8h. The Lysosomal pH was measured by pH calibration curve of + caps inside cell. The data represents average of three independent experiments and corresponding standard deviation.

4.9.2 Monitoring pH of intra and extracellular compartments by different capsules

Capsules with PEI layers were prepared to monitor the effect of PEI on lysosomal pH. Two different types of PEI layered pH sensitive capsules named as PEI capsule, [(PAH/PSS) (PEI/DEX)3PARG] & PEI-end capsule [(PAH/PSS)3(PEI/DEX) PEI], were used for this study. Another two pH sensor capsules named as (+) capsule [(PAH/PSS)4PAH] & (-) capsule [(PAH/PSS)4] were used as control. First 40000 HeLa cells were seeded in 24 well plates (1.9 cm² surface area per well; 1 mL of medium added per well) with complete cell medium for 24 h. The next day, 4 different capsules,

PEI capsules, PEI-end capsule, (+) capsule & (-) capsule were exposed to the cell at 15 capsules/cell concentrations for 2, 4, 6, 24 & 48 h in complete cell media. Chloroquine (Cq) was used as a positive control during each experiment. Specifically, 4 different capsules were exposed to the cell for 24h in serum supplemented media followed by three times washing with PBS & 25 μ M Chloroquine was exposed for 2, 4, 6 & 24h in complete cell media.

In another experiment, PEI capsule, PEI-end capsule & (+) capsule (control) were allowed to internalized into cell for 24h in complete media, followed by three times PBS wash and further a series of different concentrations of BPEI 25 kDa & LPEI 20 kDa solutions were exposed to the cell for 2, 4, 6 & 24 h. Also, 100 nM BPEI (25 kDa) was exposed in complete media for 2, 4, 6 & 24 h in terms of polyplex as prepared with BPEI 25 kDa and scrambled plasmid. At each time points 25 μ M chloroquine was used as positive control. After incubation with different sensor capsules for desired time, cells collected and fluorescence measured by FACS similarly as before.

4.10 Synthesis and characterization of PEI-polyplex

A scrambled plasmid was used to make polyplex. In a typical reaction, 7.66 μ L of 0.75 mg/ mL, Rh-B Labeled BPEI (25 kDa) mixed with 100 μ L 10 mM HEPES, pH 7.4 (Con. Of PEI = 5.76 μ g in 100 μ L) and 3.8 μ L of 1.05 mg/ mL plasmid was mixed with 100 μ L 10 mM HEPES, pH 7.4 (Con. Of plasmid = 3.99 μ g in 100 μ L). Then PEI & plasmid mixed at 1:1 ratio, vortexed 5-10 s and kept at RT for another 15 mins prior to cellular exposure. Polyplex was characterized by measuring size of it with dynamic light scattering (DLS) and measuring the zeta-potential (ζ) with laser Doppler anemometry, as carried out in a Malvern ZetasizerNano particle analyzer ZEN 3600 instrument, in 10mM HEPES (pH 7.4) buffer. (See fig. 21)

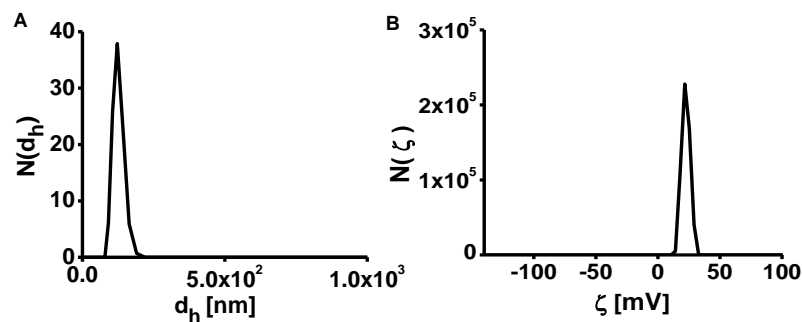


Figure 21: Characterization of Rh-B labeled PEI-plasmid polyplex. (A) Corresponds to size of polyplex in 10 mM, pH 7.4, HEPES buffer as measured by DLS. (B) Represents zeta potential of polyplex.

4.11 Co-localization study of capsule, labeled-PEI or PEI-plasmid polyplex & lysosome

Co-localization study of capsules & PEI was performed to check whether PEI and capsules co-localize into same lysosome. SNARF has broad excitation and emission spectra. Therefore, capsule was loaded with Cascade-blue dye and used for co-localization study to avoid cross talks. BPEI 25kDa was labeled with Rh-B dye and lysosome staining was done with LysoTracker-green dye. Briefly, 14000 HeLa cells per well were seeded overnight in ibidis 8-well plates (area per well: 1 cm², medium per well: 300 μ L) and next day 7 capsules/ cell was exposed for another 24h. After that 100nM of free BPEI (25 kDa) exposed for 24h and polyplex made to BPEI 25 kDa & scrambled plasmid was exposed for 6 h and 24 h. Polyplex was prepared with N/P ratio 10 and 88 nM of PEI was exposed as polyplex. After the desired incubation time, cell washed with PBS and lysosome was stained with 1 μ M LysoTracker green for 30 mins prior to imaging with a confocal microscope (Zeiss LSM 510 Meta Confocal Microscope). Fluorescence images were taken with a Plan-Apochromat 63x/1.40 Oil DIC M27 objective, and the pin hole was set to 0.86–1.32 airy units. A laser diode emitting at 405 nm and a band pass BP 420-480 emission filter were used to visualize the capsule loaded with cascade blue dye. A helium–neon laser for excitation at 543 nm and a BP 560–615 emission filter used to visualize the Rh-B dye labeled to PEI or PEI-polyplex. An argon laser for excitation at 488 nm together with a BP 505– 570 emission filter were used for recording fluorescence of Lyso-Tracker-green. Colocalization of the capsule & labeled-PEI or PEI-polyplex, capsule & lysosome, labeled-PEI or PEI-polyplex & lysosome estimated by Mander's overlap coefficient (MOC) which was calculated using ImageJ 1.42 software (NIH).

4.12 Study the effect of PEI on fluorescence of pH sensitive dye SNARF

To check whether PEI can influence the fluorescence property of SNARF, different concentrations of BPEI 25 kDa samples were added into SNARF solution and their fluorescence was monitored by fluorimeter ($\lambda_{\text{ex}} = 561 \text{ nm}$). Typically, 0.05 mg/ mL concentration of SNARF solution in two different buffer solutions (pH 4.5 & 7.5) were taken and different concentrations of BPEI 25 kDa were added with keeping final concentration of SNARF in each solution intact. Same concentration of SNARF (no PEI added) at pH 4.5 & 7.5 was used as control for each buffer. Similarly, different capsules (+ caps, PEI caps, PEI-end caps) were also dispersed into pH 7 buffer and different PEI samples were added to it keeping total capsule concentration same in different solutions for each capsule. Here different capsules into pH 7 buffer without PEI were control for each capsule. Finally (I_{640}/I_{580}) vs concentration of PEI was plotted for each sample to verify possible change in intensity ratio of SNARF in presence of PEI. Figure 22 shows no influence of PEI on fluorescence spectra of SNARF.

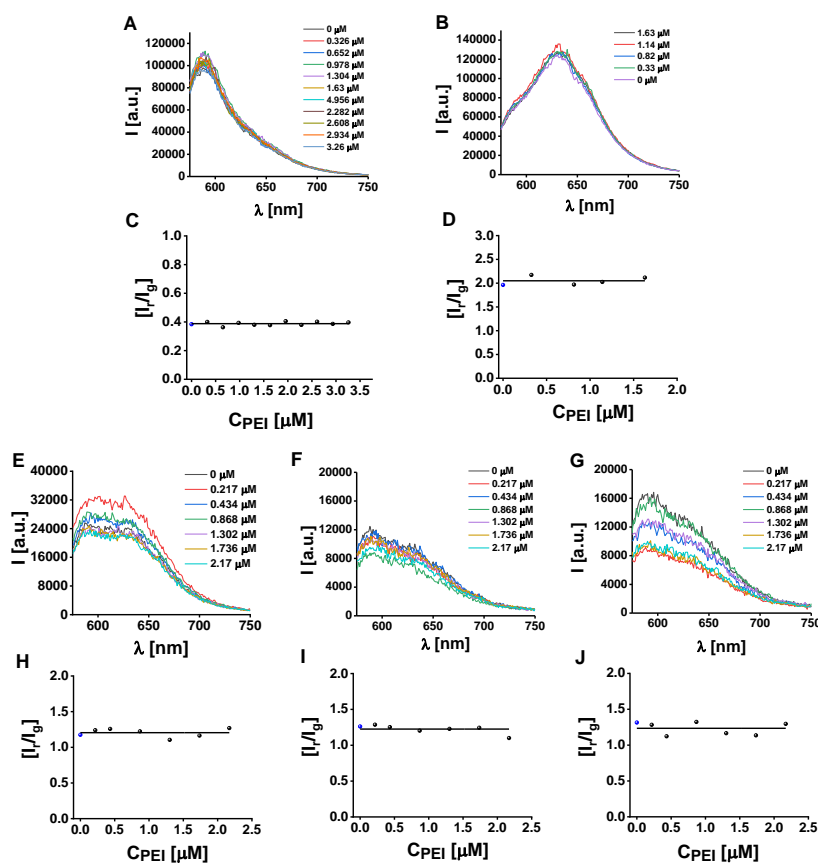


Figure 22: Study the influence of PEI on fluorescence spectra of SNARF. (A, B) represents fluorescence spectra of SNARF after adding Different concentrations of BPEI 25 kDa solution into SNARF solution at pH buffer 4.5 (A) & 7.5 (B). (C – E) fluorescence spectra of different SNARF loaded, pH sensitive capsules, (+) caps (C), PEI caps (D), PEI-end caps (E), dispersed into pH buffer 7. (F-J) corresponds to intensity ratio at 640 nm and 580 nm (I_r/I_g) vs concentrations of PEI (C_{PEI}), as analyzed from the respective fluorescence spectra (A-E).

4.13 Uptake studies by flow cytometry

4.13.1 Uptake studies of biodegradable capsules

Intracellular uptake of capsules exposed to HeLa cells was determined by flow cytometry according to previous protocols[82]. A flow cytometer (BD LSR Fortessa Biosciences, German) was used for the analysis. For that 40,000 HeLa cells were seeded per well in 24 well plates (1.9 cm² surface area per well; 1 mL of medium added per well) and incubated overnight. The next day, HeLa cells were exposed to the curcumin-loaded (PARG/ALGI)₂ and (PARG/ALGI)₂(PARG/EuL) capsules at desired concentrations $N_{capsules/cell}$ (3 - 100 capsules/cell) in complete cell medium for 24 and 48 h. After the exposure time, the supernatants of the samples were removed and the HeLa cells were washed three times with PBS (500 μ L). Then, HeLa cells were trypsinated, followed by neutralization of trypsin with complete culture medium. Next, the cells were collected into flow cytometry tubes and centrifuged at 300 rcf for 5 minutes. Finally, the cells were then suspended into 0.3 mL PBS solution. Cells were mixed very well with a pipette in order to avoid clamping of cells prior to analysis. The threshold of the forward-scattering signal in the flow cytometer was adjusted to eliminate signals from debris and smaller particles. The cells with internalized capsule were excited by an argon 488 nm laser and the emission at 540 nm was collected using a 530/30 filter. For each experiment, a minimum of 10,000 cells was sampled with the flow cytometer. A cell sample without capsule was used as control. Results represent the mean value \pm standard deviation (SD) from three independent experiments using HeLa cells at different passage numbers. Results shown in Figure 32. Here, as

additional data an overview of the cell population and respective histograms are shown in Figure 23.

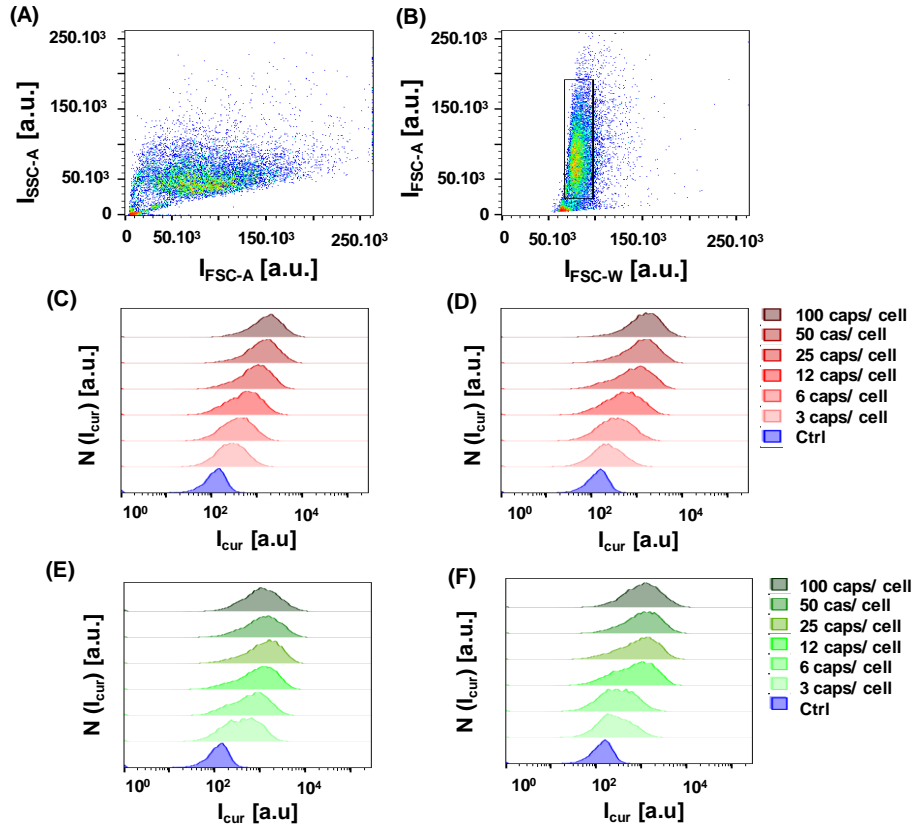


Figure 23. Uptake of (PARG/ALGI)₂ and (PARG/ALGI)₂(PARG/EuL) capsules exposed to HeLa cells as assessed by flow cytometry. (A,B) Used gating strategy in the experiments. The sample of control cells, which not exposed to capsules, shown as an example. I_{SSC} and I_{FSC} correspond to the sideward and forward scattering intensities, respectively. (C-F) Fluorescence intensity distribution $N(I_{cur})$ of cells exposed to $N_{capsules}/cell$ for 24 h and 48 h. (C,D) (PARG/ALGI)₂ capsules. (E,F) (PARG/ALGI)₂(PARG/EuL) capsules. The corresponding quantitative data shown in Figure 32 in the main manuscript. The control (Ctrl) corresponds to 0 capsules/cell.

4.13.2 Uptake studies of different pH sensor capsules

A flow cytometer (BD LSR Fortessa Biosciences, German) was used for the analysis of Intracellular uptake of 4 different capsules (+ caps, - caps, PEI caps & PEI-end caps) exposed to HeLa cells. For that, 40,000 HeLa cells were seeded per well in 24 well plates (1.9 cm² surface area per well; 1 mL of medium added per well) and incubated overnight. The next day, HeLa cells were exposed to the different capsules at concentrations $N_{\text{capsules/cell}}$ (15 & 7 capsules/cell) in complete cell medium up to 48 h. Kinetics of intracellular capsule uptake was monitored by measuring fluorescence intensity cell overtime (15, 30 min, 1, 2, 4, 6, 24, 48 h). After exposure time, the supernatants of the samples were removed and the HeLa cells were washed three times with PBS (500 μ L). Then, HeLa cells were trypsinized, followed by neutralization of trypsin with complete culture medium. Then, the cells were collected into flow cytometry tubes and centrifuged at 300g for 5 minutes. Finally, the cells were resuspended into 0.3 mL PBS solution. Cells were mixed very well with a pipette in order to avoid clamping of cells prior to analysis. The threshold of the forward-scattering signal in the flow cytometer was adjusted to eliminate signals from debris and smaller particles. The cells with internalized capsule excited by 561 nm laser and the emission at $I_r = 670 \pm 30$ nm & $I_g = 586 \pm 15$ nm were collected. For each experiment, a minimum of 10,000 cells were sampled with the flow cytometer. A cell sample without capsule was used as control. Results represent the mean value \pm standard deviation (SD) from three independent experiments using HeLa cells at different passage numbers. (See figure 41 (15caps/cell) and 24 (7caps/cell))

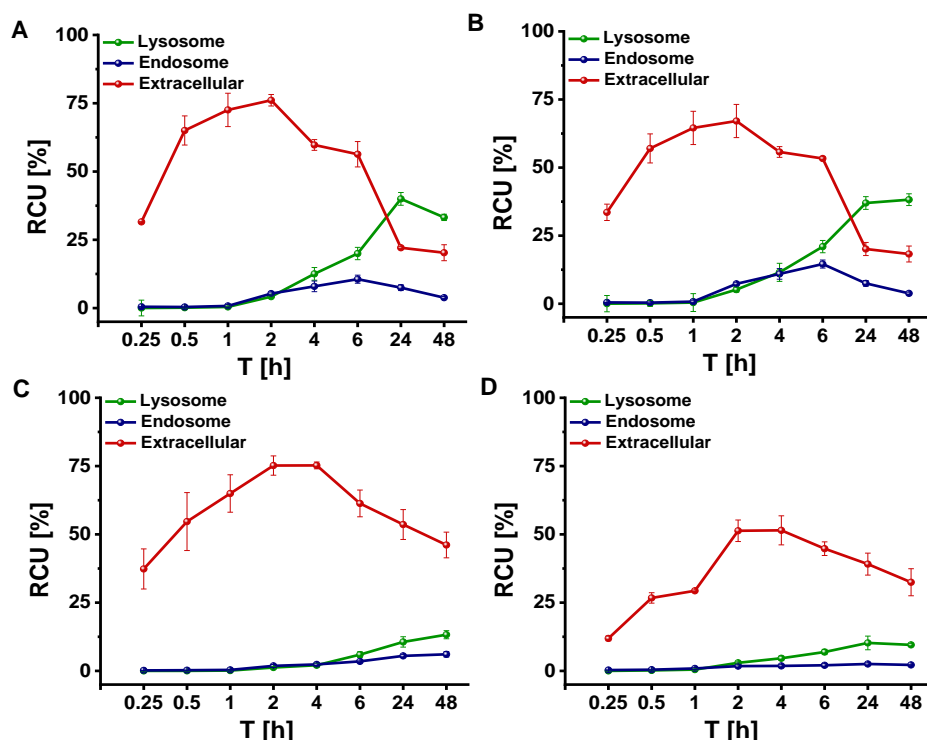


Figure 24: (A, B, C, D) represents percentage of relative capsule uptake (RCU) of different capsules, (+) capsule (A), (-) capsule (B), PEI capsule (C) and PEI-end capsule (D) over time. Here 7 capsule/ cell concentrations of each capsules were exposed to Hela cell for maximum 48 hrs.

4.13.3 Uptake study of labeled PEI

Labeling of PEI with dye and characterization

BPEI 25 kDa fluorescently labeled with either Dy-647 or Rh-B dye. The amino reactive fluorophore DY-647, containing the activated ester N-hydroxysuccinimide (-NHS), was conjugated to branched PEI. The primary and secondary amine groups of PEIs undergo a nucleophilic attack to the activated carbonyl functionality along with removing the NHS leaving group and form a stable covalent amide bond. A molar ratio of 1:10 (polymer: dye) was used as reported elsewhere. Typically, 2.8 mg of BPEI (25 kDa) were dissolved in 22 μ L of sodium bicarbonate buffer (NaHCO_3 , 0.1 M, pH 8.5) and subsequently, 1 mg of DY-647 (MW= 886.04 g/mole) dissolved in 112 μ L of DMSO (99.9%) were added and the mixture was incubated for 2 hours in dark at RT.

Similarly, BPEI was labeled by reaction of the isothiocyanate group (-SCN) of rhodamine-B (Rh-B) with primary or secondary amino groups of BPEI (25 kDa) by forming a stable thiourea bond. A molar ratio of 1:25 (polymer: dye) was used. Briefly,

1.4 mg of PEI (25 kDa) were dissolved in 250 μL of sodium bicarbonate buffer (NaHCO_3 , 0.1 M, pH 8.5) and then, 0.2 mg of Rh-B dissolved in 50 μL of DMSO (99.9%) were added followed by 2h incubation under dark at RT. For both cases, unreacted dye was separated by using PD-10 desalting columns (Cat. No.: 17-0851-01, GE Healthcare) eluted with Millie-Q water. The amount of PEI was estimated via the copper(II) polyplexation method. (See fig. 25)

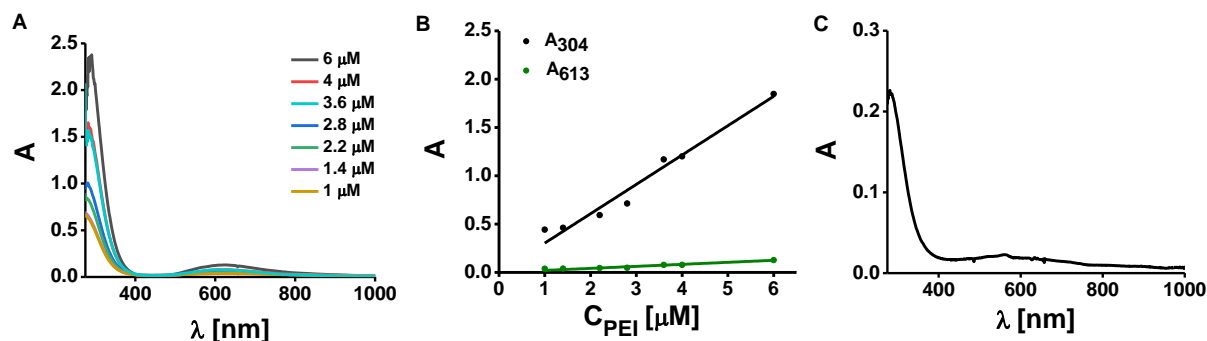


Figure 25: (A) UV-vis absorption spectrum of PEI/copper (II) complex in water with different BPEI (25 kDa) concentrations. (B) Absorption at λ_{304} & λ_{613} vs different PEI concentration (C_{PEI}) plotted and fitted with linear function. (C) Absorption spectra of Rh-B labeled PEI / copper complex in water.

Uptake study

Intracellular uptake of free BPEI 25 kDa studied with FACS. BPEI labeled with Dy-647 dye. In 24 well plates (1.9 cm^2 surface area per well; 1 mL of medium added per well), 40,000 Hela cells per well were seeded overnight. A dilution series of PEI samples (400 – 12.5 nM) were exposed to the cell in FBS supplemented media for 4h, 6h & 24 h. Similarly, different concentrations (100 – 12.5 nM) of PEI samples were also exposed to the cell for 6h without FBS containing media & 6h without FBS + 24h in FBS supplemented media. At each time-points, cells were washed with PBS for 3 times and collected cells were dispersed into fresh PBS for flow cytometric analysis. Signals from debris and smaller particles were eliminated by adjusting the threshold of the forward-scattering signal in the flow cytometer. The cells containing fluorescent labeled PEI was excited by 640 nm laser and the emission collected with 670 ± 30 filters. For each

experiment, a minimum of 10,000 cells were analyzed. A cell sample without PEI was used as a control. Intensity of PEI inside cell was calculated by subtracting the Intensity of control cell from each intensity measured from PEI containing cell ($I_{\text{PEI-cell}}$). Results represent the mean value \pm standard deviation (SD) from three independent experiments using HeLa cells at different passage numbers. (See fig 26)

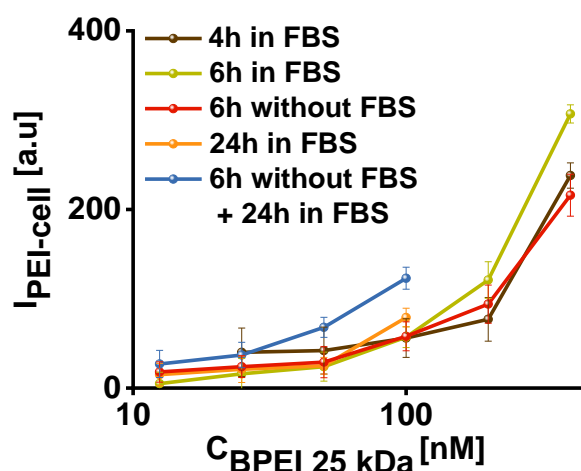


Figure 26: Uptake study of BPEI 25 kDa inside cell by FACS. BPEI 20 kDa was labeled with Dy-647 dye and different concentrations of PEI exposed to HeLa cells for 4, 6, 24 h with serum (FBS) supplemented media & without serum supplemented media for 6h. Another one was 6h without serum-supplemented media and further media was replaced with serum-supplemented media for another 24h.

5. Results and discussion

5.1 Biodegradable alginate capsules as biocompatible potential delivery agents

In the present work, we synthesized polyelectrolyte capsules with diameters below 1 μm made of the biocompatible polyelectrolytes alginate (ALGI) and poly-L-arginine (PARG) based on LbL assembly through a biocompatible synthetic route.

5.1.1 Synthesis and characterization of biodegradable alginate capsules

Two types of capsules were prepared by the LbL method. For that, a modified protocol of previously reported procedures was used.[84, 85] The capsules were composed of biodegradable polyelectrolytes, PARG and alginate (ALGI), with positive and negative

charge respectively. The overview of the synthesis strategy is illustrated in Figure 27. We selected PARG and ALGI to serve as polyelectrolytes, taking advantage of their natural, biocompatible and biodegradable origin. Curcumin was encapsulated in the capsule core as model drug (*cf.* Figure 27A-B).

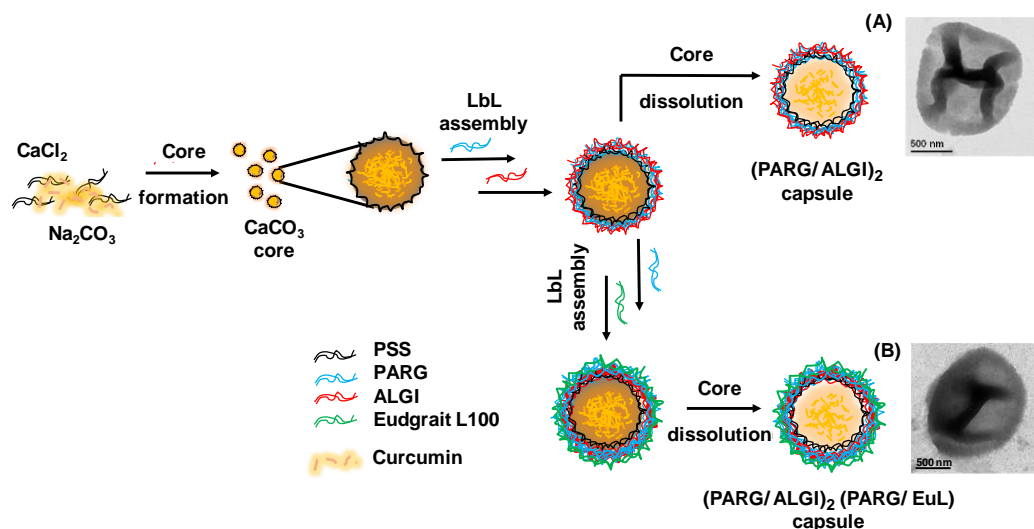


Figure 27. A schematic diagram of the synthesis of biodegradable polyelectrolyte capsules loaded with curcumin. Transmission electron microscope (TEM) images of curcumin-loaded (A) $(\text{PARG}/\text{ALGI})_2$ and (B) $(\text{PARG}/\text{ALGI})_2(\text{PARG}/\text{EuL})$ capsules after dissolution of the template cores are shown. Scale bars correspond to 500 nm.

Briefly, calcium carbonate (CaCO_3) particles of $d_h \approx 850$ hydrodynamic diameter nm, as determined by dynamic light scattering (DLS), were prepared by co-precipitation and were used as core templates (*c.f.* Figure 28F,J). To prepare curcumin-loaded capsules, curcumin was co-precipitated in the CaCO_3 particles. Both, fluorescence measurements and fluorescence microscopy (*c.f.* Figure 28C-D, A-B), confirmed the integration of the curcumin in the template core. Note that the CaCO_3 were synthesized under the presence of PSS in order to reduce size. Next, the core particles were coated with PARG and ALGI using the well-described LbL method.[43] As seen in Fig. 28K-L, a reversal of the surface charge between negative to positive zeta potential values could be observed, which verified the adsorption of polyelectrolytes in each layer. Capsules of

two bilayers were prepared and are in the following referred to as (PARG/ALGI)₂ capsules. Furthermore, in order to support and preserve the capsules in harsh pH environment (e.g. promote the efficient delivery capability through oral route), the capsules were complemented with an additional pH-sensitive EuL polymer layer and are then referred to as (PARG/ALGI)₂(PARG/EuL) capsules (*c.f.* Figure 28L). Finally, the template cores were removed, and the capsules were washed and stored in sterilized water. Then, the capsule concentration was determined by confocal laser scanning microscopy (CLSM) (as described in the experimental section), and capsules were stored in dark at 4 °C until further used. The resulting capsules exhibited hydrodynamic diameters d_h of around 885 nm ((PARG/ALGI)₂) and 916 nm ((PARG/ALGI)₂(PARG/EuL)). Capsules were uniform, well dispersed, and presented spherical shape as shown by TEM and CLSM images (*c.f.* Figure 28 E, I; A, B and the experimental section for further synthesis details). A summary of the capsule characterization including the colloidal stability and surface charge of the capsules determined using DLS in Millie-Q water, are presented in the Table 3. The found size variation between DLS measurement and TEM image analysis can be attributed to little deformation or flattening of spherical capsules under dry condition for TEM imaging.

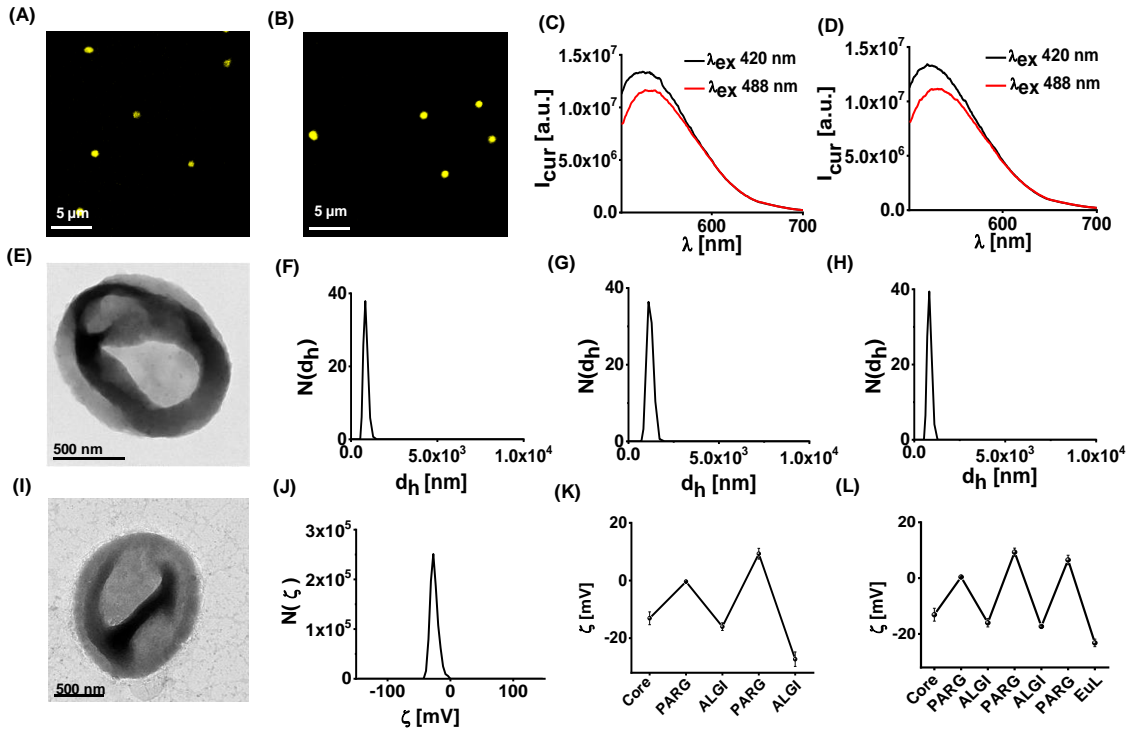


Figure 28. Characterization of the biodegradable (PARG/ALGI)₂ and (PARG/ALGI)₂ PARG/EuL) capsules. (A, B) Confocal microscopy images of curcumin-loaded (A) (PARG/ALGI)₂ and (B) (PARG/ALGI)₂(PARG/EuL) capsules after removal of the template cores. (C, D) Fluorescence spectra $I_{\text{cur}}(\lambda)$ of curcumin-loaded (C) (PARG/ALGI)₂ and (D) (PARG/ALGI)₂(PARG/EuL) capsules after removal of the template cores at different wavelength of excitation λ_{ex} . (E, I) TEM image of curcumin-loaded E) (PARG/ALGI)₂ and (F) (PARG/ALGI)₂(PARG/EuL) capsules after removal of the template cores. (F-H) Number distributions $N(d_h)$ of the hydrodynamic diameters of (F) PSS-CaCO₃ cores, (G) (PARG/ALGI)₂ capsules, and (H) (PARG/ALGI)₂(PARG/EuL) capsules as measured by DLS. Data are presented as number distributions $N(d_h)$. (J-L) Zeta potential distributions $N(\zeta)$ of (J) PSS-CaCO₃ cores, and capsules coated as function of the additional PARG/ALGI layers for (K) (PARG/ALGI)₂ and (L) of (PARG/ALGI)₂(PARG/EuL) capsules. DLS and zeta potential measurements were carried out in Millie-Q water.[86]

Capsule Type	d_{TEM} [μm]	d_h [nm]	ζ [mV]	PDI
PSS-CaCO ₃	--	856 \pm 29	-20 \pm 5	0.15 \pm 0.05
(PARG/ ALGI) ₂	1.07 \pm 0.34	885 \pm 34	-37.3 \pm 3.7	0.23 \pm 0.15
(PARG/ ALGI) ₂ (PARG/ EuL)	1.17 \pm 0.52	916 \pm 46	-39.2 \pm 4	0.27 \pm 0.035

Table 3. Colloidal properties of the capsules: The capsule diameter (d_{TEM}) obtained from TEM images, average hydrodynamic diameter d_h , zeta potential ζ , and PDI of the cores and capsules with dissolved cores. The results are presented as (mean \pm standard deviation (SD)) from three independent batches of capsules. DLS and zeta potential measurements were carried out in Millie-Q water.

5.1.2 Drug loading and encapsulation efficiency of capsules

The encapsulation efficiency (η_{EE}) and loading capacity (η_{LC}) of curcumin-loaded capsules evaluated by both, indirect and direct methods that described in the methods section. Note that the spectral and photo physical properties of curcumin are highly

sensitive to pH and solvent conditions. [87] For direct quantification of encapsulated curcumin the capsule walls were dissolved by pronase before spectroscopy. Interference of the optical properties of curcumin with those of pronase was controlled by UV-Vis absorption spectroscopy $A(\lambda)$ and fluorescence spectroscopy $I(\lambda)$ after 24 h incubation of curcumin in pronase solution at 37°, as shown in Figure 12. The absorption $A(\lambda = 420 \text{ nm})$ at 420 nm was used to calculate η_{EE} and η_{LC} , see the experimental section. The results are presented in Table 4, indicating similar η_{EE} and η_{LC} of curcumin in both types capsules. Spectroscopic measurements of the fluorescent signal of released curcumin after pronase mediated degradation (i.e. the "direct" method) of both the capsules indicated a η_{EE} of approx. 70 %. The η_{LC} values found for $(\text{PARG/ALGI})_2$ and $(\text{PARG/ALGI})_2(\text{PARG/EuL})$ capsules were approximately 15.57 and 11.24 pg curcumin/capsule as measured by the indirect method and 11.24 and 11.94 pg curcumin/capsule as measured by the direct method, respectively. Since, both types of capsules were prepared from one initial batch of CaCO_3 cores these similar results of curcumin loading were expected. The slightly different fluorescence and consequent variance of η_{LC} observed maybe attributed to the additional washing steps involved in the synthesis of the $(\text{PARG/ALGI})_2(\text{PARG/EuL})$ capsules, which may result in the loss of encapsulated curcumin or due to the counting errors of the capsules. However, it is important to mention that the η_{LC} results of both types of capsules showed, the direct and indirect methods agree remarkably well.

Capsules	η_{EE} [%] (direct method)	η_{LC} [pg/capsule] (indirect method)	η_{LC} [pg/capsule] direct method)
$(\text{PARG/ALGI})_2$	75.75 ± 2.25	15.57 ± 1.05	13.54 ± 1.86
$(\text{PARG/ALGI})_2(\text{PARG/EuL})$	71.00 ± 2.80	11.24 ± 2.15	11.94 ± 1.37

Table 4. Encapsulation efficiency (η_{EE}) and loading capacity (η_{LC}) of (PARG/ALGI)₂ and (PARG/ALGI)₂(PARG/EuL) capsules with curcumin (number of capsule batches n=2).

5.1.3 In vitro release study from different capsules

(PARG/ALGI)₂ and (PARG/ALGI)₂(PARG/EuL) capsules were loaded with curcumin as model drug to investigate the effect that the surface modifications (EuL layer) and the number of bilayers of the capsules may have on the drug release kinetics. Thus, the *in vitro* release profile of curcumin (η_{CR}) loaded (PARG/ALGI)₂ and (PARG/ALGI)₂(PARG/EuL) capsules investigated by two different approaches, the dialysis and the ultrafiltration method (see the methods section). [88, 89] For those investigations 1 mL ($n_c = 4 \times 10^7$ capsules/mL) of (PARG/ALGI)₂ and ($n_c = 4.6 \times 10^7$ capsules/mL) (PARG/ALGI)₂(PARG/EuL) capsule solution was used. In both types of the capsules, the curcumin concentration used for the release study was 40 μ g/mL. The release profile evaluated at different environmental conditions, in acidic (pH 3 and pH 5) as well as in neutral conditions (pH 7). [90] The results show that (PARG/ALGI)₂ and (PARG/ALGI)₂(PARG/EuL) capsules had an opposite pH-dependent drug release profile. (*c.f.* Figure 29A-B, C-D). (PARG/ALGI)₂ capsules exhibited higher release of encapsulated curcumin following incubation at lower pH, while (PARG/ALGI)₂(PARG/EuL) capsules released more curcumin after incubation at higher pH. Amount of released curcumin increased over the time. Notably, the tendency of the results was confirmed by the two different approaches used (the dialysis and the ultrafiltration method), which corroborates reproducibility of the found pH-dependent drug release kinetics. Moreover, the dialysis method showed that after 48 h incubation, the (PARG/ALGI)₂ and (PARG/ALGI)₂(PARG/EuL) capsules exhibited a maximum η_{CR} of 50% at pH = 3 environment and η_{CR} of 52% at pH = 7 environment, respectively (*c.f.* Figure 29 A, B). Besides, the cumulative curcumin release η_{CR} of capsules observed at 48h by the ultrafiltration method was 70% in pH = 3 environment and 71% in pH = 7 environment for the (PARG/ALGI)₂ and (PARG/ALGI)₂(PARG/EuL) capsules respectively (*c.f.* Fig. 29 D, E). The two used approaches provided similar trends in maximum η_{CR} release from (PARG/ALGI)₂ and (PARG/ALGI)₂(PARG/EuL) capsules pH 3 and 7, respectively but differed in the absolute η_{CR} value. We will attribute this

variation to the nature of the different methods, some loss of curcumin, etc. The η_{CR} behavior of $(PARG/ALGI)_2(PARG/EuL)$ was attributed to the additional EuL layer, results that were in line with previous work.[91] [92]The use of EuL on capsules could potentially be beneficial for particles that need to be preserved under harsh pH environment.[93, 94]

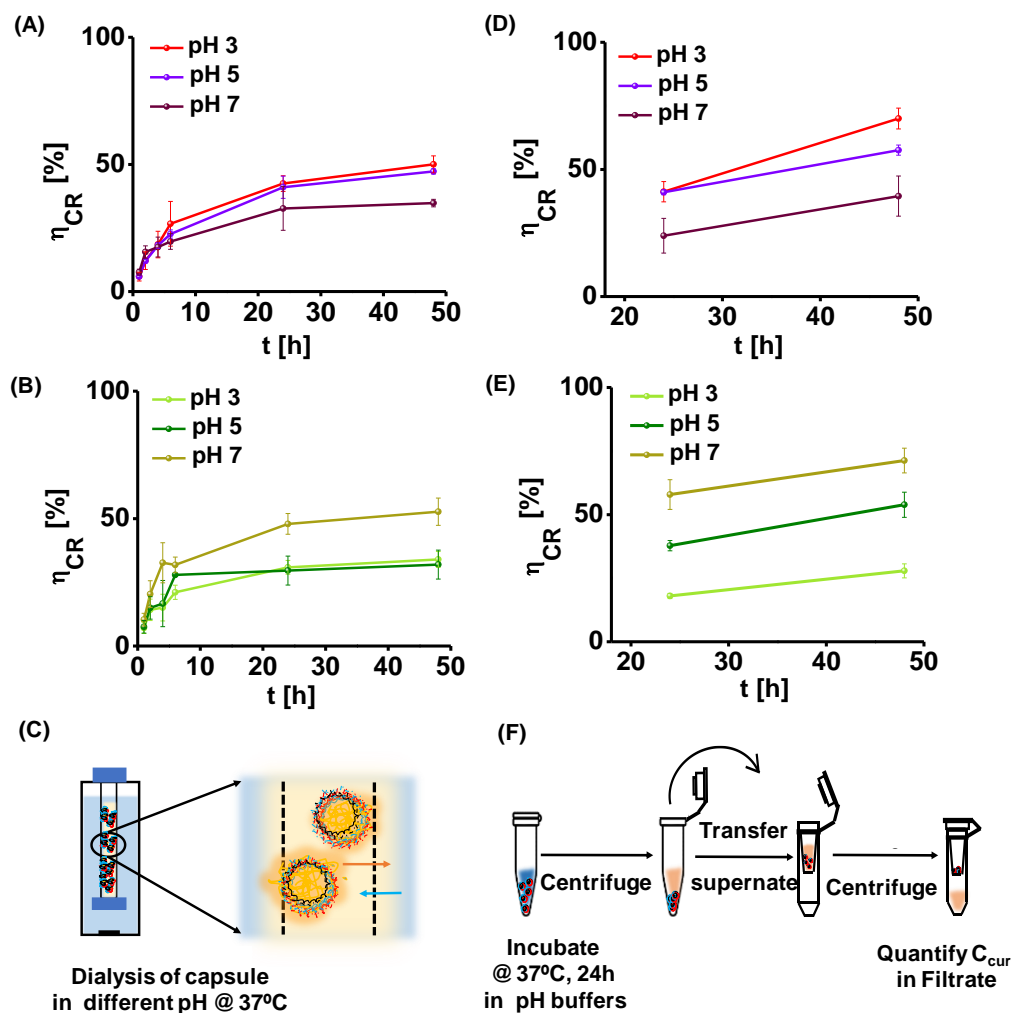


Figure 29. Release study of biodegradable curcumin-loaded $(PARG/ALGI)_2$ and $(PARG/ALGI)_2(PARG/EuL)$ capsules using the dialysis and ultrafiltration method. (A, D) Percentage of released curcumin η_{CR} from $(PARG/ALGI)_2$ capsules and (B, E) η_{CR} from $(PARG/ALGI)_2(PARG/EuL)$ capsules measured by (A, B) the dialysis and (D, E) the ultrafiltration method. The results are presented as percent of (mean \pm SD) from three

independent experiments. (C,F) represent schemes of the release study as performed by the dialysis and the ultrafiltration technique.[86]

5.1.4 Biodegradation study of capsules

The biodegradation of the capsules under different environment conditions over time was investigated by means of changes in hydrodynamic diameter d_h , zeta potential ζ , and visual inspection by confocal laser microscopy (CLSM) images (*c.f* Figure 30). Briefly, (PARG/ALGI)₂ and (PARG/ALGI)₂(PARG/EuL) capsules were incubated in 2 mg/mL pronase in phosphate buffered saline (PBS, pH 7) and in PBS buffer at pH = 7 and pH = 3 for 2, 4, 6, 24, 48, and 72 h and the biodegradation was monitored in terms of $d_h(t)$, $\zeta(t)$, and changes in CLSM images.

The degradation kinetics of (PARG/ALGI)₂ capsules depends on the pH environment. The average size of capsules incubated at pH 3 initially decreased and over time increased little bit, which has been observed at pH 7 as well as shown by the d_h measurements. Although, at pH 3 after 48h these capsules loses fluorescence, whereas at pH 7 particles were still showing fluorescence as revealed from CLSM images, suggesting loss of curcumin at pH 3 (*c.f* Figure 30). In contrary to (PARG/ALGI)₂ capsule, (PARG/ALGI)₂(PARG/EuL) capsules loses curcumin fluorescence, at pH 7 after 48h. The d_h of (PARG/ALGI)₂(PARG/EuL) capsules increases over time for incubation in both pH 3 and 7 buffers overtime, which may be because of aggregation of these capsules, instead of being degraded according to the CLSM images. In contrast to pH 7 buffers, in which, both the capsules were stable up to 24h, get degraded in the presence of pronase, even at short periods of time. A decreasing trend in capsule size as observed from d_h measurements and CLSM images and lowering of outer charge of capsules in pronase, over time, supports degradation of capsules in pronase. These data suggest that (PARG/ALGI)₂ and (PARG/ALGI)₂(PARG/EuL) are biodegradable capsules, but exhibit different pH dependence profiles, most provably due to the effect of the additional PARG/EuL bilayer.

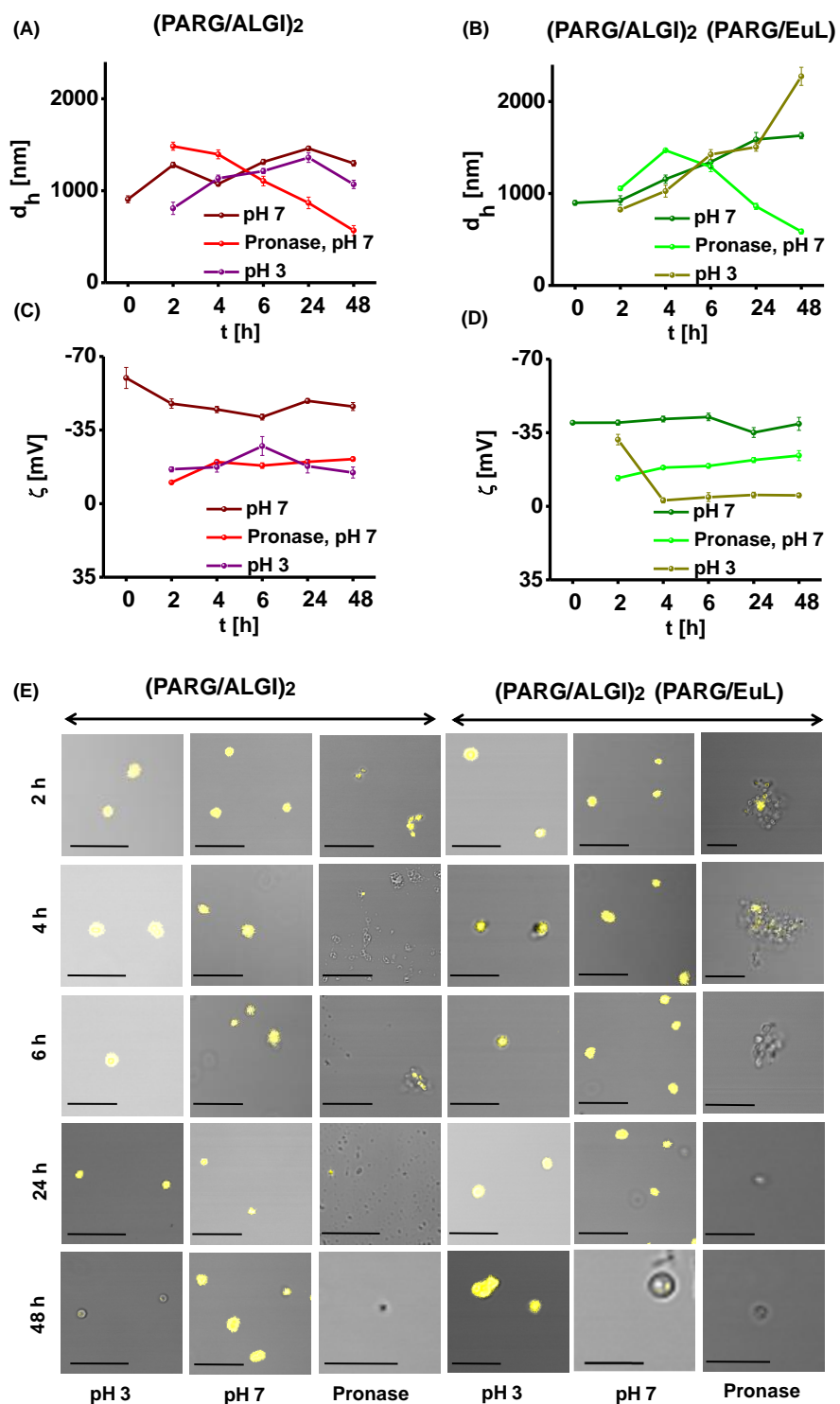


Figure 30. Biodegradability study of capsules loaded with curcumin. Curcumin-loaded (PARG/ALGI)₂ and (PARG/ALGI)₂(PARG/EuL) capsules were incubated in 2 mg/mL pronase (pH 7) and in PBS buffer at pH = 7 and pH = 3 at 37 °C. (A,B) The

hydrodynamic diameter d_h and (C,D) the zeta potential ζ of (A,C) (PARG/ALGI)₂ and (B,D) (PARG/ALGI)₂(PARG/EuL) capsules, in PBS buffer at pH = 7, and pH = 3, as well as in pronase in PBS at pH = 7 is plotted over time t . Decrease in d_h can be interpreted as degradation of the capsules, increase in d_h as agglomeration. Data correspond to (mean \pm SD) of 3 measurements. (E) Confocal images of curcumin-loaded (PARG/ALGI)₂ and (PARG/ALGI)₂(PARG/EuL) capsules at each time point of the degradation study. The scale bars correspond to 5 μ m.

5.1.5 Biocompatibility studies of capsules

In order to investigate the biocompatibility of (PARG/ALGI)₂ and (PARG/ALGI)₂(PARG/EuL) capsules, cell viability studies of HeLa cells exposed to those capsules were carried out by using the traditional Resazurin assay as previously reported [81, 95]. HeLa cells were derived from a cervical carcinoma, and those cells have been frequently employed in toxicology studies,[96] [97, 98] and thus were used as model system in this work. As seen in Figure 31, the cell viability (V) results indicated that both capsules types are not acutely toxic at the time and doses used. Only a slight decrease of cell viability was observed at higher exposure concentrations of capsules/cell added.

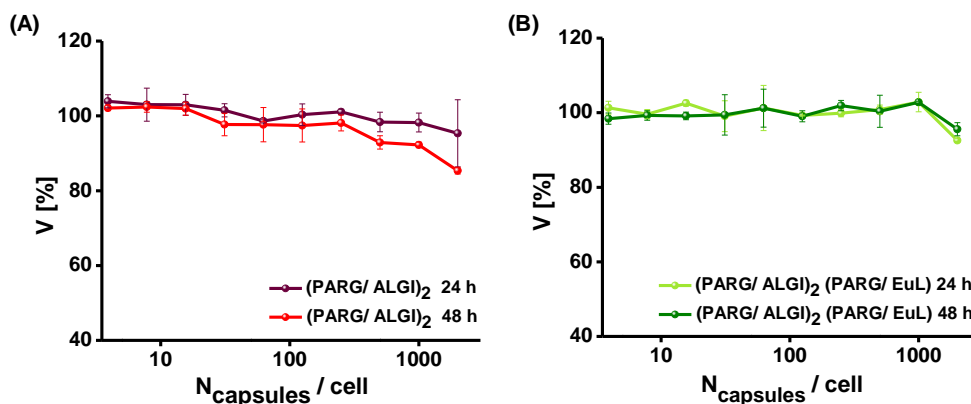


Figure 31. Biocompatibility study of curcumin-loaded biodegradable capsules. HeLa cells were incubated with various numbers capsules per cell ($N_{\text{capsules/cell}}$) in serum-supplemented media for $t = 24$ h and 48 h. Cell viability V was assessed using the

resazurin assay, for (A) $(\text{PARG}/\text{ALGI})_2$ and (B) $(\text{PARG}/\text{ALGI})_2(\text{PARG}/\text{EuL})$ capsules. Results are presented as percent of cell viability V [%] (mean \pm SD) from three independent experiments.[86]

5.1.6 Uptake studies of the capsules

Taking advantage of the intrinsic fluorescence of curcumin, uptake studies of curcumin-loaded biodegradable capsules were conducted in HeLa cells by flow cytometry and CLSM. Flow cytometry is a commonly used strategy to monitor and quantify internalization of particles by cells[99], [82], [100]. Briefly, different concentrations of $(\text{PARG}/\text{ALGI})_2$ and $(\text{PARG}/\text{ALGI})_2(\text{PARG}/\text{EuL})$ capsules (exposure concentrations $N_{\text{capsules}}/\text{cell}$) were exposed to HeLa cells for $t = 24$ h and 48 h in serum-supplemented medium. After exposure, the curcumin fluorescence I_{cur} in the cells was monitored. The internalization studies by flow cytometry indicated that capsules were uptaken in a dose dependent manner (*c.f.* Figure 32). Notably, time (24 versus 48 h) did not influence the uptake results, which might be due to cell proliferation. Moreover, the internalization of $(\text{PARG}/\text{ALGI})_2(\text{PARG}/\text{EuL})$ capsules reached a plateau as seen in Figure 32B, which was not observed for $(\text{PARG}/\text{ALGI})_2$ capsules (fig 32A). In addition, we also monitor the uptake by CLSM (*c.f.* Figure 33). For that, cells exposed to capsules at the concentration of 50 capsules/cell for 24 h. Co-localization studies were conducted and revealed that the majority of the capsules were found in the lysosomal compartments as shown by the Manders' coefficient m_1 . [99] The results indicate that $(\text{PARG}/\text{ALGI})_2$ capsules are slightly higher internalized than the $(\text{PARG}/\text{ALGI})_2(\text{PARG}/\text{EuL})$ capsules. Those results agree and complement the flow cytometry studies.

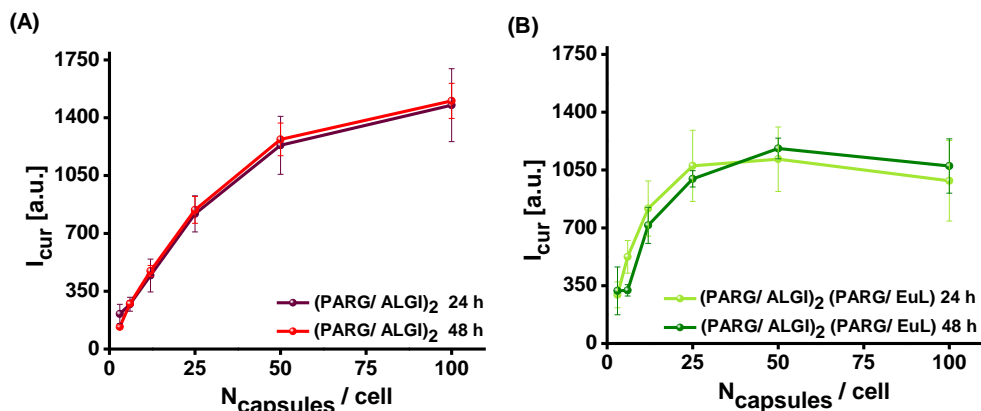


Figure 32. Uptake study of curcumin-loaded biodegradable capsules. HeLa cells were exposed to different concentrations of capsules ($N_{\text{capsules/cell}}$) for $t = 24$ h and 48 h in serum-supplemented medium. (A) $(\text{PARG}/\text{ALGI})_2$ capsules. (B) $(\text{PARG}/\text{ALGI})_2(\text{PARG}/\text{EuL})$ capsules. Cells were then analyzed by flow cytometry and the mean curcumin fluorescence I_{cur} in cell was determined. Data were derived from the curves shown in Figure 23 and represent (mean \pm SD) from three independent experiments.[86]

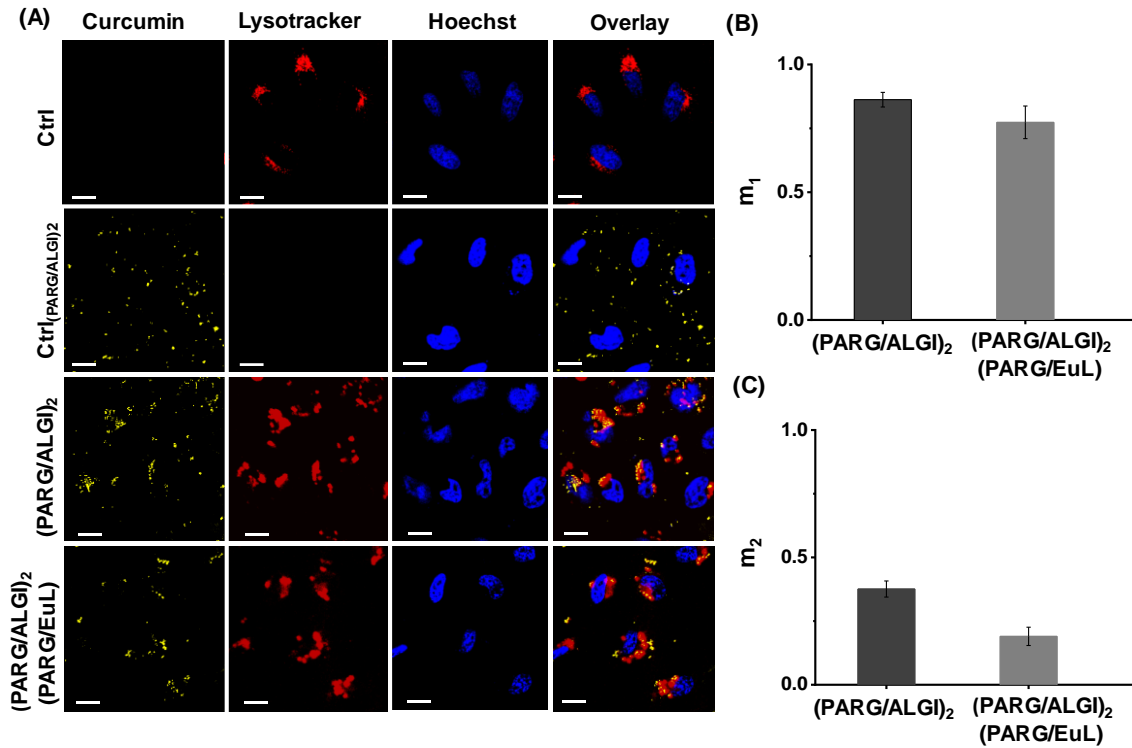


Figure 33. (A) CLSM images of cells exposed to $(\text{PARG}/\text{ALGI})_2$ and $(\text{PARG}/\text{ALGI})_2(\text{PARG}/\text{EuL})$ capsules for 24 h along with controls at 50 capsules/cell added. LysoTracker-red-DND-99 and Hoechst were used for lysosome and nucleus staining respectively. Ctrl and Ctrl $_{(\text{PARG}/\text{ALGI})_2}$ are cells without capsules added and cell with capsules added but without membrane staining, respectively. (B, C) Quantification of Manders' coefficients m_1 corresponding to the fraction of capsules in colocalization with lysosomes and m_2 corresponding to the fraction of lysosomes in colocalization with

capsules. Around 40 cells were analyzed from two independent experiments. Scale bars corresponds to 20 μm . [86]

5.2 pH-sensor capsule - a reporter of PEI-mediated Lysosomal pH change and capsule trafficking

5.2.1 Synthesis and characterization of pH sensor capsule

In our study, four different types of pH sensitive capsules were prepared loaded with a pH sensitive fluorophore, SNARF. A detailed description of synthesis is reported in experimental section. In brief, SNARF conjugated to high mol wt. dextran (170 kDa) was loaded into CaCO_3 particles by co-precipitation method. An alternative polymer layer of PAH/PSS was added, leading to the final architecture of $(\text{PAH}/\text{PSS})_4\text{PAH}$ and $(\text{PAH}/\text{PSS})_4$ which will be further designated as (+) capsule and (-) capsule respectively. In order to quantify lysosomal pH, change due to proton sponge effect of PEI, BPEI (25 kDa) was selected to make layers of capsule. Two partially biodegradable capsules with 3 BPEI layers in-between (PEI capsule) and 2 PEI layers including one end layer of PEI (PEI-end capsule) were synthesized. For making PEI capsule, 1st 2 layers of PAH/PSS were added followed by 3 bi layers of (PEI/DEX) and final layer of PARG, making final structure of $(\text{PAH}/\text{PSS})(\text{PEI}/\text{DEX})_3\text{PARG}$. In case of PEI-end capsule initial 3 bilayers were prepared with PAH/PSS, along with 3 layers of PEI/DEX/PEI, giving rise the structure of $(\text{PAH}/\text{PSS})_3(\text{PEI}/\text{DEX})\text{PEI}$. Finally, the inside CaCO_3 core was destroyed by EDTA, which leads to formation of SNARF loaded hollow capsule system of varying polymer layers. In this study, (+) and (-) capsules without any PEI layers were used as control. Confocal images of all different capsules of 4-5 μm in size are shown in (fig 34. A, E, I, M). The successful addition of alternate layers of opposite charge and the final charge of all capsules were confirmed by measuring their zeta potential values (fig 34 (B,C); (F,G); (J,K); (N,O)). The capsules show charge variation due to difference in final layer. (+) caps, (-) caps, PEI-caps and PEI-end caps have final charge of +10.09, -35.2, +7.6 and +10.14 mV respectively. Some variations in SNARF fluorescence intensity for different capsules was observed (fig 34 D, H, L, P). The (+) caps, PEI caps and PEI-end caps were synthesized from same CaCO_3 core loaded with SNARF whereas (-) caps was prepared from a separate batch. The more fluorescence of (-) capsule can be attributed for synthesizing capsules from different batches of CaCO_3 cores. Both (+)

caps and PEI-end caps showed almost similar fluorescence intensity whereas little lower intensity was found from PEI caps. This is because, during synthesis, after addition of EDTA a loss of fluorophore from PEI capsule observed.

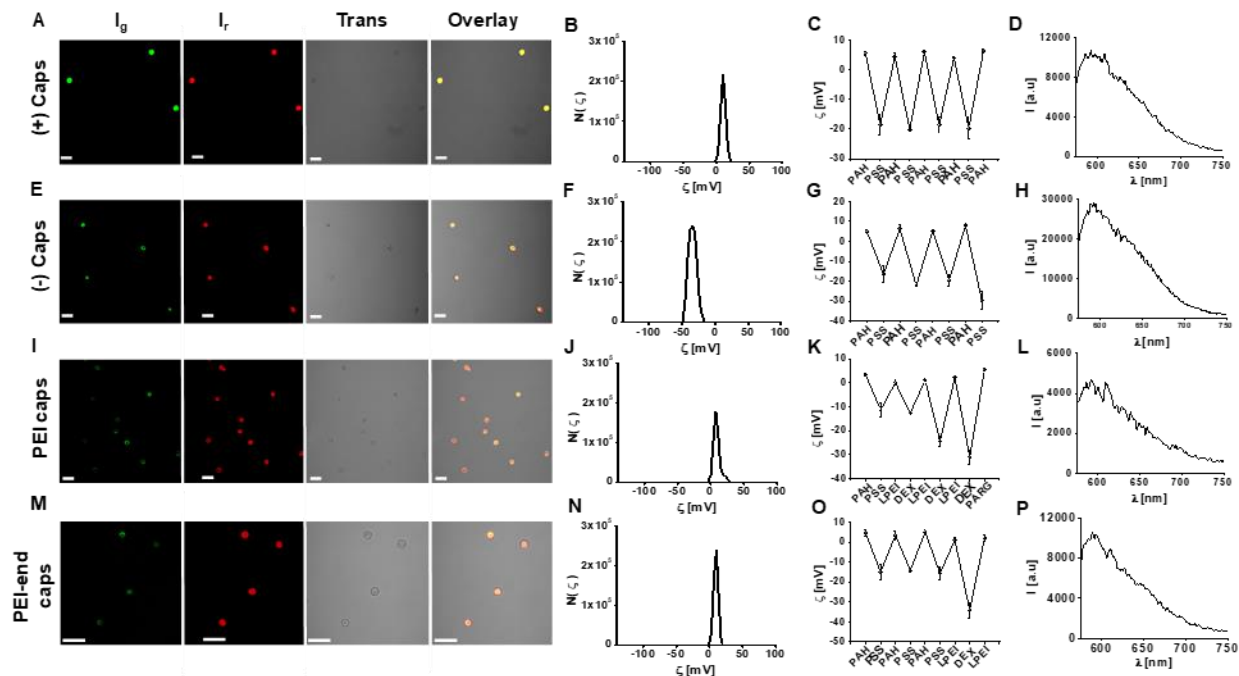


Figure 34: Characterization of SNARF loaded (PAH/PSS)4 PAH capsule [(+) caps], (PAH/PSS)4 capsule [(-) caps], (PAH/PSS)(PEI/DEX)3 PARG capsule (PEI caps) and (PAH/PSS)3(PEI/DEX) PEI capsule (PEI-end caps). (A- P) corresponds to Confocal images, zeta potential of final capsule & different layers during synthesis and fluorescence spectra of SNARF inside (+) capsule (A,B,C, D), (-) capsule (E, F, G, H), PEI capsule (I, J, K, L) and PEI-end capsule (M, N, O, P) respectively. Scale bar in each image corresponds to 10 μm.

5.2.2 pH dependence of different pH sensor capsules

All different capsules were loaded with pH-sensitive dye SNARF. The SNARF conjugated to dextran cannot pass through the capsule but capsule layers are

highly permeable to different ions in surrounding environment. Therefore, all capsules showed a pH dependent change in fluorescence property. In acidic environment, it gives more green ($I_g = I_{580}$) and less red ($I_r = I_{640}$) fluorescence whereas it becomes reverse in alkaline condition. Therefore w.r.t different pH the intensity ratio of red and green fluorescence (I_r / I_g) changes which allows us to monitor pH changes inside cell under various conditions. In fig19, pH dependent calibration curve of all capsule outside cell immersed into different pH buffers are shown. Fluorescence was measured by FACS and fluorescence spectroscopy. The pH dependent calibration curve of capsule inside cell after exposure to different pH buffers prepared by FACS analysis. The dot plot of I_r vs I_g for 4 different capsules inside cell, immersed into different buffer solutions (pH 4- 7.5) has been presented in figure 35 and corresponding pH calibration curve of each capsules are shown in figure 36

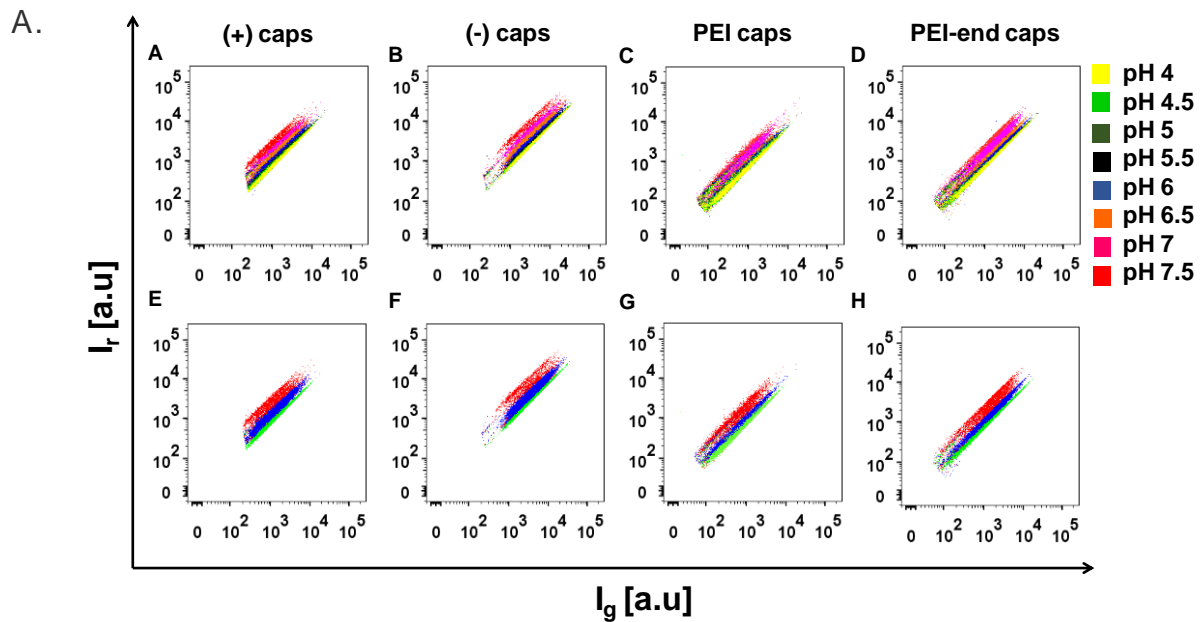


Figure 35: 2D density plots of the events recorded with FACS for 4 different capsules internalized into cells and incubated in different buffer solutions. (A- H) represents density plot of the red (I_r) and green (I_g) fluorescence signals. Each recorded event is shown as a point in the diagram. (A, E), (B, F), (C, G), (D, H) corresponds to fluorescence from 4 different capsules, (+) capsule, (-) capsule, PEI capsule, PEI-end

capsule respectively, exposed to cell for 24 h and then immersed into different buffer solutions containing nigerisin and monensin to equilibrate with buffer Ph. (E, F, G, H) Represents 2D density plots of fluorescence signals at 3 different pH (pH 7.5, pH 6 and pH 4.5), which has been used as a reference for gating lysosome, endosome and extracellular part of cell.

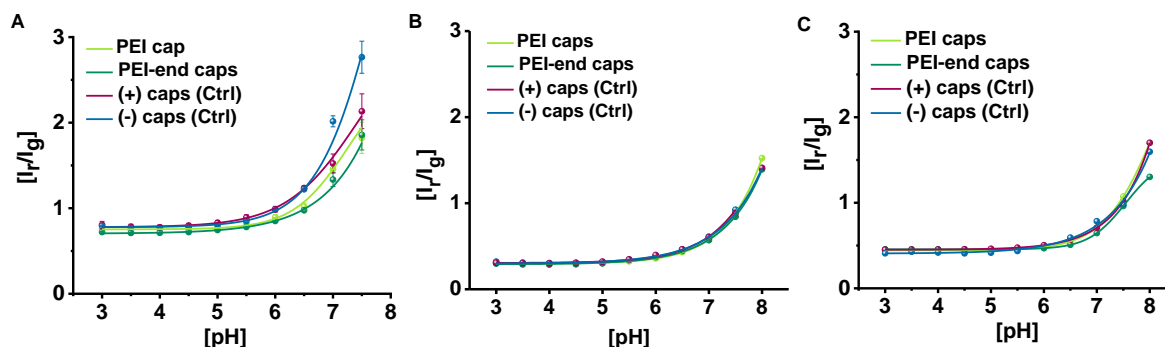


Figure 36: (A, B, C) pH Calibration curves of 4 different pH sensitive capsules, (+)/ (-) caps (Ctrl), PEI and PEI-end caps as measured by Flow cytometry (A, B) & Fluorimeter (C). (A) represents pH calibration curve of capsules inside cell after 24h and (B, C) represents pH calibration curve of capsules only. The ratio of green to red fluorescence intensity (I_r/I_g) versus the pH of different buffer solutions has been plotted in which the capsules were dispersed.

Therefore, in the CLSM image (overlay image) of capsules after exposed to the cell, capsules showing more green fluorescence correspond to that inside endolysosome and more red fluorescence represents, that are outside cell or adherent to the cell, which means exposed to alkaline cell medium, (see fig 37). In general, capsules are internalized by cell through endocytosis process; initial attachment to the cell surface followed by intracellular entry into early endosome, late endosome and finally ends up into lysosome. Along this pathway, pH around capsule varies from alkaline, to acidic. Therefore, trafficking pathway of each capsule into different intracellular compartments can be track by monitoring ratio-metric change in fluorescence readout from pH sensitive capsules.

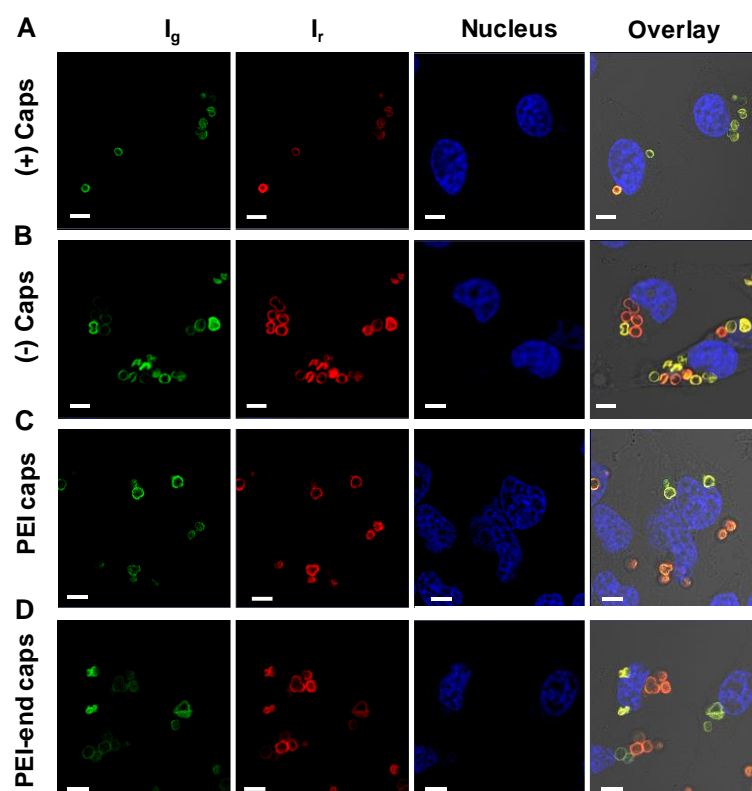


Figure 37: Confocal images of 4 different SNARF loaded pH sensitive capsules, (PAH/PSS)4PAH capsule [(+) caps] (A), (PAH/PSS)4 capsule [(-) caps] (B), (PAH/PSS)(PEI/DEX)3 PARG capsule [PEI caps] (C) and (PAH/PSS)3(PEI/DEX) PEI capsule [PEI-end caps] (D), inside cell after 24h exposure. HeLa cells were exposed to 15 capsules/ cell concentrations of different capsules for 24h. Nucleus was stained with Hoechst. Scale bar in each image corresponds to 10 μ m.

5.2.3 Cytotoxicity of different pH sensor capsules

Biocompatibility study of different capsules were performed by simple toxicity assay i.e. resazurine assay which determines cytotoxicity depending upon mitochondrial activity of viable cell. Cell viability study of different capsules showed both (+) and (-) capsules were nontoxic at 120 caps/ cell concentrations after 48h exposure. However, due to addition of PEI layers, PEI and PEI-end capsules were found more toxic to the cell (See fig.38). Therefore, for all capsules 15 caps/cell concentration was chosen as maximum concentration at which almost no toxic effects happened.

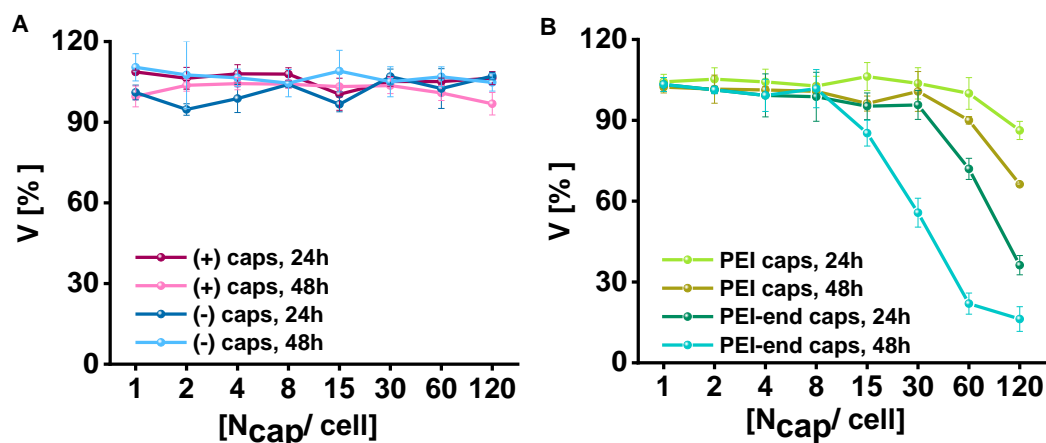


Figure 38: Biocompatibility studies of SNARF loaded (PAH/PSS)4PAH capsule [(+) caps], (PAH/PSS)4 capsule [(-) caps] (A) and (PAH/PSS)(PEI/DEX)3 PARG capsule (PEI caps) , (PAH/PSS)3(PEI/DEX) PEI capsule (PEI-end caps) (B) for 24h and 48h exposure time. HeLa cells were exposed to different capsules with a concentration range of (120-1) capsules/ cell in serum-supplemented media for 24 and 48 h separately. Results are presented as percent of cell viability V [%] (mean value) from three independent experiments.

5.2.4 Understanding the Intracellular trafficking of pH-sensor capsules by FACS

The study of capsule uptake process i.e. intracellular trafficking and intracellular pH measurement were performed by Flow cytometry (FACS) as it allows high throughput and highly quantitative analysis. For uptake study, different pH sensitive capsules exposed to Hela cells at two different concentrations (15 and 7 capsules/ cell) and internalization of capsules monitored over time. For analyzing Flow cytometry data for each sample, the first step is to isolate single cell population from cellular debris, dead cells and doublets. The two-dimensional (2D) density plots of the forward-scattering width (FSC-W) vs forward-scattering area (FSC-A) signals, for detected events of untreated HeLa cell (cell without capsule) has been shown in Figure 39A. Low forward scattering FSC-W corresponds to cellular debris and dead cells whereas high FSC-A signals represents cell doublets or clumps. Single cell population in gated region were

backgated onto forward-scattering (FSC) vs side scattering (SSC) plot. The fluorescence signals of pH sensitive SNARF capsules inside cell are shown in figure 39B as a dot plot of red vs green fluorescence signals (I_r vs I_g) as measured by FACS. Fluorescence of cell with capsule is highly distinct from fluorescence of cell without capsules. Low fluorescence signal (lower-right quadrant) corresponds to the cell without capsule and High fluorescence (I_r and I_g) shows cell with capsule.

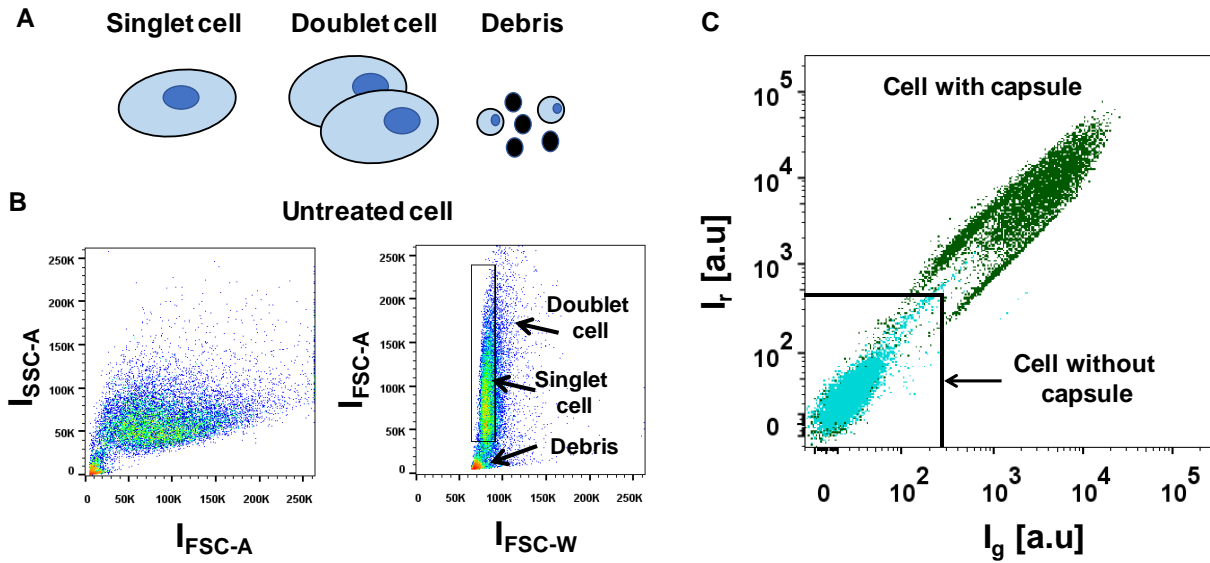


Figure 39: Gating strategy for distinguishing events for single cell interaction in FACS data. (A) Different types of cell present in a single cell population for FACS analysis. (B) Density plot of the side scattering intensity (I_{SSC-A}) vs forward scattering intensity (I_{FSC-A}) for untreated cell (cell without capsule), after gating. The isolated single cell population from doublet and debris is shown in density plot of the I_{FSC-A} vs I_{FSC-W} . Here A and W corresponds to area and width of signal. (C) Single cell-population density plot of cell with capsule and cell without capsule, after gating, represented as red intensity (I_r) vs green intensity (I_g) of SNARF capsule. Population of Cell containing capsule is highly distinct from the cell without capsule.

The fluorescent population of cell with capsule was divided into three quadrants. The local pH of capsules adherent to cell surface are in alkaline environment due to alkaline pH of PBS buffer (pH 7.4), whereas capsules inside cell are in acidic endosome (pH 5-

6) or lysosome (pH 4.5). The fluorescence cell population in pH calibration curve at pH 7.5, 6 and 4.5 are distinct from each other (see figure 35 E, F, G, H). Therefore, these populations in corresponding buffer solutions has been used as a reference for isolating extracellular (pH 7.5), endosome (pH 6) and lysosome (pH 4.5) compartments of cell. Therefore, in this way we will get four distinct percentage of cell, three numbers for cell having capsules in different compartments (extracellular, endosome, lysosome) and one number for cell not having capsule. It can be depicted as % of Cell_{w caps (in extra)}, % Cell_{w caps (in endo)}, % Cell_{w caps (in lyso)} and % cell_{w/o caps} respectively.

The % cell_{w/o caps} (red population) decreases over time, followed by increase in % Cell_{w caps (in endo)} (blue population) and % Cell_{w caps (in lyso)} (green population). Thus, relative capsule uptake into different compartments of cell can be quantify by the formula¹.

$$\text{Relative capsule uptake (RCU)} = (N_{\text{cell w caps (in X)}} / N_{\text{total}}) \times 100 \quad \dots\dots\dots (1)$$

Here, N_{cell w caps (in X)} corresponds to number of cell with capsule in x compartment, where x can be extracellular, endosome or lysosome compartment.

N_{total} is the summation of number of cell with capsule and without capsule. The 2D density plot of the red (Ir) vs green (Ig) fluorescence signals for uptake of four different capsules, (+) capsule, (-) capsule, PEI capsule and PEI-end capsule, over time presented in figure 40.

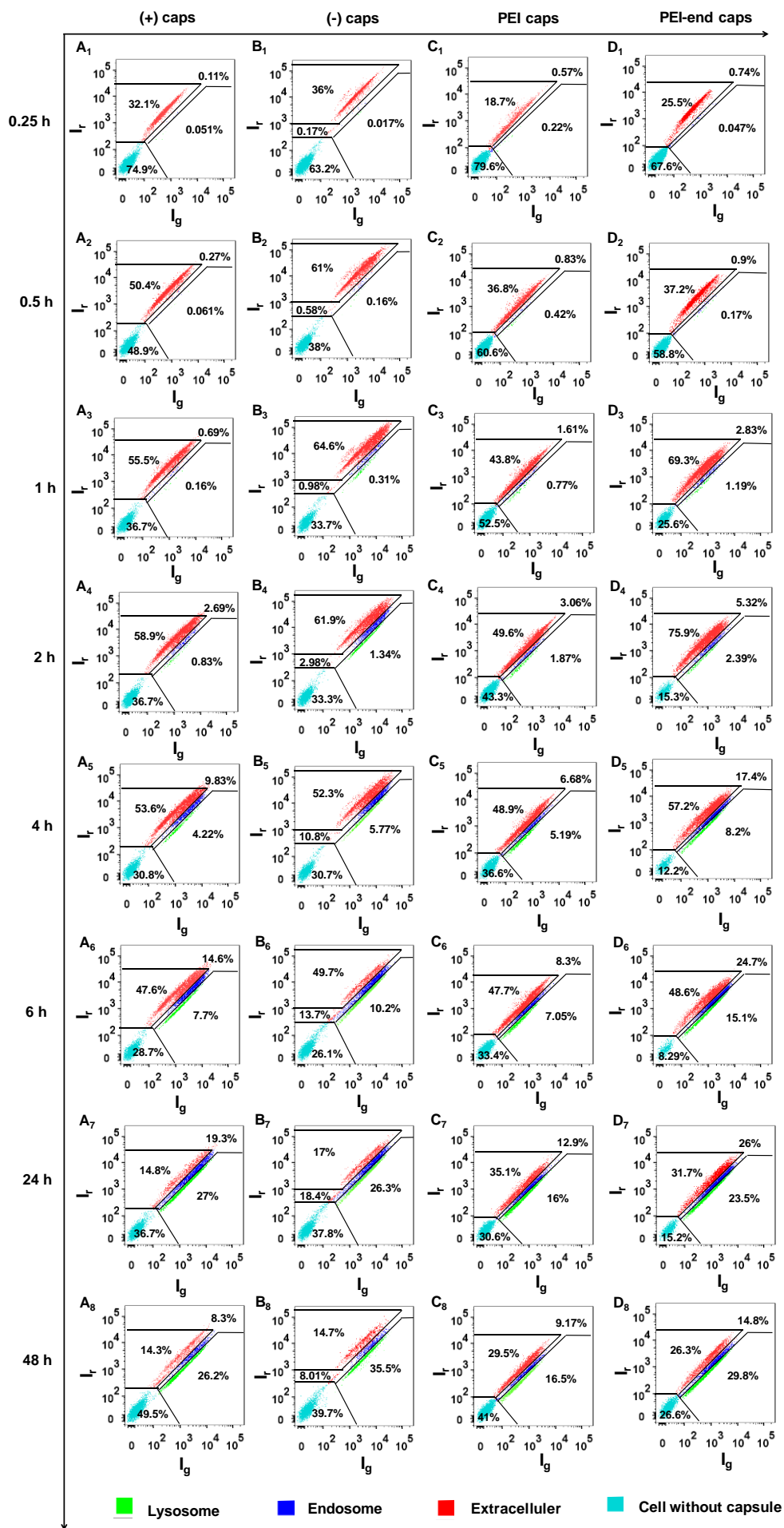


Figure 40: 2D density plot of the red (Ir) and green (Ig) fluorescence signals recorded with FACS for uptake of 4 different capsules. (A1-8, B1-8, C1-8, D1-8) represents percentage of different capsule uptake, (+) capsule (A1-8), (-) capsule (B1-8), PEI capsule (C1-8) and PEI-end capsule (D1-8) over time. Here 15 capsule/ cell concentrations of each capsules were exposed to HeLa cell for 0.25, 0.5, 1, 2, 4, 6, 24, 48 hrs. For separating uptake of capsules at lysosome, endosome and extracellular part (adherent capsules), fluorescence population (Ir vs Ig) in 2D dot plot at pH 4.5, 6 and 7.5, of each capsule, has been used as reference for gating respectively. The percentage of cell without capsule are also presented here.

Figure 41 shows relative capsule uptake (RCU) of (+) and (-) capsules, PEI capsule and PEI-end capsule into HeLa cell. FACS experiments were done as explained in the experimental section. The % of Cell_w caps (in extra) goes on increasing up to initial 2h of capsule exposure for all different capsules. So, % of Cell_w caps (in extra) reaches maximum value of $\approx 70\%$ for (+) and (-) capsule, $\approx 75\%$ for PEI-end capsule after 2h whereas it reaches to $\approx 80\%$ for PEI capsule after 1h exposure. During this period, % Cell_w caps (in endo) and % Cell_w caps (in lyso) are very low. It means almost all capsules attaches to the cell membrane by that time and it gradually enters into cell over time. After 48h, for (+) and (-) capsule, only $\approx 10\%$ capsules remain attached to the cell surface. Although at that time, % of Cell_w caps (in extra) for PEI caps and PEI-end caps were found $\approx 45\%$ and 50% respectively. After 2h almost for every capsules, % Cell_w caps (in endo) and % Cell_w caps (in lyso) increases, this is $\approx 6-10\%$ and $\approx 3-4\%$ respectively for all capsules. A maxima of % Cell_w caps (in endo) was found for (+) and (-) capsule after 6h, that is $\approx 22\%$ and $\approx 25\%$ respectively. Finally, it gradually decreases leading to increase in % Cell_w caps (in lyso) which reaches $\approx 40-45\%$ after 48h. However, in case of both PEI caps and PEI-end caps % Cell_w caps (in endo) and % Cell_w caps (in lyso) were found $\approx 18\%$ and $\approx 20\%$ respectively, after 48 h. That means sum of RCU (%) in endosome and lysosome is $\approx 35-45\%$ for all 4 types of capsules. In case of (+) and (-) capsules, most of the endosomes mature into lysosome after 48h, showing a decrease in % Cell_w caps (in endo) and increase in % Cell_w caps (in lyso). Whereas for PEI and PEI-end capsule, an inhibition in

endosome to lysosome maturation can be observed, which leads to gradual increase in both % Cell_w caps (in endo) and % Cell_w caps (in lyso). This phenomenon can be attributed to the fact that, due to buffering capacity of PEI layers present in PEI and PEI-end capsules, maturation of endosome to lysosome is delayed. Similar trend in RCU of different capsules was observed for concentration of 7 caps/ cell, showing low value of % Cell_w caps (in endo) and % Cell_w caps (in lyso) compare to the values for 15 caps/ cell. (See figure 24)

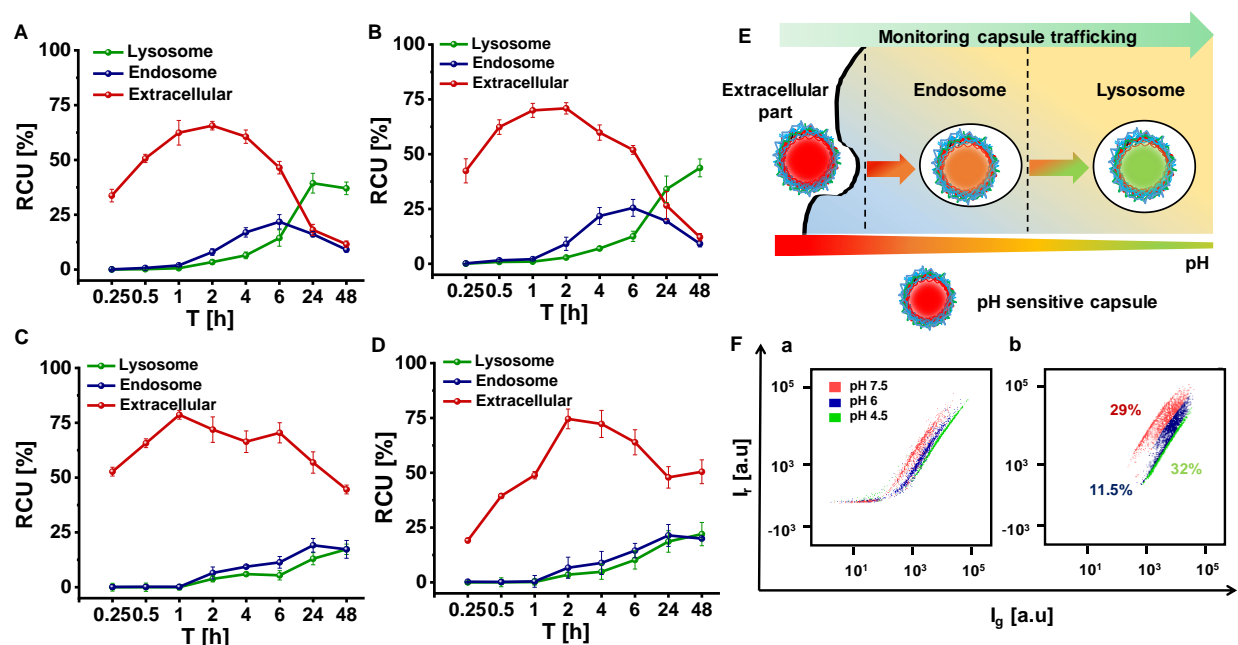


Figure 41: (A, B, C, D) represents percentage of relative capsule uptake (RCU) of different capsules, (+) capsule (A), (-) capsule (B), PEI capsule (C) and PEI-end capsule (D) over time. Here 15 capsule/ cell concentrations of each capsules were exposed to Hela cell for maximum 48 hrs. (E) Corresponds to a schematic of monitoring capsule trafficking process. (Fa) Represents fluorescence intensity measured by FACS from (+) pH sensitive capsule inside cell at different pH (4.5, 6 and 7.5) buffers. After 24h caps exposure, cells with internalized capsules were immersed into different buffers containing inophores (monensin and nigerisin) for equilibrating intracellular and extracellular buffer pH. For separating uptake of capsules at lysosome, endosome and extracellular part (adherent capsules), pH 4.5, 6 and 7.5 has been used as reference

gate respectively. (Fb) Corresponds to FACS data of relative capsules uptake into lysosome, endosome and extracellular part after 24h for (+) capsule.

5.2.5 Monitoring intracellular pH by different pH–sensor capsule

According to well accepted ‘proton sponge effect’, PEI is able to increase lysosomal pH, although experimental proof about this fact yet to be discover. Therefore, measuring lysosomal pH by different pH sensor capsules can reveal valuable information about this hypothesis. As explained earlier, PEI layers of PEI and PEI-end capsules will act as PEI source inside lysosome and corresponding local pH will be measured by monitoring pH dependent fluorescence change of SNARF embedded in each capsule. Two capsules, (+) and (-) pH sensor capsule without any PEI layers are used as control sensor in each independent experiment. To quantify local pH around each capsule, pH dependent calibration curve of respective capsule inside cell used. All these studies performed by FACS as described in experimental section. In each experiment, our positive control is chloroquine (Cq) which can increase lysosomal pH. Chloroquine is a lysosomotropic substance that can pass through cell as non-protonated form and gets protonated under acidic environment inside lysosome. It can increase lysosomal pH by blocking proton-pump activity in lysosome. In order, understand how our analysis by FACS correlates the variation in lysosomal pH to RCU in different intracellular compartments, different Cq concentration were exposed to cell for 4h. Here, I need to mention Cq was exposed after 24h internalization of pH-sensor capsule into cell. In figure 42A, pH of three different compartments i.e., pH_{extra} , pH_{endo} , pH_{lyso} are compared after Cq exposure with control sample. Here (+) pH sensor capsule used for monitoring Ph. The cell not exposed to Cq but exposed to sensor capsule used as control. A definite change in lysosomal pH from 4.5 (Ctrl) to 5.3 (Cq, 50 μ M) was observed whereas no significant change was found in pH_{extra} and pH_{endo} . However, distinct decrease in %cell_{w caps (in lyso)} and relative increase in %cell_{w caps (in endo)} and %cell_{w caps (in extra)} compare to control, has been observed w.r.t varying concentrations of Cq exposure for 4h (fig42B). The %cell_{w caps (in lyso)} decreased from 40 % (Ctrl) to 1.2 % (Cq, 50 μ M, 4h), %cell_{w caps (in endo)} increased from 6% (Ctrl) to 24% (Cq, 50 μ M , 4h) and %cell_{w caps (in extra)} also increased from 23.5% (Ctrl) to 48% (Cq, 50 μ M , 4h). The 2D dot plot of I_r vs I_g of cell_{w caps} exposed to Cq also shows a shift in cell fluorescence (Compare green

population in fig 42 C and D) i.e. decrease in %cell_{w caps} (in lyso) and shift towards red intensity in presence of Cq.

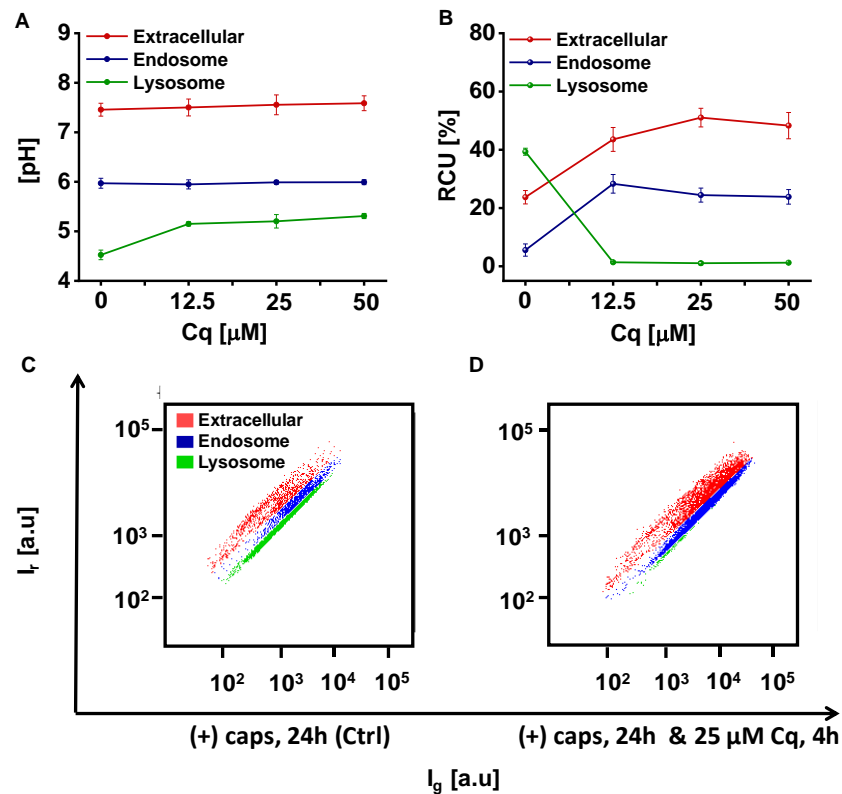


Figure 42: (A) Monitoring pH of different intracellular (lysosome & endosome) and extracellular compartments after exposing different concentrations of chloroquine (Cq) by pH sensitive (+) capsule. (B) Represents percentage of relative capsule uptake (RCU) of (+) capsule due to chloroquine (Cq) exposure for 4h. Here 15 capsule/ cell were exposed to HeLa cell for 24hrs and then different concentrations of chloroquine were exposed to the cell for 4h. (C) Represents fluorescence intensity of cell after internalization of capsule as measured by FACS. (D) Corresponds to FACS data of fluorescence intensity change for capsules uptake into lysosome, endosome and extracellular part due to 4h 25 μ M chloroquine exposure.

Data resulting from 4 different capsules exposure at two different concentrations (15 and 7 caps/ cell) and related pH_{extra} , pH_{endo} , pH_{lyso} as calculated from respective calibration curves of each capsules are presented in figure 43. The pH was monitored over time and for each capsule 25 μM Cq exposed to cell was used as positive control at each time points. All pH analysis, as well as capsule trafficking analysis, were performed from independent pH calibration curve of different capsules (after 24h capsule exposure), prepared at each individual experiment. For PEI and PEI-end capsules, exposure at 15 caps/ cell concentration, a slight difference in pH_{lyso} (ΔpH_{lyso}) can be observed even after 2h which increases more after 24 and 48h compare to (+) and (-) capsules (control). The pH_{lyso} as measured by (+) caps and (-) caps after 6h caps internalization is 5.1 and 4.9 respectively whereas by PEI and PEI-end capsules it was reported as 5.37 and 5.67 respectively. After 24h, the pH_{lyso} reported by (+) caps, (-) caps, PEI and PEI-end capsules was 4.7, 4.8, 5.26 and 5.47 respectively. (See fig 43A)

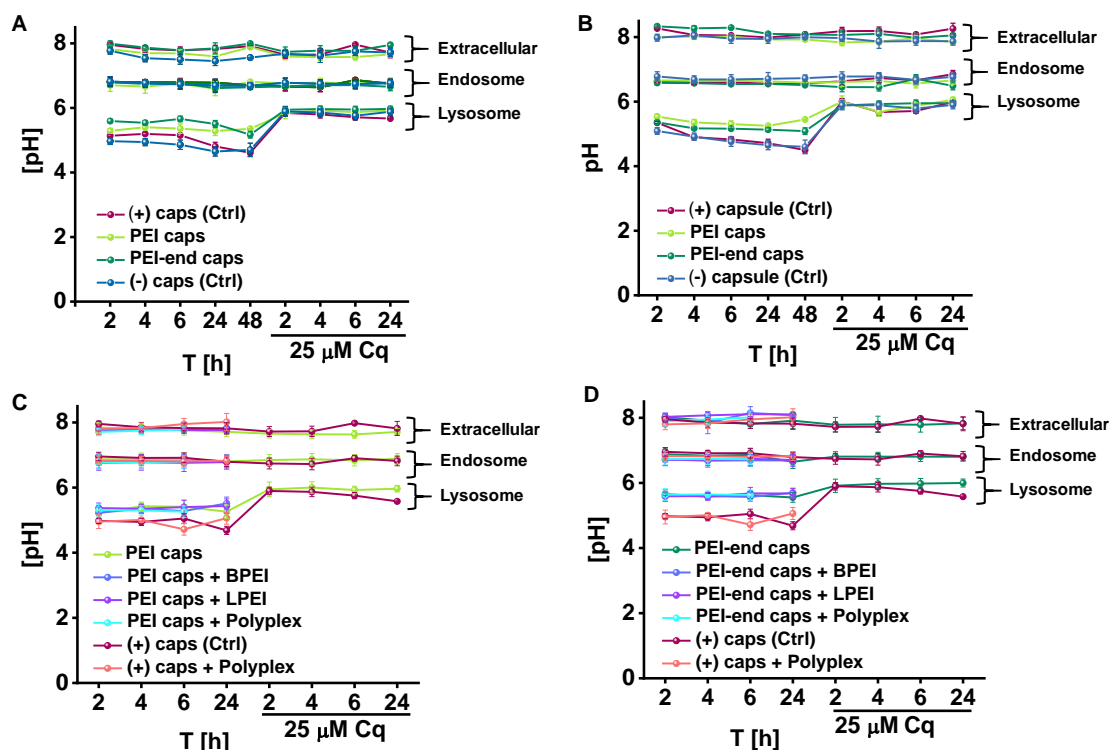


Figure 43: (A, B) Monitoring pH change of intracellular (lysosome & endosome) and

extracellular parts over time due to PEI, using 4 different pH sensitive capsules, (PAH/PSS)4PAH capsule [(+) caps], (PAH/PSS)4 capsule [(-) caps], (PAH/PSS)(PEI/DEX)3 PARG capsule (PEI caps) and (PAH/PSS)3(PEI/DEX) PEI capsule (PEI-end caps). Different capsules exposed at 15 caps/ cell (A) & 15 caps/ cell (B) concentration to the HeLa cell. (A) Represents change in lysosomal pH due to 3 PEI layers at PEI capsule and 2 PEI layers at PEI-end capsule. (+)/ (-) capsule used as control (Ctrl). (C, D) corresponds to quantification of cellular pH values due to further exposure of BPEI 25 kDa, LPEI 20 kDa and PEI-plasmid polyplex. After 24h exposure of PEI capsule, (+) capsules (C) and PEI-end capsule, (+) capsules (C), 200 nM BPEI (25 kDa), 300 nM LPEI (20 kDa) and polyplex were exposed. Here (+) capsule was used as a control. In all study (A, B, C, D) chloroquine (Cq) was used as a positive control. 25 μ M chloroquine was exposed for 2, 4, 6 and 24h after 24h exposure of different capsules.

Similar result was found in pH analysis with 7 caps/ cell concentration, Δ pH_{lyso} becomes significant after 6h followed by reaching maximum after 48h (see fig 43B). Although, we can see little variation in pH values of lysosome reported by (+) and (-) capsule. Here, our major concern was to observe whether pH_{lyso} changes because of PEI layers and the pH analysis is based on pH-calibration curve of respective pH-sensor capsules. All the 4 capsules are able to quantify Δ pH_{lyso} in presence of Cq also. Therefore, we should always consider this pH determination as relative analysis not absolute measurement.

In order to look into lysosomal pH variation as reported by different capsules in more details, intensity ratio (I_r/ I_g) at lysosomal compartment in FACS data plotted over time and compared with their respective pH calibration curve. A decreasing plateau in pH_{lyso}, of HeLa cell observed over time reported by all capsules (figure 44 B, D, F, H). For (+) and (-) capsule pH_{lyso} varies between \approx (5.2-4.7) whereas for PEI and PEI-end capsule it was found between \approx (5.5-5.3) within 2 to 48h time window. In a recent study on lysosomal pH using quantitative ratio metric fluorescence microscopy, reported 'peripheral lysosomes are less acidic than juxtanuclear ones despite their comparable buffering capacity'. The reduced acidifying ability of peripheral lysosomes is a result of

an increased passive (leak) permeability to protons, together with reduced vacuolar H⁺-adenosine triphosphatase (V-ATPase) activity. Therefore, a plausible reason for decreasing trend in pH_{lyso} over time could be trafficking of internalized capsules containing lysosome from peripheral site to juxtannuclear site. The increased pH_{lyso} due to exposure of Cq as measured by (+) and (-) pH-sensor capsule was \approx (5.5-5.7). However, for the same Cq exposure, PEI and PEI-end capsule reported the pH_{lyso} as \approx 5.8 (see, figure 44 A, C, E, G). A slight higher pH reported by PEI layered capsules can be addressed to the presence of additional PEI layers in it. This additional PEI layer can further contribute to the increase in pH_{lyso} due to Cq exposure. In another experiment, all different capsules were 1st exposed for 24h and then extra BPEI, LPEI and polyplex were exposed to the cell. In figure 43 C, D, Δ pH_{lyso} among PEI, PEI-end capsule and (+) capsule can be seen but no Δ pH_{lyso} were found for further exposure of PEI or PEI-polyplex. Now, to detect any influence of PEI on lysosomal pH, it is necessary that sensor capsule should report the pH of the particular lysosome that contain PEI. Since, capsules are quite big in size compare to the simple polymer or PEI-polyplex, we suppose, there might be rare possibility of co-localization into same lysosome. Therefore, we performed co-localization study of sensor capsule, PEI and lysosome that explained in next paragraph. Nevertheless, no significant changes in Δ pH_{extra} and Δ pH_{endo} found in all experiments. This we have to address to the limitation of this analysis technique. However, in terms of RCU in different intracellular compartments, a distinct anomaly observed between control capsule and PEI layered capsules which shown in fig 41 and explained in section 5.2.5.

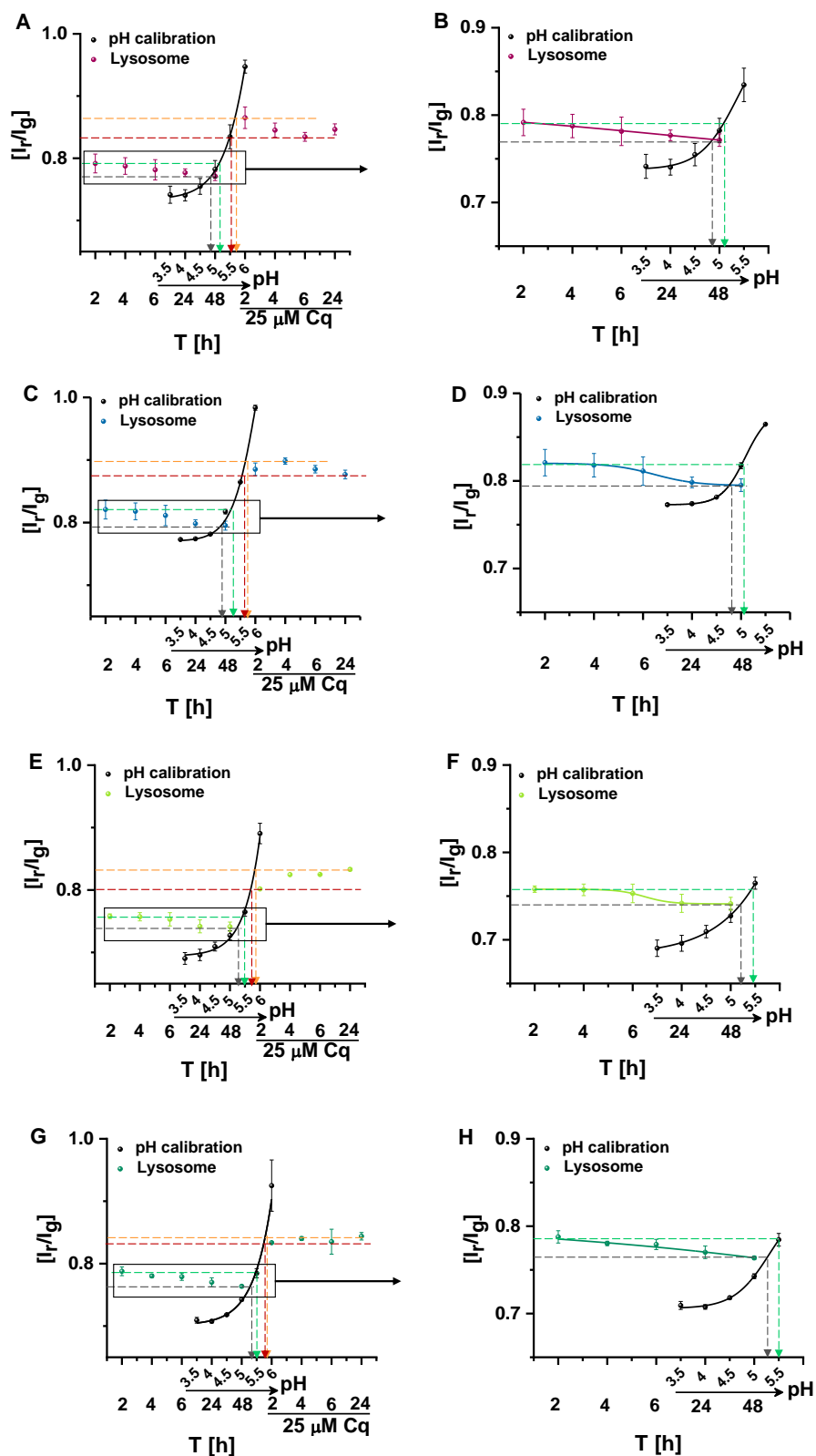


Figure 44: Lysosomal pH quantification using 4 different pH sensitive capsules,

(+) capsule (A, B), (-) capsule (C, D), PEI capsule (E, F), PEI-end capsule (G, H). Change in intensity ratio (I_r/I_g) of different capsules inside cell over time, has been plotted for each capsule and compared with their respective pH calibration curves. Calibration curves were prepared after 24h capsules exposure to the cell. Change in Intensity ratio can be seen due to further exposure of 25 μ M chloroquine (Cq) for 2, 4, 6, 24h after 24h cellular uptake of each capsules. (B, D, F, H) Corresponds to enlarged view of the lysosomal part of cell and shows time dependent decrease in lysosomal pH as found for every capsule.

5.2.6 Co-localization study of pH-sensor capsule, PEI and lysosome

The most important criteria for efficient quantification of lysosomal Δ pH is, both the sensor capsules and reagent specific for pH change should be in same lysosome. Therefore, a detailed investigation on lysosomal pH change performed with different PEI samples (BPEI 2, 25, 60 kDa and LPEI 20, 250 kDa) as mentioned in experimental section. For that, the nontoxic concentration range of different PEI samples selected from a series of dose-dependent cell viability experiments of different PEI samples (see figure 18). Since we wanted to transfer both sensor capsule and PEI into same lysosome, we designed two experimental methods. In 1st (+) caps allowed to enter into cell for 24h, followed by different PEI samples were exposed and pH_{lyso} monitored over time by FACS. Whereas, the 2nd experiment was co-exposure of capsules and PEI samples, where capsules exposed for 4h followed by exposure of different PEI samples. The reason to keep 4h interval between capsule and PEI exposure in 2nd experiment was bigger particle like capsules (5 μ m) require longer time to enter into cell than small polymer like PEI. In the same way as mentioned before, we quantified pH_{lyso} after exposure of different PEI samples. Here, control was cell exposed to caps but not PEI and positive control was cell exposed to Cq. Since lysosomal pH is also dependent upon capsule trafficking three different pH calibration curves with varying capsule exposure time (8h, 24h and 48h) used for pH analysis. For instance, pH calibration curve after 24h caps exposure used for analyzing pH_{lyso} after 24h PEI exposure. In case of 1st experiment pH_{lyso} after 24h PEI exposure was quantified with pH calibration curve after 48h capsule exposure as this corresponds to capsule internalization up to 48h. (figure 19 D, E). For each individual experiment, a set of time dependent pH calibration

curve used for analysis. In figure 20 and 45, pH_{lyso} quantified for 1st and 2nd experiments, after exposing different PEI samples with a series of concentrations, are reported. In case of (8+24)h a slight deviation from control pH_{lyso} observed for all PEI samples in figure 20. Similar phenomenon also observed for BPEI 2, 25 kDa and LPEI 250 kDa after 24h exposure in 2nd experiment (fig 45 A, B, E). However, considering the standard deviation from different experiments, this pH shift found in these studies clearly cannot be associated with change in pH_{lyso} due to PEI exposure.

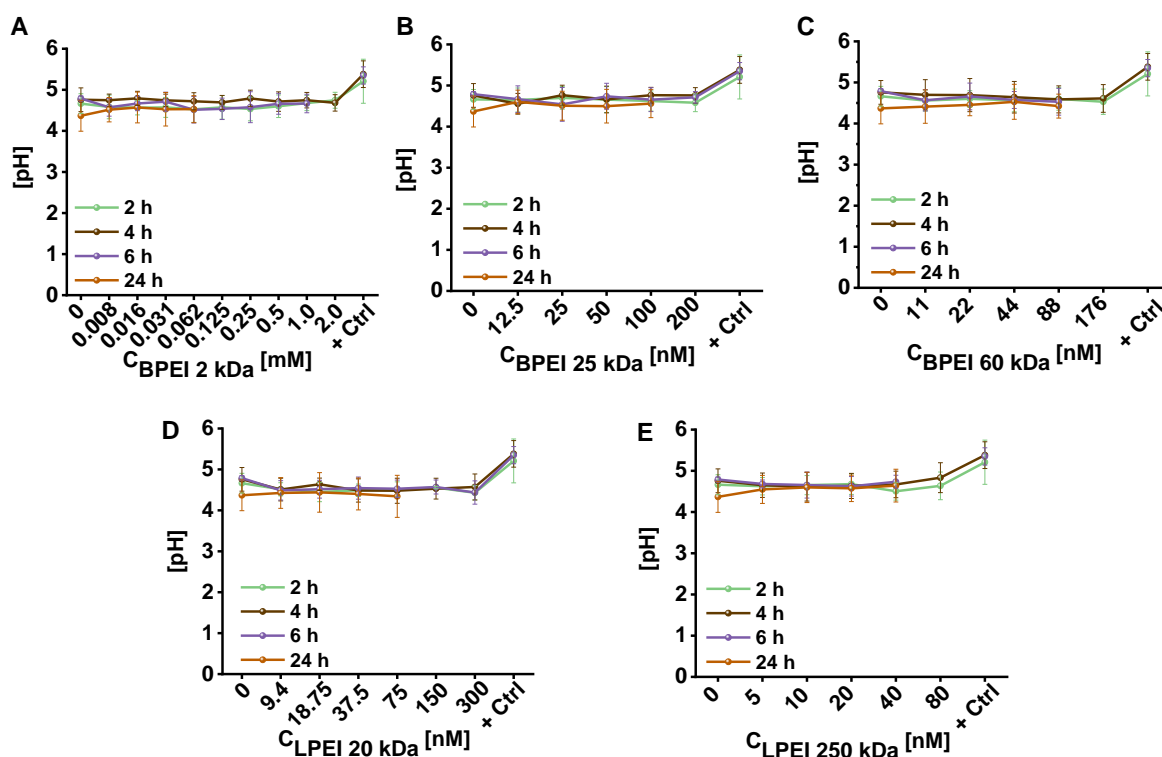


Figure 45: Lysosomal pH measurement in response to different branched (A-C) and linear (D, E) polyethylenimine (BPEI & LPEI) over time. Hela cells were allowed to internalize + ve pH sensor capsule at 15 caps/ cell in serum supplemented media for 4 h followed by exposure to series of dilutions of different PEI samples for 2, 4, 6 & 24 h. The Data point at zero corresponds to reference cell or control. As + Control (+ ctrl) 25 μ M chloroquine solution was exposed to cells for 2h, 4h and 6h. The Lysosomal pH measured from pH calibration curve of + caps inside cell. The data represents average of three independent experiments and corresponding standard deviation.

In order to confirm co-localization of pH-sensor capsule and PEI or PEI-polyplex, in same lysosome, co-localization study was performed as described in SI. Here scrambled DNA was used to make polyplex as our main aim was to see effect of PEI on pH_{lyso} . As excitation and emission spectra of SNARF covers a quite broad spectral window, we were unable to perform direct co-localization with pH sensor capsule and PEI with any labeled fluorophore. Therefore, capsule was loaded with cascade blue dextran, BPEI 25 kDa labeled with Rhodamine-B and lysosome was stained with LysoTracker-green dye. Quantification of mender's overlap co-efficient revealed very low overlap between PEI and capsule for both PEI and polyplex. (see figure 46 C, G, K). That means possibility of finding capsule and PEI, as free PEI or polyplex, into one lysosome is very low. Therefore, it can happen the pH sensor capsule is reporting the pH of different lysosome having no PEI in it or with insufficient PEI content for showing lysosomal pH change.

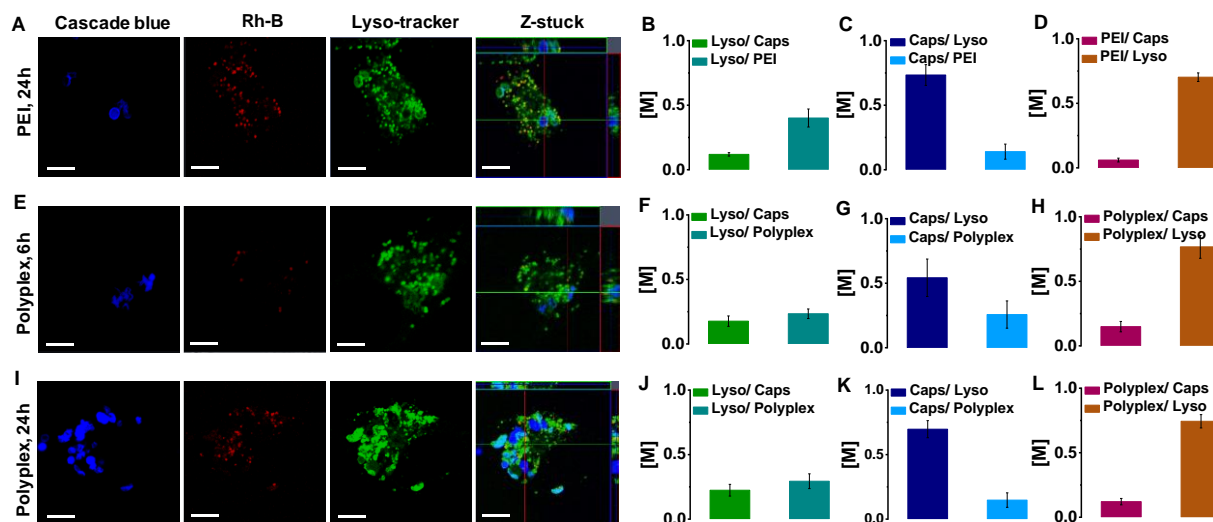


Figure 46: Confocal image of capsule, lysosome, PEI (A) & capsule, lysosome, PEI-plasmid polyplex (E, I) co-localization. PEI was labeled with Rh-B dye and capsule was loaded with cascade blue dye. HeLa cells were exposed to 7 capsules/ cell concentrations of (PAH/PSS)₄ capsules for 24h. After that PEI exposed for 24h (A) and Rh-B labeled PEI-plasmid polyplex exposed for 6 & 24h (E, I). lysosome was stained with Lyso-Tracker green. (B C, D) corresponds to mender's overlap co-efficient (M) for lysosome (lyso), capsule (caps), PEI after 24h & (F, G, H), (J, K, L) corresponds to

lysosome (lyso), capsule (caps), PEI-plasmid polyplex (polyplex) overlap after 6h and 24h respectively. (B,F, J) Overlap of lysosome with capsule & PEI or polyplex, (C,G, K) Overlap of capsule with lysosome & PEI or polyplex, (D, H, L) Overlap of PEI or polyplex with lysosome & capsule. Scale bar in each image corresponds to 10 μ m.

6. Conclusion and outlook

In summary, two application of LbL PEC has been presented, one about fabrication of a new biocompatible drug delivery system and another is about intracellular pH-sensing through PEC by high throughput analysis technique using FACS.








The presented 1st work provides an assessment of the in vitro biocompatibility, stability, and biodegradability of $(\text{PARG/ALGI})_2$ and $(\text{PARG/ALGI})_2(\text{PARG/EuL})$ capsules. Capsules were shown to be biodegradable. Hereby $(\text{PARG/ALGI})_2$ capsules degraded faster at acidic pH = 3, in contrast to $(\text{PARG/ALGI})_2(\text{PARG/EuL})$ capsules, which exhibit better stability at lower pH. However, both capsules were degraded in presence of pronase. In addition, the drug release studies indicated reverse drug release kinetics. The maximum release profile found for $(\text{PARG/ALGI})_2$ capsules occurred at lower pH, while the maximum release profile of $(\text{PARG/ALGI})_2(\text{PARG/EuL})$ capsules was found to be at physiological pH. The release kinetics showed thus that the additional EuL layer on the capsules protected the release at acidic environment. Moreover, capsules showed acceptable biocompatibility in HeLa cells. The uptake studies revealed that capsules were internalized into cells in a concentration dependent manner. $(\text{PARG/ALGI})_2$ and $(\text{PARG/ALGI})_2(\text{PARG/EuL})$ capsules thus allow for the delivery of encapsulated compounds to cells with the possibility to tune the release kinetics by the outer EuL layer.








In my second work PEC based pH-sensor was used to validate ‘proton sponge effect’ hypothesis of PEI, which is explained elaborately in introduction. Here we assessed influence of PEI on lysosomal pH by making pH-sensor PEC with additional outer layers of PEI. Comparing the pH_{lyso} as reported by PEI caps and PEI-end caps with our control sensor (+)/ (-) caps, we found a little increase in pH after 6h, which was more prominent at 24h exposure time. This analysis was performed with FACS and we demonstrated a high throughput analysis technique of intracellular pH change. Nevertheless, the uptake

studies of different pH-sensor capsule allowed us to monitor particle trafficking in terms of capsule, into different intracellular compartments (extracellular, endosome, lysosome) over time, considering the pH variation of these compartments. This analysis revealed initially 1h required for capsules attachment to the cell afterwards it starts to internalize into endosome and lysosome over time. After 24h the % Cell_w caps (in extra) decreases and % Cell_w caps (in endo) and % Cell_w caps (in lyso) increases. However, the intracellular uptake kinetics of control sensor capsules was different from PEI-layered capsule. For control pH-sensor, capsule lysosome increases following decrease in endosome, which indicates maturation of endosome to lysosome over time. Whereas in case of PEI-layered pH-sensor, increase of capsule in both endosome and lysosome suggest PEI layer in capsule inhibits maturation of endosome into lysosome by preventing acidification. Therefore, according to our study with PEC based pH-sensor, we can conclude that PEI is capable of manipulating lysosomal pH due to its buffering capacity. This is also a reason for their improved transfection efficiency. Although until now, there was no direct experimental proof about this special characteristic of PEI.

The PEC system show potential for application as biodegradable drug delivery system and for pH-sensing inside cell. Delivery of therapeutics through biodegradable carrier improves bioavailability of poorly water-soluble drugs especially in case of oral drug delivery. However, large size of this system is still a major concern for drug delivery and sensing application. Another major challenge of capsule based ion-sensor is the problem of cross talk between different fluorophores. Since, capsules can load high content of fluorophores in it, sensitivity of fluorescence dependent sensing analysis increases. However, this advantage sometime introduces cross-talk challenges while study with multiple fluorophore labeled particle is concerned.

7. List of Hazardous Substances used according to GHS

Substances	GHS pictograms	Hazard Sentences	Precaution Sentences
Ethanol	  GHS02, GHS07 Danger	H225–H319	P210–P305 + P351 + P338–P370 + P378–P403 + P235
Hydrochloric acid, 37 %	  GHS05, GHS07 Danger	H302+ H314+ H318+ H335	P260 + P264 + P270 + P271 + P280 + P301 + P330 + P331 + P303 + P361 + P353
Sodium Alginate	Not hazardous substance.		
Sodium chloride	Not hazardous substance.		
Sodium hydroxide	 GHS05 Danger	H224	P210
EDTA, Disodium, Dihydrate	 GHS07	H302 + H315 + H319 + H335	P261 + P264 + P270 + P280 + P271
Poly(sodium-p-styrenesulfonate)	Not hazardous substance.		
Poly(allylamine hydrochloride)	 GHS07	H302-H317	P280

Poly-L-arginine hydrochloride	Not hazardous substance.		
Polyvinyl pyrrolidone	Not hazardous substance.		
Curcumin	Not hazardous substance.		
Sodium dodecyl sulfate	   GHS02, GHS07	H228-H302 + H332-H315-H318-H335-H412	P210-P261-P280-P301 + P312 + P330-P305 + P351 + P338 + P310-P370 + P378
Poly(ethyleneimine)	  GHS07, GHS09	H302-H411	P273
Sodium carbonate	 GHS07	H319	P264-P280-P305 + P351 + P338-P337 + P313
Citric acid	 GHS07	H319	P264-P280-P305 + P351 + P338-P337 + P313
Dextran sulfate sodium salt	Not hazardous substance.		

References

1. Caruso, F., R.A. Caruso, and H. Möhwald, *Nanoengineering of Inorganic and Hybrid Hollow Spheres by Colloidal Templating*. Science, 1998. **282**: p. 1111-1114.
2. Sukhorukov, G.B., et al., *Stepwise polyelectrolyte assembly on particle surfaces: a novel approach to colloid design*. Polymers for Advanced Technologies, 1998. **9**(10-11): p. 759-767.
3. Dejugnat, C., D. Halozan, and G.B. Sukhorukov, *Defined Picogram Dose Inclusion and Release of Macromolecules using Polyelectrolyte Microcapsules* Macromolecular Rapid Communications, 2005. **26**: p. 961-967.
4. Dejugnat, C. and G.B. Sukhorukov, *pH-responsive properties of hollow polyelectrolyte microcapsules templated on various cores*. Langmuir, 2004. **20**(17): p. 7265-7269.
5. Volodkin, D.V., et al., *Matrix polyelectrolyte microcapsules: New system for macromolecule encapsulation*. Langmuir, 2004. **20**(8): p. 3398-3406.
6. Antipov, A.A., et al., *Fabrication of a Novel Type of Metallized Colloids and Hollow Capsules*. Langmuir, 2002. **18**(17): p. 6687-6693.
7. Moya, S.E., et al., *Composite lipid polyelectrolyte capsules templated on red blood cells: fabrication and structural characterisation*. Medical & Biological Engineering & Computing, 2003. **41**(4): p. 504-508.
8. Trushina, D.B., T.V. Bukreeva, and M.N. Antipina, *Size-Controlled Synthesis of Vaterite Calcium Carbonate by the Mixing Method: Aiming for Nanosized Particles*. Crystal Growth & Design, 2016. **16**(3): p. 1311-1319.
9. Skorb, E.V. and H. Möhwald, *"Smart" Surface Capsules for Delivery Devices*. Advanced Materials Interfaces, 2015. **1**(6): p. n/a-n/a.
10. Renjie, Z., et al., *Self-assemblies of Luminescent Rare Earth Compounds in Capsules and Multilayers*. Adv Colloid Interface Sci, 2014. **207**(1): p. 361-375.
11. Kolesnikova, T.A., A.G. Skirtach, and H. Möhwald, *Red Blood Cells and Polyelectrolyte Multilayer Capsules: Natural Carriers Versus Polymer-Based Drug Delivery Vehicles*. Expert Opinion on Drug Delivery, 2013. **10**(1): p. 47-58.
12. Skirtach, A., A. Yashchenok, and H. Mohwald, *Encapsulation, release and applications of LbL polyelectrolyte multilayer capsules*. CHEMICAL COMMUNICATIONS, 2011. **47**(48): p. 12736-12746.
13. Liu, X.Y., et al., *Multilayer microcapsules as anti-cancer drug delivery vehicle:deposition,sustained release,and in vitro bioactivity*. Macromolecular Bioscience, 2005. **5**(12): p. 1209-1219.
14. Antipov, A.A., et al., *Polyelectrolyte multilayer capsule permeability control*. Colloids and Surfaces, A: Physicochemical and Engineering Aspects, 2002. **198**(Sp. Iss. SI): p. 535-541.
15. Gao, H., et al., *Intracellularly Biodegradable Polyelectrolyte/Silica Composite Microcapsules as Carriers for Small Molecules*. Acs Applied Materials & Interfaces, 2016. **8**(15): p. 9651-9661.
16. Kastl, L., et al., *Multiple internalization pathways of polyelectrolyte multilayer capsules into mammalian cells*. ACS Nano, 2013. **7**(8): p. 6605-6618.
17. Zyuzin, M.V., et al., *Comprehensive and Systematic Analysis of the Immunocompatibility of Polyelectrolyte Capsules*. Bioconjugate Chemistry, 2017. **28**: p. 556-564.
18. Hartmann, R., et al., *Stiffness-dependent in vitro uptake and lysosomal acidification of colloidal particles*. Angewandte Chemie International Edition, 2015. **54**(4): p. 1365-1368.
19. Sun, H.L., et al., *The role of capsule stiffness on cellular processing*. Chemical Science, 2015. **6**(6): p. 3505-3514.
20. Shimoni, O., et al., *Shape-Dependent Cellular Processing of Polyelectrolyte Capsules*. ACS Nano, 2013. **7**(1): p. 522-530.

21. Zhao, S., et al., *The Future of Layer-by-Layer Assembly: A Tribute to ACS Nano Associate Editor Helmut Möhwald*. ACS Nano, 2019.
22. Hanafy, N.A.N., et al., *Control of colloidal CaCO₃ suspension by using biodegradable polymers during fabrication*. Beni-Suef University Journal of Basic and Applied Sciences, 2015. **4**(1): p. 60-70.
23. Parakhonskiy, B., et al., *The influence of the size and aspect ratio of anisotropic, porous CaCO₃ particles on their uptake by cells*. J Nanobiotechnology, 2015. **13**(1): p. 53.
24. Zhou, Z., et al., *Nonviral cancer gene therapy: delivery cascade and vector nanoproperty integration*. Advanced drug delivery reviews, 2017. **115**: p. 115-154.
25. Gilleron, J., et al., *Image-based analysis of lipid nanoparticle-mediated siRNA delivery, intracellular trafficking and endosomal escape*. Nature biotechnology, 2013. **31**(7): p. 638-646.
26. Rivera_Gil, P., et al., *Intracellular processing of proteins mediated by biodegradable polyelectrolyte capsules*. Nano Letters, 2009. **9**(12): p. 4398-4402.
27. Ott, A., et al., *Light-addressable and degradable silica capsules for delivery of molecular cargo to the cytosol of cells*. Chemistry of Materials, 2015. **27**: p. 1929-1942.
28. Zhu, D., et al., *Remotely controlled opening of delivery vehicles and release of cargo by external triggers*. Advanced Drug Delivery Reviews, 2019. **138**: p. 117-132.
29. Skirtach, A.G., et al., *Laser-induced release of encapsulated materials inside living cells*. Angew. Chem. Int. Ed., 2006. **45**: p. 4612-4617.
30. Skirtach, A.G., et al., *Remote activation of capsules containing Ag nanoparticles and IR dye by laser light*. Langmuir, 2004. **20**(17): p. 6988-6992.
31. Muñoz Javier, A., et al., *Photoactivated release of cargo from the cavity of polyelectrolyte capsules to the cytosol of cells*. Langmuir, 2008. **24**: p. 12517-12520.
32. Radt, B., T.A. Smith, and F. Caruso, *Optically addressable nanostructured capsules*. Advanced Materials, 2004. **16**(23-24): p. 2184-2189.
33. Palankar, R., et al., *Controlled intracellular release of peptides from microcapsules enhances antigen presentation on MHC class I molecules*. Small, 2009. **5**(19): p. 2168-2176.
34. Ochs, M., et al., *Light-addressable capsules as caged compound matrix for controlled in vitro release*. Angewandte Chemie International Edition, 2013. **52**(2): p. 695-699.
35. Hühn, D., et al., *Photostimulated Au nanoheaters in polymer and biological media: characterization of mechanical destruction and boiling*. Advanced Functional Materials, 2012. **22**(2): p. 294-303.
36. Huang, J., K.S. Jackson, and C.J. Murphy, *Polyelectrolyte wrapping layers control rates of photothermal molecular release from gold nanorods*. Nano Lett., 2012. **12**(6): p. 2982-2987.
37. del Mercato, L.L., et al., *LbL multilayer capsules: recent progress and future outlook for their use in life sciences*. Nanoscale, 2010. **2**(4): p. 458-467.
38. Kantner, K., et al., *Laterally and temporally controlled intracellular staining by light-triggered release of encapsulated fluorescent markers*. Chemistry A European Journal, 2018. **24**: p. 2098-2102.
39. Kim, H., et al., *Visible light-triggered on-demand drug release from hybrid hydrogels and its application in transdermal patches*. Advanced healthcare materials, 2015. **4**(14): p. 2071-2077.
40. Masereel, B., L. Pochet, and D. Laeckmann, *An overview of inhibitors of Na⁺/H⁺ exchanger*. European Journal of Medicinal Chemistry, 2003. **38**(6): p. 547-554.
41. Cannell, M.B. and M.V. Thomas, *Intracellular ion measurement with fluorescent indicators*. Flux, 1994. **2**(1): p. 317-345.
42. Kantner, K., et al., *Particle-Based Optical Sensing of Intracellular Ions at the Example of Calcium - What are the Experimental Pitfalls?* Small, 2015. **11**: p. 896-904.

43. del Mercato, L.L., A.Z. Abbasi, and W.J. Parak, *Synthesis and characterization of ratiometric ion-sensitive polyelectrolyte capsules*. Small, 2011. **7**: p. 351-363.
44. del Mercato, L.L., et al., *Multiplexed sensing of ions with barcoded polyelectrolyte capsules*. ACS Nano, 2011. **5**(12): p. 9668-9674.
45. Lee, K.Y. and D.J. Mooney, *Alginate: properties and biomedical applications*. Progress in polymer science, 2012. **37**(1): p. 106-126.
46. Goh, C.H., P.W.S. Heng, and L.W. Chan, *Alginates as a useful natural polymer for microencapsulation and therapeutic applications*. Carbohydrate Polymers, 2012. **88**(1): p. 1-12.
47. Orive, G., et al., *Biocompatibility of alginate-poly-L-lysine microcapsules for cell therapy*. Biomaterials, 2006. **27**(20): p. 3691-3700.
48. Sergeeva, A.S., D.A. Gorin, and D.V. Volodkin, *In-Situ Assembly of Ca-Alginate Gels with Controlled Pore Loading/Release Capability*. Langmuir, 2015. **31**(39): p. 10813-10821.
49. Lengert, E., et al., *Hollow silver alginate microspheres for drug delivery and surface enhanced Raman scattering detection*. RSC Advances, 2016. **6**(24): p. 20447-20452.
50. Chiang, C.-Y. and C.-C. Chu, *Synthesis of photoresponsive hybrid alginate hydrogel with photo-controlled release behavior*. Carbohydrate Polymers, 2015. **119**: p. 18-25.
51. Cong, Z., et al., *A novel controlled drug delivery system based on alginate hydrogel/chitosan micelle composites*. International Journal of Biological Macromolecules, 2018. **107**: p. 855-864.
52. Zintchenko, A., et al., *Simple modifications of branched PEI lead to highly efficient siRNA carriers with low toxicity*. Bioconjug Chem, 2008. **19**(7): p. 1448-55.
53. Boeckle, S., et al., *Melittin analogs with high lytic activity at endosomal pH enhance transfection with purified targeted PEI polyplexes*. J Control Release, 2006. **112**(2): p. 240-8.
54. von Harpe, A., et al., *Characterization of commercially available and synthesized polyethylenimines for gene delivery*. J Control Release, 2000. **69**(2): p. 309-22.
55. Beyerle, A., et al., *Poly(ethylene imine) Nanocarriers Do Not Induce Mutations nor Oxidative DNA Damage in Vitro in MutaMouse FE1 Cells*. Molecular Pharmaceutics, 2011. **8**(3): p. 976-981.
56. Abdallah, B., et al., *A powerful nonviral vector for in vivo gene transfer into the adult mammalian brain: Polyethylenimine*. Human Gene Therapy, 1996. **7**(16): p. 1947-1954.
57. Gebhart, C.L. and A.V. Kabanov, *Evaluation of polyplexes as gene transfer agents*. Journal of Controlled Release, 2001. **73**(2-3): p. 401-416.
58. Shim, M.S. and Y.J. Kwon, *Acid-responsive linear polyethylenimine for efficient, specific, and biocompatible siRNA delivery*. Bioconjug Chem, 2009. **20**(3): p. 488-99.
59. Lee, M., et al., *Target-Specific Gene Silencing of Layer-by-Layer Assembled Gold-Cysteamine/siRNA/PEI/HA Nanocomplex*. ACS NANO, 2011. **5**(8): p. 6138-6147.
60. Behr, J.P., *The proton sponge: A trick to enter cells the viruses did not exploit*. Chimia, 1997. **51**(1-2): p. 34-36.
61. Akinc, A., et al., *Exploring polyethylenimine-mediated DNA transfection and the proton sponge hypothesis*. Journal of Gene Medicine, 2005. **7**(5): p. 657-663.
62. Boussif, O., et al., *A versatile vector for gene and oligonucleotide transfer into cells in culture and in vivo: polyethylenimine*. Proc Natl Acad Sci U S A, 1995. **92**(16): p. 7297-301.
63. Pack, D.W., et al., *Design and development of polymers for gene delivery*. Nat. Rev. Drug Discovery, 2005. **4**(7): p. 581-593.
64. Creusat, G., et al., *Proton sponge trick for pH-sensitive disassembly of polyethylenimine-based siRNA delivery systems*. Bioconjug Chem, 2010. **21**(5): p. 994-1002.
65. Antipov, A.A., et al., *Carbonate microparticles for hollow polyelectrolyte capsules fabrication*. COLLOIDS AND SURFACES A-PHYSICO-CHEMICAL AND ENGINEERING ASPECTS, 2003. **224**(1-3): p. 175-183.

66. De_Geest, B.G., et al., *Polyelectrolyte microcapsules for biomedical applications*. Soft Matter, 2009. **5**(2): p. 282-291.
67. Lee, J.S., et al., *Layer-by-layer assembled charge-trap memory devices with adjustable electronic properties*. Nature Nanotechnology, 2007. **2**(12): p. 790-795.
68. Parakhonskiy, B.V., et al., *Colloidal micro- and nano-particles as templates for polyelectrolyte multilayer capsules*. Adv. Colloid Interface Sci., 2014: p. DOI: 10.1016/j.cis.2014.01.022.
69. Navolokin, A.N., et al., *Systemic Administration of Polyelectrolyte Microcapsules: Where Do They Accumulate and When? In Vivo and Ex Vivo Study*. Nanomaterials, 2018. **8**(10).
70. De Geest, B.G., et al., *Polymeric Multilayer Capsule-Mediated Vaccination Induces Protective Immunity Against Cancer and Viral Infection*. ACS Nano, 2012. **6**(3): p. 2136-2149.
71. Winter, S., et al., *Back to the roots: photodynamic inactivation of bacteria based on water-soluble curcumin bound to polyvinylpyrrolidone as a photosensitizer*. Photochemical & Photobiological Sciences, 2013. **12**(10): p. 1795-1802.
72. Yang, D.H., et al., *Preparation of poly-L-lysine-based nanoparticles with pH-sensitive release of curcumin for targeted imaging and therapy of liver cancer in vitro and in vivo*. Drug Delivery, 2018. **25**(1): p. 950-960.
73. Kottegoda, N., et al., *Urea-Hydroxyapatite Nanohybrids for Slow Release of Nitrogen*. ACS Nano, 2017. **11**: p. 1214-1221.
74. Ashraf, S., et al. *pH sensitive polyelectrolyte microcapsules as carrier system for delivery and sensing in cells*. in *Nanobio Europe - 6th International Congress & Exhibition on Nanobiotechnology*. 2010. Münster.
75. Funhoff, A.M., et al., *Endosomal escape of polymeric gene delivery complexes is not always enhanced by polymers buffering at low pH*. Biomacromolecules, 2004. **5**(1): p. 32-39.
76. Benjaminsen, R.V., et al., *The possible "proton sponge" effect of polyethylenimine (PEI) does not include change in lysosomal pH*. Mol Ther, 2013. **21**(1): p. 149-57.
77. Decher, G., *Fuzzy nanoassemblies: Toward Layered Polymeric Multicomposites*. Science, 1997. **277**: p. 1232-1237.
78. Muñoz_Javier, A., et al., *Uptake of colloidal polyelectrolyte coated particles and polyelectrolyte multilayer capsules by living cells*. Advanced Materials, 2008. **20**(22): p. 4281-4287.
79. Schuler, C. and F. Caruso, *Decomposable hollow biopolymer-based capsules*. Biomacromolecules, 2001. **2**(3): p. 921-6.
80. Dittert, L.W., T. Higuchi, and D.R. Reese, *Phase solubility technique in studying the formation of complex salts of triamterene*. Journal of Pharmaceutical Sciences, 1964. **53**(11): p. 1325-1328.
81. Nold, P., et al., *Optimizing conditions for labeling of mesenchymal stromal cells (MSCs) with gold nanoparticles: a prerequisite for in vivo tracking of MSCs*. Journal of Bionanotechnology, 2017. **15**: p. 24.
82. Ma, X., et al., *Colloidal Gold Nanoparticles Induce Changes in Cellular and Subcellular Morphology*. ACS Nano, 2017. **11**: p. 7807-7820.
83. Rivera Gil, P., et al., *pH sensitive capsules as intracellular optical reporters for monitoring lysosomal pH changes upon stimulation*. Small, 2012. **8**(6): p. 943-948.
84. De Koker, S., et al., *Polymeric multilayer capsules delivering biotherapeutics*. Advanced Drug Delivery Reviews, 2011. **63**(9): p. 748-761.
85. Ambrosone, A., et al., *Control of wnt/ β -catenin signaling pathway in vivo via light responsive capsules*. ACS Nano, 2016. **10**: p. 4828-4834.
86. Roy, S., et al., *Biodegradable alginate polyelectrolyte capsules as plausible biocompatible delivery carriers*. ACS Applied Bio Materials, 2019.

87. Bhopate, D.P., et al., *A highly selective and sensitive single click novel fluorescent off–on sensor for copper and sulfide ions detection directly in aqueous solution using curcumin nanoparticles*. New Journal of Chemistry, 2015. **39**(9): p. 7086-7096.
88. Zambito, Y., E. Pedreschi, and G. Di Colo, *Is dialysis a reliable method for studying drug release from nanoparticulate systems?—A case study*. International Journal of Pharmaceutics, 2012. **434**(1): p. 28-34.
89. Huang, J., et al., *Layer-by-layer assembled milk protein coated magnetic nanoparticle enabled oral drug delivery with high stability in stomach and enzyme-responsive release in small intestine*. Biomaterials, 2015. **39**: p. 105-113.
90. Wang, N., et al., *Magnetic nanoparticles (MNPs) covalently coated by PEO-PPO-PEO block copolymer for drug delivery*. Journal of Colloid and Interface Science, 2013. **395**: p. 50-57.
91. Hao, S., et al., *Preparation of Eudragit L 100-55 enteric nanoparticles by a novel emulsion diffusion method*. Colloids and Surfaces B: Biointerfaces, 2013. **108**: p. 127-133.
92. Liu, K., et al., *pH-responsive liposomes self-assembled from electrosprayed microparticles, and their drug release properties*. Colloids and Surfaces A: Physicochemical and Engineering Aspects, 2018. **537**: p. 20-27.
93. Joshi, M., *Role of eudragit in targeted drug delivery*. Vol. 5. 2013. 58-62.
94. Thakral, S., N.K. Thakral, and D.K. Majumdar, *Eudragit: a technology evaluation*. Expert Opin Drug Deliv, 2013. **10**(1): p. 131-49.
95. Feliu, N., et al. *Systems biology approaches reveal low-dose effects of dendrimers - abstract*. in *248th American Chemical Society National Meeting & Exposition*. 2014. San Francisco, CA, USA.
96. Al-Rawi, M., S. Diabate, and C. Weiss, *Uptake and intracellular localization of submicron and nano-sized SiO₂ particles in HeLa cells*. Archives of Toxicology, 2011. **85**(7): p. 813-826.
97. Mukherjee, S.G., et al., *Comparative in vitro cytotoxicity study of silver nanoparticle on two mammalian cell lines*. Toxicol In Vitro, 2012. **26**(2): p. 238-51.
98. Chakraborty, I., et al., *Protein-Mediated Shape-Control of Silver Nanoparticles*. Bioconjugate Chemistry, 2018. **29**: p. 1261–1265.
99. Zhu, D., et al., *Detailed investigation on how the protein corona modulates the physicochemical properties and gene delivery of polyethylenimine (PEI) polyplexes*. Biomaterials Science, 2018. **6**: p. 1800-1817.
100. Summers, H.D., et al., *Quantification of Nanoparticle Dose and Vesicular Inheritance in Proliferating Cells*. Acs Nano, 2013. **7**(7): p. 6129-6137.

A. Acknowledgments

This thesis was prepared at the University of Hamburg, in the Department of Chemistry in the Center for Hybrid Nanostructure (CHyN) under supervision of Professor Dr. Wolfgang J. Parak, Prof. Alf Mews as 2nd supervisor and co-supervision of Dr. Neus Feliu Torres.

First, I would like to thank Prof. Dr. Wolfgang J Parak for entrusting me with this highly interesting research topic and for giving me the opportunity to be a member of his research group. I am especially grateful to Dr. Neus Feliu Torres for her provided freedom in my research and her guidance. I am also honored to have Prof. Alf Mews as my second supervisor from the University of Hamburg (UHH) and my previous second supervisor Prof. Dr. Martin Koch from the Philipps-University of Marburg.

I would like to specially acknowledge Prof. Antonios G. Kanaras from the University of Southampton, UK for sending samples for collaborative project, Nancy Elbaz for collaborative work. I acknowledge the support of Mrs Marta Gallego Gonzalez from CIC Biomagune for measuring the TEM images. Also, Dr. Indranath Chakraborty from UHH for doing my ICP-MS measurements. Stefanie Kramer and Andreas Rentzos from the Philipps-University of Marburg and also, Petra Roth and Marten Rittner from UHH for administrative and technical support during my PhD research years in both the Universities.

Additionally, I want to thank members from PIER graduate school who helped me to integrate into different career development programs in UHH, Mrs. Anika Ostermaier-Grabow for coordinating 'dynaMENT, women in natural science' program and giving me an opportunity to participate in it. I'm also very thankful to Prof. Dr. Carmen Herrmann for being my mentor in 'dynaMENT' program and for all the fruitful advices she gave for my future career development.

My special thanks go to Prof. Dr. Wolfgang J Parak and Dr. Neus Feliu Torres for evaluating of this thesis. Moreover, I thank Prof. Carmen Herrmann and Prof. Dr. Dorota Koziej for being members of the examination committee.

Furthermore, I would like to thank my present and previous colleagues from the Biophotonik group at the UHH and Philipps-University of Marburg for the great working atmosphere and all memorable moments together. Especially I would like to thank my friend and previous colleague Karl V L Kraft for helping me with German language translation for PhD scholarship applications. I really appreciate the time of my colleagues, Dr. Dingcheng Zhu and Dr. Mikhail V. Zyuzin, for the valuable discussions at different stages of my PhD research work.

Special thanks go to my husband Dr. Indranath Chakraborty for his support, understanding and all scientific advices. Moreover, I dearly thank my family and friends for their support and patience during the last years. THANKS!!